



University of Kentucky
UKnowledge

University of Kentucky Doctoral Dissertations

Graduate School

2007

FUNCTIONALIZATION OF FLUORINATED SURFACTANT TEMPLATED SILICA

Gifty Osei-Prempeh
University of Kentucky, gosei2@uky.edu

[Right click to open a feedback form in a new tab to let us know how this document benefits you.](#)

Recommended Citation

Osei-Prempeh, Gifty, "FUNCTIONALIZATION OF FLUORINATED SURFACTANT TEMPLATED SILICA" (2007).
University of Kentucky Doctoral Dissertations. 542.
https://uknowledge.uky.edu/gradschool_diss/542

This Dissertation is brought to you for free and open access by the Graduate School at UKnowledge. It has been accepted for inclusion in University of Kentucky Doctoral Dissertations by an authorized administrator of UKnowledge. For more information, please contact UKnowledge@lsv.uky.edu.

ABSTRACT OF DISSERTATION

Gifty Osei-Prempeh

The Graduate School
University of Kentucky
2007

FUNCTIONALIZATION OF FLUORINATED SURFACTANT TEMPLATED SILICA

ABSTRACT OF DISSERTATION

A dissertation submitted in partial fulfillment of the requirements for the degree of Doctor of Philosophy in the College of Engineering at the University of Kentucky

By
Gifty Osei-Prempeh

Lexington, Kentucky

Director: Dr. Barbara L. Knutson, Professor of Chemical Engineering

Lexington, Kentucky

2007

Copyright © Gifty Osei-Prempeh 2007

ABSTRACT OF DISSERTATION

FUNCTIONALIZATION OF FLUORINATED SURFACTANT TEMPLATED SILICA

Surfactant templating provides for the synthesis of ordered mesoporous silica and the opportunity to tailor the pore size, pore structure, particle morphology and surface functionality of the silica through the selection of synthesis conditions and surfactant template. This work extends the synthesis of nanostructured silica using fluorinated surfactant templates to the synthesis of organic/inorganic composites. The effect of fluorinated surfactant templates ($C_6F_{13}C_2H_4NC_5H_5Cl$, $C_8F_{17}C_2H_4NC_5H_5Cl$ and $C_{10}F_{21}C_2H_4NC_5H_5Cl$), which have highly hydrophobic fluorocarbon tails, on functional group incorporation, accessibility, and silica textural properties is examined and compared to properties of hydrocarbon surfactant ($C_{16}H_{33}N(CH_3)_3Br$, CTAB) templated silica. Hydrocarbon (vinyl, n-decyl and 3-aminopropyl) and fluorocarbon (perfluoro-octyl, perfluorodecyl) functional group incorporation by direct synthesis is demonstrated, and its effects on silica properties are interpreted based on the aggregation behavior with the surfactant templates.

Silica materials synthesized with CTAB possess greater pore order than materials synthesized with the fluorocarbon surfactants. The incorporation of the short vinyl chain substantially reduces silica pore size and pore order. However, pore order increases with functionalization for materials synthesized with the fluorinated surfactant having the longest hydrophobic chain.

The incorporation of longer chain functional groups (n-decyl, perfluorodecyl, perfluoro-octyl) by direct synthesis results in hexagonal pore structured silica for combinations of hydrocarbon/fluorocarbon surfactant and functional groups. The long chain of these silica precursors, which can be incorporated in the surfactant micelle core, affect the pore size less than vinyl incorporation. Synthesis using the longer chain fluorosurfactant ($C_8F_{17}C_2H_4NC_5H_5Cl$) template in ethanol/water solution results in highest incorporation of both n-decyl and the fluorocarbon functional groups, with a corresponding loss of material order in the fluorinated material. Matching the fluorocarbon surfactant ($C_6F_{13}C_2H_4NC_5H_5Cl$) to the perfluoro-octyl precursor did not show improved functional group incorporation. Higher incorporation of the perfluoro-octyl functional group was observed for all surfactant templates, but the perfluoro-decyl silica is a better adsorbent for the separation of hydrocarbon and fluorocarbon tagged anthraquinones.

Incorporating a reactive hydrophilic functional group (3-aminopropyl) suggests further applications of the resulting nanoporous silica. Greater amine incorporation is achieved in the CTAB templated silica, which has hexagonal pore structure; the order and surface area decreases for the fluorinated surfactant templated material.

KEYWORDS: Nanoporous silica, fluorocarbon surfactants, CO₂ capture, organic/inorganic composites, surfactant templating

Gifty Osei Prempeh

August 20, 2007

FUNCTIONALIZATION OF FLUORINATED SURFACTANT TEMPLATED SILICA

By

Gifty Osei-Prempeh

Dr Barbara L. Knutson

Director of Dissertation

Dr Barbara L. Knutson

Director of Graduate Studies

August 20, 2007

RULES FOR THE USE OF DISSERTATIONS

Unpublished dissertations submitted for the Doctor's degree and deposited in the University of Kentucky Library are as a rule open for inspection, but are to be used only with due regard to the rights of the authors. Bibliographical references may be noted, but quotations or summaries of parts may be published only with the permission of the author, and with the usual scholarly acknowledgments.

Extensive copying or publication of the dissertation in whole or in part also requires the consent of the Dean of the Graduate School of the University of Kentucky.

A library that borrows this dissertation for use by its patrons is expected to secure the signature of each user.

Name

Date

DISSERTATION

Gifty Osei-Prempeh

The Graduate School
University of Kentucky

2007

FUNCTIONALIZATION OF FLUORINATED SURFACTANT TEMPLATED SILICA

DISSERTATION

A dissertation submitted in partial fulfillment of the
requirements for the degree of Doctor of Philosophy in the
College of Engineering
at the University of Kentucky

By
Gifty Osei-Prempeh

Lexington, Kentucky

Director: Dr. Barbara L. Knutson, Professor of Chemical Engineering

Lexington, Kentucky

2007

Copyright © Gifty Osei-Prempeh 2007

ACKNOWLEDGEMENTS

My special thanks go to my advisor, Dr Barbara Knutson, for her invaluable guidance and counseling through out this research and particularly in the writing of this dissertation. She has been a great inspiration to me during my time here at UK and hope to draw on that in the future. I would also like to thank Dr Rankin and Dr Lehmler for their substantial contributions to this project. Thanks to my Ph.D. committee for their time and advice.

I am also grateful to my friends and colleagues for their support. My parents and sister, though far away, also played an important role in this work by means of their advice and encouragement. Finally, I am thankful for my husband, Alex, he has been my greatest strength and bulwark. I dedicate this dissertation to my daughter, Ama, for her to know that it is not impossible to set high goals because they are achievable if you believe in yourself.

TABLE OF CONTENTS

Acknowledgments.....	iii
List of Tables.....	viii
List of Figures.....	ix
Chapter One: Introduction.....	1
1.1 Research Hypothesis.....	2
1.2 Research Objectives.....	3
Chapter Two: Background.....	5
2.1 Silica.....	5
2.2 Porous Material.....	5
2.3 Surfactant Templated Mesoporous Silica.....	7
2.3.1 Surfactants.....	7
2.3.2 Mesoporous Silica Templating Mechanism.....	17
2.3.3 Silica Polymerization Steps.....	19
2.3.4 M41S Family of Materials and Others.....	20
2.3.5 Fluorinated Surfactant Templating.....	22
2.3.6 Ordered Organic-Inorganic Mesoporous Silica.....	26
2.4 Material Characterization Techniques.....	28
2.4.1 Fourier Transform Infra-red Spectroscopy (FTIR).....	28
2.4.2 Thermogravimetric Analysis (TGA).....	30
2.4.3 X-Ray Diffraction (XRD).....	31
2.4.4 Transmission Electron Microscopy (TEM).....	34

2.4.5 Nitrogen Adsorption Analysis.....	35
Chapter Three: Fluorinated Surfactant Templating of Vinyl-Functionalized Nanoporous Silica.....	38
3.1 Summary.....	38
3.2 Introduction.....	39
3.3 Materials and Methods.....	41
3.3.1 Surfactant Synthesis.....	41
3.3.2 Materials Synthesis.....	42
3.3.3 Materials Characterization.....	44
3.4 Results and Discussion.....	45
3.4.1 FTIR Analysis.....	45
3.4.2 Powder X-ray Diffraction Analysis.....	45
3.4.3 Transmission Electron Microscopy.....	48
3.4.4 Nitrogen Adsorption Analysis.....	48
3.4.5 Vinyl Accessibility Analysis.....	53
3.5 Conclusions.....	55
Chapter Four: Fluorocarbon and Hydrocarbon Functional Group Incorporation into Nanoporous Silica Employing Fluorinated And Hydrocarbon Surfactants as Templates.....	57
4.1 Summary.....	57
4.2 Introduction.....	58
4.3 Materials and Methods.....	62
4.3.1 Synthesis of Mesoporous Silica.....	64
4.3.2 Materials Characterization.....	65
4.4 Results and Discussion.....	66

4.4.1 Functional Group Incorporation.....	66
4.4.2 Hydrophobicity of Functionalized Silica Materials.....	72
4.4.3 Structural Properties of Functionalized Silica.....	73
4.5 Conclusions.....	80
Chapter Five: Application of Fluoro-Functionalized Mesoporous Silica To Fluorous Separations.....	82
5.1 Summary.....	82
5.2 Introduction.....	83
5.3 Materials and Methods.....	87
5.3.1 Materials.....	87
5.3.2 Synthesis of Mesoporous Silica.....	88
5.3.3 Materials Characterization.....	89
5.3.4 Partitioning of Anthraquinone Dyes Onto Functionalized Mesoporous Silica.....	91
5.3.5 Fluorous-Solid Phase Extraction (F-SPE).....	91
5.4 Results and Discussion.....	93
5.4.1 Silica Materials as Packing for Dyes Separation.....	100
5.5 Conclusions.....	107
Chapter Six: Direct Synthesis and Accessibility of Amine-Functionalized Nanoporous Silica.....	109
6.1 Summary.....	109
6.2 Introduction.....	110
6.3 Materials and Methods.....	114
6.4 Results and Discussion.....	118

6.4.1	Chemical Analysis of Functional Group Incorporation.....	119
6.4.2	Pore Structure Size and Order of Synthesized Materials.....	124
6.4.3	Accessibility of Amine Functionalized Group.....	130
6.4.4	Characterization of Synthesized Silica by CO ₂ Capture.....	132
6.5	Conclusions.....	138
Chapter Seven:	Conclusions and Future Work.....	140
7.1	Conclusions.....	140
7.2	Future Work.....	144
Appendix A		
KJS and Adsorption Potential Methods.....		147
Appendix B		
FTIR of Representative Surfactants and Silica Precursors Used in This Investigation.....		151
Appendix C		
FTIR of CTAB and HFOPC Templated Vinyl Functionalized Silica.....		153
Appendix D		
Perfluoro-decyl (F ₈ H ₂) Functionalized Mesoporous Silica Synthesized in Homogeneous (water/ethanol) Solution using CTAB and HFOPC Templates.....		155
Appendix E		
Synthesis of organic functionalized silica using cetyltrimethyl pyridinium bromide (CPB) template.....		158
APPENDIX F		
CO ₂ Capture from Humid and Low Concentration CO ₂ Streams.....		161
References.....		163
Vita		185

LIST OF TABLES

Table 2.1, Packing parameter, shape of surfactant and structure of micelles.....	9
Table 2.2, Critical Micelle Concentration (CMC) of Surfactants.....	13
Table 2.3, Comparison of texture properties of nanoporous silica particles obtained by perfluoro-alkylpyridinium chloride surfactants templating.....	23
Table 3.1, Molar ratios of reactants used in material synthesis.....	43
Table 3.2, Summary of the textural properties of all the materials.....	52
Table 4.1, Organic content of functionalized materials.....	70
Table 4.2, Structural properties of fluorocarbon and hydrocarbon functionalized Materials.....	77
Table 5.1, Organic content and textural properties of functionalized and non-functionalized materials.....	99
Table 5.2, Partition behavior of HC- and FC- dyes in eluent solvents.....	105
Table 5.3, Anthraquinone dye separation by fluorous-solid phase extraction (F-SPE) using a 0.2 g packed column.....	106
Table 6.1, Elemental nitrogen analysis of the non-functionalized and amine-functionalized material.....	123
Table 6.2, Materials textural properties of non-functionalized, amine-functionalized, and bi-functionalized (amine-fluorocarbon) silica as a function of surfactant template.....	130
Table 6.3, CO ₂ capacity of synthesized silica as measured in dry CO ₂ as a function of Temperature.....	137
Table D1, Molar ratios of reagents.....	155
Table D2, Organic content from TGA analysis.....	156
Table E1 Molar ratios of reagents.....	158
Table F1 Amount of CO ₂ adsorbed from humid pure CO ₂ stream.....	162

LIST OF FIGURES

Figure 2.1, Liquid crystal phases A) hexagonal, B) lamellar and C) bicontinuous cubic.....	10
Figure 2.2, Phase diagram of hydrocarbon surfactant – aqueous solution mixtures showing location of hexagonal (H_1), normal bicontinuous cubic (V_1), and lamellar (L_α) liquid phases, aqueous nonmicellar solution (W), micellar solution (L_1), liquid surfactant containing water (L_2), and solid surfactant (S).....	10
Figure 2.3, Co-existence of two kinds of mixed micelles observed by Asakawa et al; FC-fluorocarbon, HC-hydrocarbon.....	15
Figure 2.4, Mechanism of mesoporous silica formation.....	18
Figure 2.5, Thermogram.....	30
Figure 2.6, Incident rays on three parallel equidistant planes.....	31
Figure 2.7, X-Ray Diffraction Patterns.....	32
Figure 2.8, Types of physisorption isotherms.....	37
Figure 3.1, Powder X-ray diffraction patterns of A) CTAB template materials, B) HFOPC template materials, C) HFDePC template materials and D) HFDoDePC template materials.....	47
Figure 3.2, TEM images of A) v4-CTAB B) v6-HFOPC C) v6-HFDePC and D) v4-HFDoDePC.....	49
Figure 3.3, Nitrogen adsorption isotherms of a) v4-CTAB-d b) v4-CTAB c) v6-CTAB d) CTAB e) v4-HFDePC f) v6-HFDePC, g) HFDePC h) v4-HFOPC i) v6-HFOPC, j) HFOPC.....	50
Figure 3.4, Pore size distributions calculated using the BJH method with a modified Kelvin equation.....	51
Figure 3.5, Bromination reaction plots of A) samples prepared with 4 TEOS: 1 VTES and B) samples prepared with 6 TEOS: 1 VTES.....	54
Figure 4.1, Structures of precursors: A) tetraethoxysilane (TEOS) B) n-decyl triethoxysilane (H_{10} TES) and C) heptadecafluoro-1,1,2,2-tetrahydrodecyl triethoxysilane (F_8H_2 TES).....	63

Figure 4.2, Structures of surfactants: A) tridecafluoro-1,1,2,2-tetrahydro-octyl pyridinium chloride (HFOPC) B) heptadecafluoro-1,1,2,2-tetrahydro-decyl pyridinium chloride (HFDePC) and C) cetyltrimethylammonium bromide (CTAB).....	63
Figure 4.3, FTIR plots of as-synthesized and extracted A) CTAB templated, B) HFOPC templated, and C) HFDePC templated silica.....	68
Figure 4.4, Sample TGA plots of HFDePC, H ₁₀ -HFDePC and F ₈ H ₂ -HFDePC.....	70
Figure 4.5, Images of water droplet on A) HFDePC templated silica, B) H ₁₀ -HFDePC and C) F ₈ H ₂ -HFDePC.....	73
Figure 4.6, Powder X-ray diffraction plots of A) CTAB templated, B) HFOPC templated, and C) HFDePC templated silica materials.....	74
Figure 4.7, Representative TEM images of A) H ₁₀ -CTAB, B) F ₈ H ₂ -CTAB, C) H ₁₀ -HFOPC, D) F ₈ H ₂ -HFOPC, E) H ₁₀ -HFDePC, and F) F ₈ H ₂ -HFDePC.....	75
Figure 4.8, Nitrogen adsorption isotherm and pore size distribution of A) CTAB templated, B) HFOPC templated, and C) HFDePC templated silica materials.....	79
Figure 5.1, Hydrocarbon-tagged anthraquinone (Sudan blue II [Bis(butylamino)anthraquinone]) (left); and fluorocarbon-tagged anthraquinone dye (1-fluoro, 4-pentadecafluoro-1,1-dihydro-octylamino-anthraquinone).....	88
Figure 5.2, FTIR profile of A) F ₆ H ₂ -CTAB template before and after extraction; B) F ₈ H ₂ -HFDePC before and after extraction; and C) HFDePC templated materials.....	94
Figure 5.3, Sample TGA plot of HFDePC, F ₈ H ₂ -HFDePC and F ₆ H ₂ -HFDePC.....	96
Figure 5.4, Powder X-ray diffraction plots of A) F ₆ H ₂ functionalized B) F ₈ H ₂ functionalized silica materials.....	98
Figure 5.5 SEM image of A) F ₈ H ₂ -CTAB B) F ₈ H ₂ -HFOPC and C) F ₈ H ₂ -HFDePC.....	101
Figure 5.6 A) Mixture of HC- and FC-tagged anthraquinones loaded on column. Elution behavior of HC- and FC-tagged anthraquinone (blue and orange dyes, respectively) on B) fluoroflash fluoro-functionalized silica gel and, C) F ₈ H ₂ - HFDePC column.....	102

Figure 5.7, Dye elution plots of hydrocarbon-tagged anthraquinone (HC-dye) and fluorocarbon-tagged anthraquinone (FC-dye) on A) functionalized silica gel, B) F ₈ H ₂ -CTAB, and C) F ₈ H ₂ -HFDePC.....	104
Figure 6.1, FTIR plots of A) CTAB templated AP- silica materials; B) HFOPC templated AP-silica materials; C) HFDePC templated AP-F ₆ H ₂ -silica and D) AP-HFDePC.....	120
Figure 6.2, TGA plot of A) HFDePC B) AP-HFDePC and C) AP-F ₆ H ₂ -HFDePC.....	123
Figure 6.3, Powder X-ray diffraction plots of non-functionalized, amine-functionalized, and bi-functionalized (amine and fluorocarbon) silica materials templated with A) CTAB; B) HFOPC; and C) HFDePC.....	125
Figure 6.4, Sample TEM images of A) AP-CTAB B) AP-HFOPC C) AP-HFDePC D) AP-F ₆ H ₂ -CTAB E) AP-F ₆ H ₂ -HFOPC and F) AP-F ₆ H ₂ -HFDePC.....	126
Figure 6.5, Nitrogen adsorption isotherm and pore size distribution of A) CTAB templated materials B) HFOPC templated materials and C) HFDePC template materials.....	129
Figure 6.6, Confocal microscopy images of A) AP-CTAB B) AP-HFOPC C) AP-HFDePC.....	132
Figure 6.7, Solution phase concentration of FITC during incorporation into amine functionalized silica.....	132
Figure 6.8, FTIR of AP-HFDePC before and 15 minutes after CO ₂ adsorption.....	138
Figure A1, High resolution α_s -plot	148
Figure A2, Adsorption potential plot for v6-HFOPC.....	150
Figure B1 FTIR of representative surfactants.....	151
Figure B2 FTIR of precursors.....	152
Figure C1 FTIR of A) CTAB templated and B) HFOPC templated vinyl functionalized silica.....	154
Figure D1 FTIR of A) CTAB template and B) HFOPC template materials.....	156
Figure D2 XRD patterns of A) CTAB template and B) HFOPC template silica materials synthesized in homogeneous water/ethanol solution.....	157

Figure E1 XRD patterns of CPB template silica materials.....	159
Figure E2 Comparison of XRD patterns for F ₆ H ₂ -CTAB and F ₆ H ₂ -CPB.....	160

CHAPTER 1

INTRODUCTION

Porous materials have been demonstrated for a wide range of applications, such as catalysis, separation and sensing, which make use of their high surface area to volume ratio. In catalysis, porous materials are applied as catalyst support by incorporating inorganic, organic and bio-molecule active sites.¹ Organic functionalized porous materials are also employed as solid supports for HPLC, SPE and membrane separations. Porous materials incorporated with enzymes, antibodies and dyes are used as sensors to provide fluorescence, optical and electrochemical responses to external stimulation.² Emerging areas of application of porous materials include drug delivery³, energy (e.g. hydrogen storage) and environmental remediation (e.g. CO₂ capture and storage).⁴ The matrices of porous materials are formed by polymers, carbon, metals, alumino-silicate and oxides. In the 1990's researchers at Mobil Oil Co. synthesized hexagonal, cubic and lamellar uniform pore structured silica by sol-gel techniques using alkylammonium bromide surfactants as template.⁵ Subsequent investigations have focused on tailoring the silica pore structure through the synthesis conditions and type of template (hydrocarbon cationic surfactants (e.g. CTAB)⁶, anionic surfactant (e.g. sodium dodecylsulfate, SDS)⁷, neutral surfactants⁸, block co-polymers⁹ and fluorocarbon surfactants^{10,11}).

Cationic fluorinated surfactants (a series of perfluoroalkylpyridinium chloride) have recently been demonstrated as templates for the synthesis of a range of structured nanoporous silica.^{10, 12-15} Varied particle morphology (irregular, spherical, elongated) and

pore structure (disordered, hexagonal, mesh phase) have been obtained as a function of synthesis conditions, chain length and structure of surfactant template. The ability to tailor the pore size and structure of porous materials using fluorinated surfactant templates provides unique application opportunities.

Organic functional groups, metals and bio-molecules have been incorporated into surfactant template nanoporous silica for further applications as adsorbents for separation¹⁶, CO₂ capture¹⁷, catalyst support¹⁸, heavy metal removal¹⁹ and sensing²⁰. The functionalization of the porous silica is achieved by either post-synthesis grafting of already synthesized silica or direct ‘one-pot’ synthesis (i.e. co-condensation of a mixture of tetraalkoxysilane and organic functionalized alkoxy silane).²¹ Direct synthesis results in silica materials with high loading and uniform distribution of functional group.^{22,23} However, the accessibility of the functional group depends on its location and orientation during self-assembly of the template molecules and the precursors.²⁴ Functional groups that are incorporated into the aggregated surfactant micelle (core of the micelle) will be highly accessible after the surfactant template is extracted.

1.1 Research Hypothesis

The hypothesis of this research is that the use of fluorinated surfactants as templating agents will lead to improved opportunities to tailor the pores of organic-functionalized silica materials. Specifically, the higher hydrophobicity of the fluorinated surfactant templates relative to traditional hydrocarbon surfactant templates is expected to drive the organic functional groups (both hydrocarbon and fluorocarbon) of silica precursors towards the core of the surfactant aggregates during the direct synthesis process, altering pore size, order, and potentially the orientation of the organic functional

group of the resulting materials. The resulting porous materials are expected to have functional groups well aligned along the pore channel, providing accessible and highly functionalized porous surfaces.

1.2 Research Objectives

The aim of the research is to demonstrate the synthesis, characterization and possible applications of organic functionalized nanoporous silica templated using fluorinated surfactants (i.e., $C_6F_{13}C_2H_4NC_5H_5Cl$ (HFOPC), $C_8F_{17}C_2H_4NC_5H_5Cl$ (HFDePC), $C_{10}F_{21}C_2H_4NC_5H_5Cl$ (HFDDePC)). The textural properties (such as pore structure and order, pore volume, and specific surface area) and functional group accessibility or applicability of the silica materials are compared to functionalized materials obtained using a traditional cationic hydrocarbon, $C_{16}H_{33}N(CH_3)_3Br$ (CTAB), as a template. The materials characterization techniques employed in this investigation include powder X-ray diffraction (XRD), nitrogen sorption at 77K, transmission electron microscopy (TEM), Fourier transform infra-red spectroscopy (FTIR) and thermogravimetric analysis (TGA).

Chapter 2 presents a brief background on surfactant templated nanoporous silica, fluorinated surfactants, and relevant materials characterization techniques. Chapter 3 demonstrates the direct synthesis of organic functional silica using fluorinated surfactant templates. Vinyl functionalized silica is characterized as a function of surfactant template (fluorocarbon surfactant of different hydrophobic tail length and CTAB) and the accessibility of the vinyl functional group is measured by a bromination reaction. The effect of the lipophobicity and hydrophobicity of fluorocarbons on organic functionalization by direct synthesis is examined in Chapters 4 and 5 using pairs of

fluorocarbon/hydrocarbon templates and silica precursors. Surfactant/functional group (decyl, perfluoro-decyl) combinations and the subsequent effect on degree of functional group incorporation and silica meso-structure properties are presented in Chapter 4. Chapter 5 compares the properties of perfluoro-octyl and perfluoro-decyl functionalized silica and their application as sorbents in separating hydrocarbon and fluorocarbon tagged anthraquinones by fluorous-solid phase extraction (F-SPE). In Chapter 6 the effect of incorporating a hydrophilic reactive functional group (3-aminopropyl) on nanoporous silica properties is described. The characterization of these materials by CO₂ sorption suggests their potential for CO₂ capture.

CHAPTER 2

BACKGROUND

A brief outline of silica, types of porous materials; their synthesis procedure and areas of application is given. A description of surfactants and their aggregation behavior is provided with an introduction to surfactant templating of mesoporous silica. The chapter continues with a summary of synthesis processes that have yielded silica with different mesostructures and pore sizes. Also presented are procedures used in functionalizing the porous silica and the analytical techniques employed in characterizing the porous silica.

2.1 Silica

Silica (SiO_2) occurs naturally as quartz, tridymite, cristobalite, coesite and opal. Quartz is the most abundant silica forming the highest constituent in gravel and beach sand. Silica has several different crystalline structures. As sand, silica is used for making glass and fused silica, its rock crystal is used in electronic equipment and the colored crystals of silica have gem value.²⁵ Silica, however, can be manufactured in the form of sols or gels. These silicas can be formed as colloidal silicas, pyrogenic (or fumed) silica and silica xerogels, and as precipitated silica.²⁶ Silica has been applied as fillers, lubricants, adsorbents and support for solid phase syntheses. Silica can be porous or non-porous.

2.2 Porous Materials

Porous materials can be classified, on the basis of their pore structure, as open or closed. Due to the large surface area to pore volume ratio of porous materials they have

application in many fields. Open pore materials, particularly functionalized materials, are useful in adsorption, catalysis and sensing; closed pore materials are used in sonic and thermal insulation and for applications that require light weight materials. Porous materials are also classified according to their pore sizes. Materials with pores less than 2 nm in diameter are micropores; mesopores are between 2 nm and 50 nm; and pores greater than 50 nm are macropores.²⁷ Examples of pore shape and morphology include cylindrical, spherical and slit shaped. Common solid porous materials can be classified as polymeric, carbon, metals, alumino-silicate and oxides.²⁷

Polymeric porous materials are used as stationary support in chromatography, catalysis, for biologically active materials and as membranes. They are used in tissue engineering as scaffolds²⁸, for drug delivery²⁹ and in sensing. Some of the techniques used to prepare porous polymers include radiation polymerization³⁰, emulsion polymerization³¹, condensation polymerization³² and chain polymerization³³.

Activated carbon, carbon aerogels, carbon nanotubes are examples of carbon based porous materials. Porous carbon materials are synthesized from wood³⁴, resins³⁵, aqueous gels³⁶, and by crystal templating³⁷. These materials are used as catalyst supports³⁸, capacitors³⁹ and for hydrogen storage^{40,41}

The strength of porous metals makes them ideal for use in aggressive environments and at high temperatures and pressures. They have been used in aerospace technology, atomic energy, electrochemistry, machinery and in buildings, with applications as noise reducers, impact energy absorbers, electromagnetic wave shields and heat exchangers.⁴² Examples of metals found in porous powder form are iron, aluminum, brass, bronze,

copper, lead, silver and nickel. They are produced by mechanical, chemical or electrochemical methods.⁴³

Other porous materials are single inorganic oxides such as silica, alumina, titania, ceria and mixed oxides (e.g., titania silica, barium titanate, indium tin-oxide and lithium nickel manganate). Porous oxides are synthesized by the sol gel technique, coprecipitation, and flame hydrolysis. Zeolites can also be considered as a mixed oxide since they are composed of alumina (Al_2O_3) and silica (SiO_2). However, they are crystalline aluminosilicates with a cage structure. There are 40 naturally occurring forms and 150 synthesized types of zeolites.⁴⁴ Zeolites are generally synthesized by sol gel technique in basic medium.⁴⁵ They are mainly microporous with pores sizes less than 2 nm. Some of the uses of porous oxides including zeolites are adsorbents, catalysts, catalyst supports, moisture control agents and in building materials. When a structure directing agent (e.g. surfactant) is incorporated during synthesis of the oxides, materials with ordered pore structure can be obtained at the appropriate synthesis condition. During synthesis the inorganic oxide condenses around the self-assembled structure of the structure directing agent (template). After removal of the template the pores of the inorganic oxide take the shape of the structure directing agent, as described below.

2.3 Surfactant Templated Mesoporous Silica

2.3.1 Surfactants




Surfactants are surface active agents that, at low concentrations, alter (usually reduce) the surface or interfacial energies when adsorbed onto a surface or interface.⁴⁶ They have an amphipathic structure with a lyophilic (hydrophilic) head group and a lyophobic (hydrophobic) tail. Surfactants are classified as anionic (negatively charged

head group), non-ionic (no charge on the head group), zwitterionic (both positive and negative charges on the head group) and cationic (positively charged head group).⁴⁷ In solution the surfactants tend to aggregate at the surface or into micelles, if the concentration of the surfactant is above the critical micelle concentration (CMC), so as to minimize unfavorable interactions with the bulk solvent. The formation of micelles is governed by molecular interactions (e.g. van der Waals forces, hydrogen bonding and electrostatic forces) and hydrophobic interactions.⁴⁸ The major aggregates formed are spherical (normal or inverted) micelles, cylindrical (rodlike) micelles or lamellar (bi-layer) structures, based on the concentration and shape of surfactant. Vesicles, which are spherical structures made up of bi-layer lamellar structures, can also form in solution²². The micellar shape can be interpreted by the space occupied by the hydrophobic and hydrophilic portions of the surfactant based on the packing parameter, $v_H/l_c a_o$ (Table 2.1), where v_H is the volume occupied by hydrophobic tail, l_c is the length of hydrophobic tail in the micellar core, and a_o is the cross-sectional area of the hydrophilic head group.^{46,49} A surfactant packing parameter of 1 (surfactant molecule of cylindrical shape) is associated with a surfactant aggregate (Table 2.1) of zero curvature, in which lamellar phases are preferred. If the surfactant parameter is less than 1 (conical shaped surfactant molecule), spherical or cylindrical micelle shapes are preferred by the surfactant aggregate. For surfactant parameter greater than 1 (surfactant molecule of reversed conical shape), the surfactant aggregates prefer negative curvature spherical structures.⁴⁶ Factors that affect the effective surfactant parameter include solubilization of hydrocarbon chain in the core of the micelles, which increases v_H . a_o also varies with electrolyte content, temperature, pH and the presence of additives. Additives such as

medium chain alcohols, which are solubilized in the head group region of the aggregate, increase the value of a_0 .⁴⁵

An increase in surfactant concentration above the CMC causes the individual micellar structures to pack together into different geometric structures called liquid crystal phases. Liquid crystals possess molecules arranged in solid crystal form but have the fluid movement of a liquid. Spherical micelles pack into cubic crystal phase however, cubic crystal phases are also formed from bi-continuous structures (Figure 2.1).⁴⁶ Cylindrical micelles pack into hexagonal crystal phase and lamellar structures into lamellar crystal phase (Figure 2.1).⁴⁶ A phase diagram representing the various micellar phases and the conditions appropriate for their formation is shown in Figure 2.2. For most fluorinated surfactants, the cubic phase region in the phase diagram is replaced by intermediate mesh lyotropic mesophases (e.g. random mesh and rhombohedral mesh phases).⁵⁰

Table 2.1 Packing parameter, shape of surfactant (adapted from Finnema⁴⁹) and structure of micelles⁴⁶

Value of $v_H/l_c a_0$	Shape of Surfactant Molecule	Structure of Micelle
0 - 1/3		Spherical in aqueous media
1/3 - 1/2		Cylindrical in aqueous media
1/2 - 1		Lamellar in aqueous media
> 1		Inverse (reversed) micelles in nonpolar media

Increase in the chain length of the hydrophobic tail group reduces the solubility of the surfactant in aqueous solution, giving the surfactants a higher tendency for

aggregation and allowing the formation of closer packed aggregates. The melting point of the surfactant also increases with an increase in hydrophobic chain length. Introducing branching in the surfactant hydrophobic tail causes a decrease in the solubility of the branched tail surfactant, resulting in more loosely packed, thermally unstable aggregates.⁴⁵

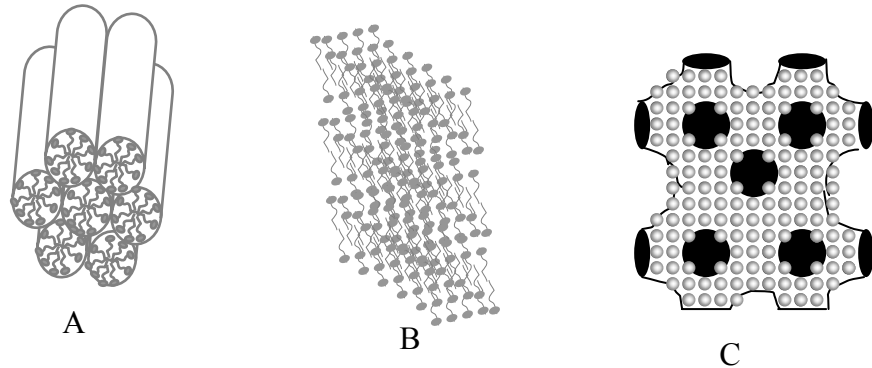


Figure 2.1 Liquid crystal phases A) hexagonal, B) lamellar and C) bicontinuous cubic (adapted from Rosen⁴⁶)

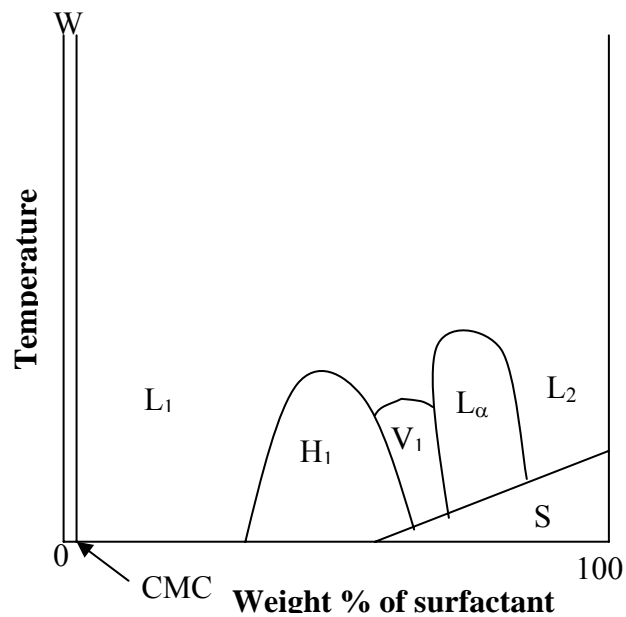


Figure 2.2 Schematic phase diagram of hydrocarbon surfactant – aqueous solution mixtures showing location of hexagonal (H_1), normal bicontinuous cubic (V_1), and lamellar (L_α) liquid phases, aqueous nonmicellar solution (W), micellar solution (L_1), liquid surfactant containing water (L_2), and solid surfactant (S) (adapted from Rosen⁴⁶).

Substitution of fluorine (which is highly electronegative) for the smaller hydrogen atom in the surfactant hydrophobic group greatly affects the properties of the surfactant. There is increase in the volume of the surfactant chain due to the larger area occupied by the $-\text{CF}_2-$ group (the cross-sectional area of a fluorinated surfactant tail is $\sim 31.5 \text{ \AA}^2$ compared to $\sim 21.4 \text{ \AA}^2$ for a hydrocarbon surfactant tail⁵¹), which contributes to the stiffness of the resulting fluorocarbon chain. The fluorocarbon chains possess less conformational freedom and weaker van der Waals interactions than hydrocarbon chains, contributing to the differences in the phase behavior of fluorocarbon and hydrocarbon surfactants.^{52,53} Although fluorinated surfactants aggregate in aqueous solution to form the same major assembled phases (L_1 , H_1 , L_α) as observed in hydrocarbon-water solutions, they are more likely to form unusual intermediate phases between the hexagonal and lamellar phase rather than the cubic phase formed by hydrocarbon surfactants.⁵⁴ This is because fluorinated surfactants form aggregates with lower interfacial curvature when compared to hydrocarbon surfactants due to the stiffer backbone of the fluorinated chain.⁵¹

The increased hydrophobicity of fluorinated surfactants cause them to aggregate at lower surfactant concentrations, as evidenced by their enhanced ability to lower surface tension and their lower critical micelle concentration relative to their hydrocarbon counterparts. In comparison to hydrocarbon surfactants, fluorinated surfactants require low concentrations of salt to cause phase change (elongation) from spherical to

cylindrical micelles.⁵³ When surfactant concentration is increased, fluorinated surfactant micelles are elongated much earlier than hydrocarbon surfactants.³⁰ Fluorinated surfactants are also lyophobic. In addition to their ease of self-assembly, fluorinated surfactants also possess greater thermal stability than their hydrocarbon analogues.^{46,51} They are also highly soluble in low surface tension fluids like supercritical carbon dioxide and fluorinated solvents. These properties of fluorinated surfactants are due to their strong intra-molecular bonds and weak intermolecular interactions.⁵⁶

Model Hydrocarbon Surfactants: Alkyltrimethylammonium Bromide Surfactants

CTAB, a common cationic surfactant, is a member of the series of alkyltrimethylammonium bromide ($\text{CH}_3-(\text{CH}_2)_{n-1}-\text{N}(\text{CH}_3)_3\text{Br}$, C_nTAB) surfactants, where n could be 6, 8, 10, 12, 14, 16 or 18. These surfactants have been studied in aqueous medium and observed to form aggregates (or micelles) with spherical, cylindrical, cubic and lamellae structures.⁵⁷ The critical micelle concentration (CMC) of alkyltrimethylammonium bromide surfactants decreases with increases in the alkyl chain length due to increased hydrophobicity of the surfactants (Table 2).⁵⁸ A change in the headgroup from a trimethylammonium to a pyridinium also affects the CMC. For the same alkyl chain of $n = 16$, the trimethylammonium surfactant has a CMC of 0.98 mmol/kg but the pyridinium surfactant's CMC is 0.78 mmol/kg at the same system temperature (20°C).⁵⁷ This difference in CMCs indicates a decrease due to the bulky pyridinium headgroup. Counterions also affect the CMC of this series of surfactants, as summarized in Table 2.2. A counterion that is able to move closer to the headgroup region and bind strongly can lead to a decrease in headgroup repulsion. A decrease in surfactant CMC occurs due to reduction in headgroup repulsion. For cationic surfactants

I⁻ has the highest binding strength followed by Br⁻ and then Cl⁻.⁵⁹ As such, the surfactants that have a Cl⁻ counter-ion aggregate at a higher concentration than those with Br⁻ counter-ion.

Table 2.2 Critical Micelle Concentration (CMC) of Surfactants

Surfactant	Critical Micelle Concentration (CMC), mM									
	Hydrophobic Chain Length	n=6	n=8	n=10	n=11	n=12	n=13	n=14	n=15	n=16
C _n H _{2n+1} -N-(CH ₃) ₃ Br						15.1 ^a		3.90 ^a		0.98 ^a
C _n H _{2n+1} -N-(CH ₃) ₃ Cl						21.0 ^d		5.60 ^d		1.25 ^a
C _n H _{2n+1} -C ₅ H ₅ NBr				18.6 ^b	11.7 ^a	4.6 ^b	2.7 ^b	1.3 ^b	0.78 ^a	
C _n H _{2n+1} -C ₅ H ₅ NCl						15.5 ^c		4.0 ^c		0.88 ^a
C _n F _{2n+1} C ₂ H ₄ -C ₅ H ₅ NCl	16.2 ^c	2.6 ^c	0.33 ^c							

^a Mata et al⁵⁹ (20 °C); ^b Lah et al⁶⁰ (25 °C); ^c Wang et al⁶² (25 °C); ^d A. Rodríguez et al⁶¹ (25 °C)

Model fluorinated surfactant series: Perfluoro-alkylpyridinium chloride salts

Perfluorinated alkylpyridinium chloride salts (C_nF_{2n+1}C₂H₄-C₅H₅NCl, also cationic surfactants) have a partially fluorinated tail and a pyridinium headgroup. Similar to alkyltrimethylammonium bromide and alkylpyridinium bromide, the perfluoro-alkylpyridinium bromide surfactants have CMC's that decrease with increase in hydrophobic tail length.⁶² The actual CMC values are much lower than those of the hydrocarbon surfactants with same carbon chain length (Table 2.2) and headgroup. The CMC of n = 6 perfluoro-alkylpyridinium chloride surfactant is almost the same as that of n = 12 alkylpyridinium chloride. Pyridinium compounds have lower CMCs because the planar pyridinium headgroups can be packed more easily than trimethylammonium

headgroups.⁴⁶ The perfluoro-alkylpyridinium chloride surfactants have been observed to form L₁, isotropic micellar phase; H₁, hexagonal phase; R, centered rectangular phase and T, centered trigonal phase (rhombohedral) and random mesh phase.⁵¹

Mixed hydrocarbon and fluorocarbon surfactant systems

Hydrocarbon and fluorocarbon surfactant mixtures have been extensively studied.^{52,63-67} Based on relative surfactant tail length, concentration, system temperature and addition of salts the surfactant mixture can phase separate into two different types of micellar phases or form a single micellar phase with de-mixed fluorocarbon-rich and hydrocarbon-rich regions. Complete mixing of the surfactants to form single phase micelles is also possible.^{65,66}

Almgren et al^{65,67} studied the mixing of perfluorodecylpyridinium chloride (HFDePC) and cetyltrimethylammonium chloride (CTAC). Demixed hydrocarbon rich and fluorocarbon rich micelles were observed to co-exist in solution. An increase in temperature favored mixing of the surfactants. Above a critical demixing temperature of 42°C, only mixed micelles formed. Asakawa et al⁶⁶ also investigated the micellar behavior of mixtures of lithium perfluorononanoate (C₈F₁₇COOLi, LiPFN) with lithium dodecyl sulfate (C₁₂H₂₅SO₄Li, LiDS), lithium perfluoro-1-octanesulfonate (C₈F₁₇SO₃Li, Li-FOS) with lithium dodecyl sulfate (C₁₂H₂₅SO₄Li, LiDS) and lithium perfluorononanoate (C₈F₁₇COOLi, LiPFN) with lithium tetradecyl sulfate (C₁₄H₂₉SO₄Li, LiTS). They also observed that for concentrations where two segregated hydrocarbon and fluorocarbon micellar phases were initially present, an increase in system temperature increased surfactant miscibility. This led to the formation of a single type of mixed

micelles. However, addition of salt (LiCl) increased micellar size and resulted in phase segregation within the micelle (Figure 2.3).⁶⁶

The aggregation behavior of the hydrocarbon functionalized precursor and the fluorocarbon surfactant and that of the fluorocarbon functionalized precursor and the hydrocarbon surfactant discussed in chapters 4 and 5 is comparable to mixed hydrocarbon/fluorocarbon surfactants.

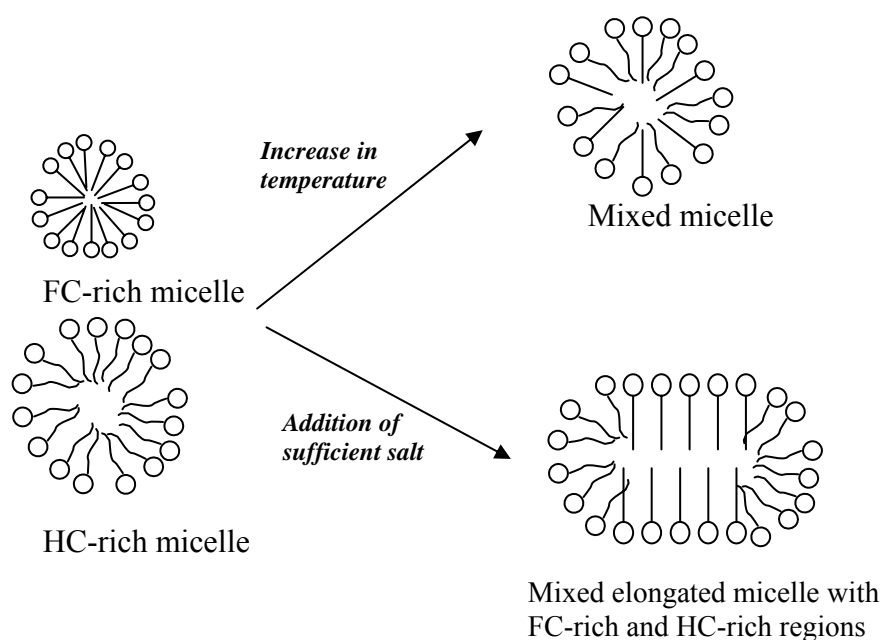


Figure 2.3 Co-existence of two kinds of mixed micelles observed by Asakawa et al⁶⁶; FC-fluorocarbon, HC-hydrocarbon.

Effect of alkane addition to cationic surfactant solutions

Hydrophobic molecules are solubilized into the hydrophobic portion of surfactant aggregates when added to aqueous surfactant solutions. This causes a shift in the balance of intermolecular forces, which affects the micellar shape and aggregation number.⁶⁸ Tornblom and Henrikson⁶⁸ investigated the solubilization of different alkanes (n-hexane,

n-octane, n-decane, n-dodecane and their cyclic versions) in 0.37 mol/kg cetyltrimethylammonium bromide (CTAB) solution. They observed an initial elongation of the cylindrical micelles due to mixing of the alkane with the surfactant hydrophobic tail until a saturation point. Above the saturation point the alkane dissolve in the core of the micelle. At a certain concentration above the saturation point (transition concentration) a transition from initial cylindrical (rod) shaped micelle to spherical structure with increase in micellar radius was observed. Hoffmann and Ulbricht⁶⁹ also examined the solubilization of n-hexane, n-octane, n-decane, n-dodecane and n-tetradecane in cationic surfactants [tetradecyltrimethylammonium bromide (TTAB) and cetyltrimethylammonium bromide (CTAB)] and demonstrated a transition from rodlike micelles to spherical micelles with increase in alkane concentration in the core of the micelles. The saturation and transition concentrations of the alkanes observed by Tornblom and Henrikson⁶⁸, similar to the investigation by Hoffmann and Ulbricht⁶⁹, decreased with increasing alkane chain length. The amount of alkane required (concentration) for transition from elongated (rod-like) to gluobular (spherical) micelles also decreased with increase in temperature.

Effect of alcohol addition to cationic surfactant solutions

Investigations on alcohol (C_nOH) addition to cationic surfactants (C_nTAB) suggest that the chain length of the alcohol dictates its role in surfactant micellation.^{70,71} Karukstis et al⁷⁰ observed that during aggregation the alcohol acts as a co-solvent, co-aggregate or co-surfactant to the surfactant depending on the relative chain length of the alcohol and surfactant. For $C_{16}TAB$, methanol (C_1OH) and ethanol (C_2OH) act as cosolvents due to their high water solubility and shorter chain. They are not able to

penetrate the surfactant micelle but slightly modify the solvent environment around the micelle. This leads to an increase in critical micelle concentration and a decrease in surfactant aggregation number.⁷² However, alcohols from propanol to decanol are able to solubilize in the palisade region of the C₁₆TAB and act as co-aggregates. Their presence in the palisade region reduces the headgroup surface charge, resulting in closer packing of the surfactants. Alcohols of the same chain length or slightly larger than the surfactant hydrophobic tail act as a co-surfactant by replacing a surfactant molecule or inserting between two surfactant molecules in an aggregate. For example, C₈OH and C₁₀OH alcohols act as co-surfactants for C₁₂TAB. When alcohol acts as a co-surfactant, the Coloumbic repulsive forces of the micellar molecules decrease, while the hydrophobic forces between the surfactant aggregate molecules increase. This leads to much closer packing of the surfactants in the micelle.⁷⁰

The incorporation of the functional groups discussed in chapters 3, 4, 5 and 6 can be related to alcohol aggregation with surfactants.

2.3.2 Mesoporous Silica Templating Mechanism

Ordered mesoporous silica was first discovered by researchers in Mobil Oil Co. in the 1990's⁵ by utilizing the surfactant templating mechanism. The surfactant aggregates (micelles) serve as a structure directing agent during the silica synthesis (Figure 2.4).

Initially the silica precursor was thought to condense and polymerize around already formed surfactant liquid crystals (LC). However, since the concentration of surfactant used during synthesis is usually lower than the critical micelle concentration (CMC) for liquid crystal (LC) phase formation, recent investigations have suggested that the templating mechanism is influenced by numerous factors that drive electrostatic

assembly through non-covalent bonding (ionic bonds, van der Waals forces, hydrogen bond and dipole-dipole bonds).⁷³⁻⁷⁵ The factors include the type of precursor used, type of surfactant (cationic, anionic, or non-ionic), relative concentrations of the surfactant to the inorganic species (e.g. Si), the pH of the synthesis medium (acidic or basic) and temperature.^{76,77}

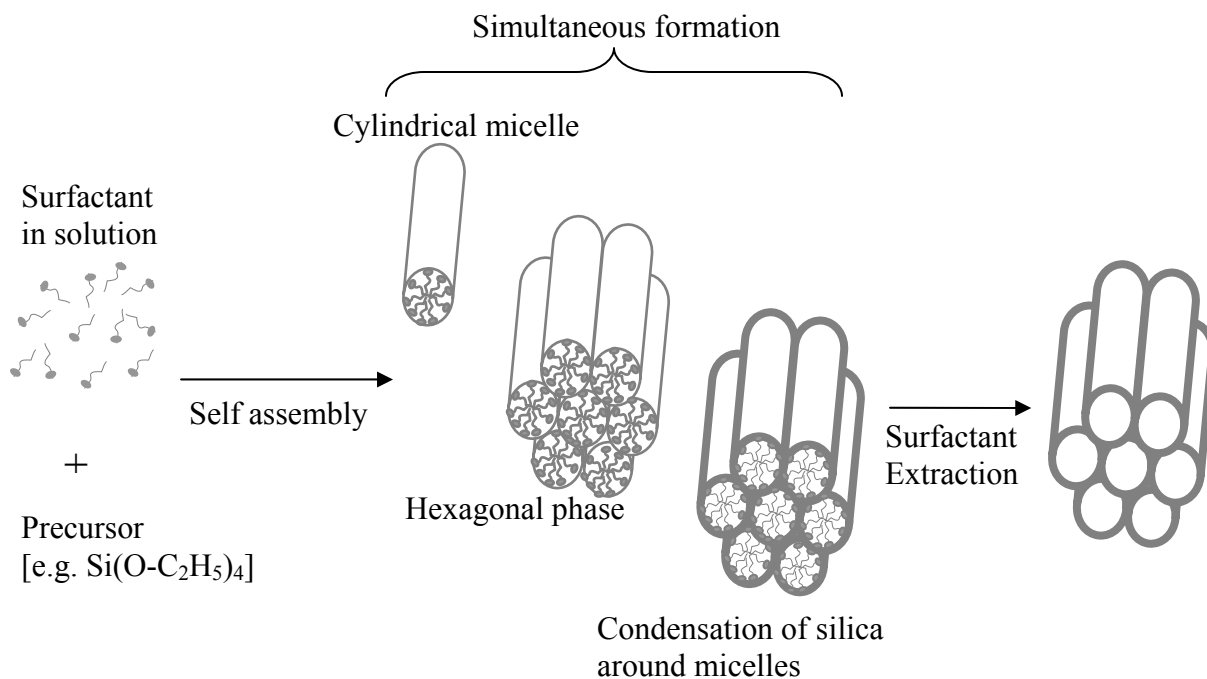


Figure 2.4 Mechanism of mesoporous silica formation, adapted from Beck et al, 1992⁵.

A number of pathways have been proposed for the templating mechanism: (1) Direct co-condensation of anionic inorganic species (I^-) with a cationic surfactant (S^+) to give assembled ion pairs (S^+I^-); (2) Use of an anionic surfactant (S^-) to direct the cationic inorganic species (I^+) to self-assemble through ion pairs (S^-I^+) Pathways 3 and 4 follow the mediation of a counter ion in the assembly of a surfactant and inorganic species of the same charge: (3) The mediation of self assembly of positive surfactant and inorganic

species by a negative counter ion, X^- , where $S^+X^-I^+$ (where $X=Cl^-$ or Br^- , for example); (4) The mediation of self assembly of negative surfactant and inorganic species by a positive counter ion, X^+ ; $S^-X^+I^-$ (where $X=Na^+$ or K^+ , for example); (5) A neutral (S^0I^0) path is believed to occur between a neutral primary amine surfactant (S^0) and the silica species through hydrogen bonding interaction.⁷⁶

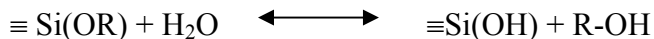
2.3.3 Silica Polymerization Steps

The polymerization of silica from the precursor solution proceeds via two reaction steps catalyzed by an acid or base, necessary due to the low hydrolysis rate of the precursors. A schematic of the reaction sequence is shown below, where R is an alkyl group (e.g. methyl, ethyl...). Silicon alkoxide precursors undergo hydrolysis, in which the alkoxide groups (OR) are replaced by hydroxyl groups (OH) (Step 1). The resulting silanol groups further undergo condensation, where water or alcohol is released from the formation of siloxane bonds (Si-O-Si) (steps 2a and 2b) to form a gel (acid catalyzed) or powder particles (base catalyzed).⁷⁸ Formation of long polymers to produce a gel occurs when synthesis occurs in a low water content medium under acid catalysis (which increases hydrolysis rate). However, under basic conditions with high water content, three dimensional polymer particles form. The particles gel by agglomeration.⁷⁹

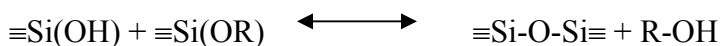
Complete hydrolysis is usually not obtained before condensation starts. Ethanol is sometimes added to the synthesis medium to obtain a homogeneous solution; silicon alkoxides are not soluble in water but soluble in ethanol. On the other hand, the presence of alcohol can favor the reverse reactions, esterification to the original precursor or hydrolyzed precursor.⁷⁸

Schematic of reactions taking place during silica formation

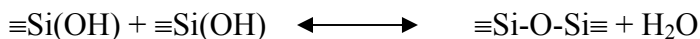
1. Hydrolysis



2a. Alcohol Condensation



2b. Water Condensation



2.3.4 M41S Family of Materials and Others

The surfactant templating mechanism was employed by researchers in Mobil to synthesize porous silica, labeled as the M41S family of materials (hexagonal phase MCM-41; cubic phase MCM-48; and lamellar phase MCM-50). These materials possess very high surface areas ($\sim 700\text{m}^2/\text{g}$) and pore-volumes with tunable pore sizes (between 2.7 - 6.7 nm from single chain alkylammonium hydrocarbon surfactant of length 10 to 22 carbons⁸⁰), and narrow pore size distributions.⁵ The materials were synthesized using cationic surfactants of the alkyl-trimethylammonium bromide series and under basic conditions. The three phases (hexagonal, cubic and lamella) were obtained from different reagent ratios by hydrothermal synthesis at 100 °C.⁸¹

Since the synthesis of the first MCM-41 by the researchers in Mobil, various investigators have used different recipes and synthesis conditions to synthesize 2-D hexagonal mesoporous silica. For example, Kumar et al employed room temperature synthesis conditions.⁸² Other families of mesoporous silica materials, representing a broad range of templates, templating mechanisms, and pore structures, have been

synthesized, from less ordered HMS and KIT to ordered SBA, MSU-V, and FSM-16 (described below).

Pinnavaia and Tanev⁸³ synthesized hexagonal pore ordered mesoporous silica (HMS) utilizing the neutral, S^0I^0 , synthesis route. Primary amines of carbon chain length from C8 to C18 were used as the structure directing agents. The materials were found to be less ordered when compared to MCM-41. Disordered but hydrothermally more stable KIT-1 was synthesized from sodium silicate, HTAC1 (surfactant), and ethylenediaminetetraacetic acid tetrasodium salt ($EDTANa_4$) by Ryoo et al.⁸⁴

Non-ionic surfactants like ethylene oxide and block co-polymer templates, (e.g., Pluronic P123 ($EO_{20}-PO_{70}-EO_{20}$)) have been used as templates for mesoporous silica of both hexagonal and cubic structures.^{85,86} Zhao et al⁸⁵ used ethylene oxide and polyalkylene oxide block-copolymers to synthesize mesoporous silica materials under strong acidic conditions. The templating route is suggested to follow hydrogen and counter ion mediating assembly ($S^0H^+(XI^+)$). These materials, labeled SBA, show a range of structures for both nonionic surfactant and block co-polymer templates. Well ordered structures (i.e., cubic, hexagonal and lamellar structures) were observed and dependent on template and synthesis conditions. The alkyl-ethylene oxide surfactant favored the formation of cubic structures and the tri-block-co-polymer favored hexagonal pore structures.⁸⁵ KIT-6, a cubic pore structured mesoporous silica, was synthesized using mixtures of triblock copolymer Pluronic P123 and butanol (cosolute) as templates.⁸⁶ Synthesis was performed in acidic condition with tetraethoxysilane or sodium silicate as the silica source.

MSU-V, characterized by a porous lamellar structure with vesicle-like particle morphology, was synthesized using neutral diamine bolaamphiphiles, which act as both a structure directing agent and a nanoreactor.^{87,88} The diamine bolaamphiphile was a significant factor in the direction and extent of growth of the silica framework and final morphology of the particles. Depending on the alkyl chain length of the diamine group, particles with either micropores or mesopores were obtained.

In most examples of synthesis of mesoporous, silica alkoxysilanes are employed as the silica precursor. However, hexagonal ordered pore structured silica was synthesized from layered polysilicate kanemite labeled FSM-16.⁸⁹ The pore structure is due to the ion exchange of the interlayered Na⁺ ions for alkyltrimethylammonium ions.

The synthesis of microporous materials (pore diameter < 2 nm) is limited in single chain hydrophobic surfactants, in which carbon chain lengths greater than 10 are generally required to make silica with stable ordered pores. These templates produce silica with pore sizes larger than 2 nm using general synthesis approaches. Some of the techniques used to make microporous materials are the use of short double tail dialkyl-diammonium surfactants and solvent evaporation method,⁹⁰ whereby reduction in solvent concentration cause liquid crystal formation of the surfactant template.

2.3.5 Fluorinated Surfactant Templating

Since the discovery of the M41S materials, the structure directing agents used for mesoporous silica synthesis have been almost exclusively hydrocarbons with hydrophilic head groups. Well-ordered materials with pore sizes in the mesoporous range have been obtained using these templates. The potential exists that fluorinated surfactants of shorter, single hydrophobic tails (8 carbons or less) can be used to produce materials with pore

sizes that can bridge the pore size range between zeolites (pore sizes less than 1.3 nm) and those of MCM-41 type materials (greater than 2.7 nm obtained from single chain hydrocarbon based templates).⁹¹

Table 2.3 Comparison of texture properties of nanoporous silica particles obtained by perfluoro-alkylpyridinium chloride surfactants templating^{10,12-15}

Surfactant	Synthesis medium*	Particle Morphology	Pore Structure	Pore Size, nm	Total Surface Area, m ² /g
C ₂ F ₅ C ₂ H ₄ -NC ₅ H ₅ ·Cl	Aqueous	irregular	wormlike	1.60	819
C ₄ F ₉ C ₂ H ₄ -NC ₅ H ₅ ·Cl	Aqueous	irregular	wormlike	2.19	884
C ₄ F ₉ C ₂ H ₄ -NC ₅ H ₅ ·Cl	Homogeneous	spherical	wormlike	2.19	577
C ₆ F ₁₃ C ₂ H ₄ -NC ₅ H ₅ ·Cl	Aqueous	irregular	2D-HCP	2.62	981
C ₆ F ₁₃ C ₂ H ₄ -NC ₅ H ₅ ·Cl	Homogeneous	spherical	wormlike	2.42	875
(CF ₃) ₂ C ₅ F ₉ CH ₂ CH ₂ -NC ₅ H ₅ ·Cl	Aqueous	spherical	wormlike	2.76	943
(CF ₃) ₂ C ₅ F ₉ CH ₂ CH ₂ -NC ₅ H ₅ ·Cl	Homogeneous	spherical	wormlike	2.56	897
C ₈ F ₁₇ C ₂ H ₄ -NC ₅ H ₅ ·Cl	Aqueous	elongated	mesh phase	1.95	851
C ₈ F ₁₇ C ₂ H ₄ -NC ₅ H ₅ ·Cl	Homogeneous	spherical	radial 2D-HCP	2.72	977
(CF ₃) ₂ C ₇ F ₁₃ CH ₂ CH ₂ -NC ₅ H ₅ ·Cl	Aqueous	Round/flat sheet	disordered	3.34	590
(CF ₃) ₂ C ₇ F ₁₃ CH ₂ CH ₂ -NC ₅ H ₅ ·Cl	Homogeneous	Spherical/irregular	disordered		321
C ₁₀ F ₂₁ C ₂ H ₄ -NC ₅ H ₅ ·Cl	Aqueous	Crumpled sheet	disordered	2.89	512
C ₁₀ F ₂₁ C ₂ H ₄ -NC ₅ H ₅ ·Cl	Homogeneous	spherical/irregular	disordered lamellar	3.32	216

*Homogenous synthesis media refers to ethanol/water synthesis media

Cationic fluorinated surfactant templates (perfluoroalkylpyridinium chloride, C_nF_{2n+1}C₂H₄-NC₅H₅·Cl) for synthesis of porous silica materials have been investigated in collaboration between the laboratories of Drs. Rankin, Lehmler, and Knutson.^{10,12-15} A

series of the straight chain surfactant with $n = 2, 4, 6, 8$ and 10 and some branched surfactants $(CF_3)_2C_nF_{2n-1}CH_2CH_2-NC_5H_5\cdot Cl$ (where $n = 5$ and 7) were demonstrated for the synthesis of nanoporous silica with a range of morphologies. Table 2.3 gives details of the surfactant used, synthesis medium, particle morphology, pore structure and size and total surface area of materials obtained.

The much shorter perfluorinated surfactant, pentafluoro-1,1,2,2-tetrahydro-butyl $(C_2F_5C_2H_4-NC_5H_5\cdot Cl)$, was used under basic conditions employing three different surfactant to Si ratios.¹⁵ An increase in surfactant/Si ratio promoted gelation during the synthesis. Low surfactant/Si ratios (0.16 and 0.62) resulted in unusually large pore sizes (11.1 nm and 17.8 nm, respectively), with no observable order. At a higher surfactant/Si ratio of 1.39 , wormlike pore structure with a silica pore size of 1.6 nm was obtained. Generally, an increase in hydrophobic tail length leads to increase in silica pore size. The smaller pore size of 1.6 nm for $C_2F_5C_2H_4-NC_5H_5\cdot Cl$ template silica follows the trend observed for the straight chain perfluoroalkylpyridinium chloride surfactants (Table 2.3). Homogenous ethanol/water solutions were sometimes employed as synthesis media for nanoporous silica templated by cationic fluorinated surfactants. Materials made in homogeneous solutions with the perfluoroalkylpyridinium chloride surfactants had spherical morphology¹³, as observed previously for traditional hydrocarbon surfactant templated materials synthesized from homogenous solutions.⁹²⁻⁹⁶

Stebe and colleagues¹¹ have investigated the phase properties and use of a nonionic fluorinated surfactant, $F(CF_2)_8C_2H_4(OC_2H_4)_9OH$, in the preparation of ordered porous silica. 2-D hexagonal pore structured silica was synthesized using the nonionic fluorinated surfactant at 80 °C. At temperatures lower than 80 °C only wormlike pore

structures were observed. An increase in synthesis temperature from 40 °C to 80 °C resulted in increased pore sizes of the mesoporous silica. For example, a pore size increase from 1.7 nm (40 °C) to 4.6 nm (80 °C) was observed at a 10 wt% surfactant concentration. Surfactant concentration also affected the pore size, which increases with increasing surfactant concentration. Fluorinated surfactant templated materials displayed better pore organization and possessed larger pores than materials made with corresponding hydrocarbon surfactant (C₁₆(EO)₁₀). In a separate investigation by Meng et al⁹⁷, the partially fluorinated surfactant FSO-100 (CF₃(CF₂)₄(EO)₁₀, Dupont) served as a template for silica with hexagonal pore structure. Two sets of materials were synthesized, one in acidic medium and the other in neutral medium. Increasing the synthesis temperature in both synthesis resulted in improved pore ordering and larger pores; materials synthesized in acidic medium showed an increase in pore size from 1.6 nm (room temperature) to 3.0 nm (100 °C). The materials templated with fluorinated surfactants had higher hydrothermal and mechanical stability than MCM-41.

In addition to surfactant templating approaches using a single surfactant, hydrocarbon-fluorocarbon surfactant mixtures have been investigated as templating agents. Xiao et al^{98,99} used a mixture of fluorocarbon surfactant (C₃F₇O(CFCF₃CF₂O)₂CFCF₃CONH(CH₂)₃N⁺(C₂H₅)₂CH₃I, FC-4) and triblock copolymer surfactant (EO₂₀PO₇₀EO₂₀, Pluronic P123) to synthesize 2-D hexagonal pore structured mesoporous silica in acidic medium at high temperatures (160 °C – 220 °C). The resulting materials had very high hydrothermal stability; the hexagonal pore order was maintained with little loss in surface area and pore volume after treatment in boiling water for 80 hours. The fluorocarbon and hydrocarbon surfactant mixture is believed to

form mixed micelles instead of separate micellar phases. Cubic pore structured materials have also been synthesized by Xiao et al⁹⁹ and Han and Ying¹⁰⁰ when a mixture of the fluorocarbon surfactant FC-4 and triblock co-polymer F127 (EO₁₀₆PO₇₀EO₁₀₆) was used as templates in acidic medium. The synthesis conditions used by Han and Ying¹⁰⁰ resulted in very fine particles (particle size between 50 nm to 300 nm). It was suggested that the particle size growth is controlled by the presence of the fluorocarbon surfactant, which aggregates around the formed silica particle templated by the hydrocarbon copolymer. The proposed assembly mechanism was by the S⁺XI⁺ interaction.

2.3.6 Ordered Organic-Inorganic Mesoporous Silica

Tailoring the surface of the mesoporous silica materials has a broad range of applications. Functional groups (i.e., metals (e.g. Au, Ce, Fe),^{18,101-103} organic compounds (e.g. vinyl, 3-aminopropyl, phenyl, thiol)¹⁰⁴⁻¹⁰⁸ and biomolecules (e.g. cyclodextrin, peptides, drugs)¹⁰⁹⁻¹¹² have been incorporated into ordered porous silica for applications ranging from heavy metals (Pd, Hg, Cr(IV), Cu) removal¹¹³⁻¹¹⁶ to drug delivery¹¹⁷⁻¹²¹. For example, gold incorporated mesoporous silica was used as a catalyst for CO oxidation.¹⁸ Hampsey et al¹²² also employed palladium functionalized mesoporous silica for the hydrodechlorination of 1,2-dichloroethane with complete conversion. Silica materials incorporated with an organic functionality (e.g., amines) have been utilized for a range of applications, including the removal of metals, such as Cu¹²³ from aqueous solution, and as solid adsorbents for CO₂ capture.¹²⁴ Amine functionalized materials have also been applied as catalysts for reactions, such as the Knoevenagel reaction.¹²⁵ Organic functionalized mesoporous silica (e.g. C₁₈ modified mesoporous silica) has been applied

as chromatographic packing in the separation of aromatic hydrocarbons and proteins.¹²⁶ The well ordered pore structure of mesoporous silica materials also provide an effective matrix for incorporating drug molecules since the rate of release of the drug can be better estimated. Drugs such as atenolol¹¹⁰ and ibuprofen¹¹¹ have been incorporated into mesoporous silica. Other bio-molecules, such as enzymes (thermolysin and lysozyme)¹²⁷ and proteins (RNase A¹²⁸), have been immobilized on the surface of the nanoporous silica and their activity after incorporation analyzed.

Several methods can be used to create organic-inorganic hybrid materials through the incorporation of organic functional group in porous silica material. These methods include post synthesis grafting techniques,^{129,130} which may consist of (i) adsorbing of the organic species into the pores of the porous silica, and (ii) covalent bond attachment of the functional group to the silica support. Alternative incorporation methods are the ship-in-bottle technique (piece-by-piece construction of the organic material within the pores of the silica)²¹, the ‘one-pot’ synthesis technique, which involves the direct co-condensation of the precursor and functionalized precursor.^{21,132-134}

The reaction pathway for the direct synthesis of organic functionalized silica is identical to the reaction pathway for silica synthesis. An alkoxy group in the silica precursor is replaced with the desired functional group (i.e., organic groups such as vinyl (vinyltriethoxysilane), aminopropyl (3-aminopropyltriethoxysilane) and mercaptopropyl (3-mercaptopropyltriethoxysilane)), where the functional group is linked to the silicon of a silane molecule. The functional group can also be attached by being bridged between two silane molecules (e.g., ethylene bridged (1,2-bis (triethoxy silyl) ethane)¹³⁵ and phenylene bridged (1,4-bis(triethoxysilyl)benzene).¹³⁶ In contrast to post-synthesis grafting, the

direct synthesis method results in high functional group loading. However, less ordered pore structure in the materials is obtained as the functional group loading increases.^{22,23} A decrease in pore size from mesopores to micropores has also been observed²³ as the loading of functional group increases. The decrease in pore size is due to the aggregation behavior of the functional group with the surfactants. As discussed in section 2.3.1 incorporation of alcohols of all chain lengths lead to a decrease in micellar size (pore size). The decrease in pore size is also attributed to the presence of the functional group within pore wall after surfactant extraction.

In silica synthesis by direct co-condensation, the availability of the functional groups is dependent on the interaction between surfactant template and the functional group. A functional group that is favorably incorporated in the surfactant micelle during assembly and synthesis would be easily accessible in the resulting pores.²⁴ Unfavorable interactions would cause the functional group to become part of the silica matrix and inaccessible, or may cause the ordered framework to collapse upon removal of template.²⁴

2.4 Material Characterization Techniques

The following characterization techniques provide information on the effects of the synthesis process on the mesostructure and surface and bulk properties of the silica.

2.4.1 Fourier Transform Infra-red Spectroscopy (FTIR)

The photon energy of infrared rays (wavelength range of 2500 to 16000 nm) are just strong enough to cause vibrational excitation of molecules with covalent bonds. The vibrational motions exhibited by molecules are characteristic of their atomic makeup and bonding structure. When an infrared radiation is passed through a sample it absorbs some

of the radiation, which leads to vibration of the atoms in the sample. The frequencies of vibration of the various atoms of the sample are observed as peaks in absorption spectra. The energy difference between the vibrational energy states of an atom is equal to the absorbed energy (ΔE). This is given by¹³⁷:

$$\Delta E = E_{vib1} - E_{vib2} = h\nu = \frac{hc}{\lambda} \quad (2.1)$$

where h is Planck's constant, λ is the wavelength and c speed of light.

The possible vibrational modes of atoms are stretching (symmetric and asymmetric) and bending (scissoring, rocking, wagging, and twisting). Rotational energies of the atoms are accounted for in the IR spectrum. The rotational energy can be added to (rotation speeds up) or subtracted from (rotation slows down) the vibrational energy. Fourier Transform Infra-red Spectroscopy (FTIR), relative to infra-red spectroscopy, shows improved quality of the infrared spectra and reduction in the time required to obtain a spectrum.¹³⁸ FTIR instruments use an interferometer to obtain an interferogram (i.e. interference pattern obtained from reflected beams), which is then passed through the sample; information at every wavelength is read by the detector during rapid scanning of the interferometer. Early IR instruments are dispersive instruments, where a grating or prism is used to separate the wavelengths of light in the spectral range after it has passed through the sample. Each wavelength is directed individually through a slit to the detector (slow process).¹³⁹ FTIR is used to obtain absorption spectra of a compound which show unique reflections of the molecular structure of that compound. This information can be used to identify unknown samples, to analyze sample for composition and also to quantify sample components.

2.4.2 Thermogravimetric Analysis (TGA)

During thermal analysis, material samples gain or lose weight due to thermal events, such as decomposition, oxidation or reactions taking place at particular temperatures. Thermogravimetric analysis (TGA) is the thermal analysis of a sample whereby the mass of the sample is measured as a function of temperature and time under controlled temperature in a chosen environment (e.g. air, nitrogen).^{140,141} TGA is used to obtain characteristic qualitative (composition) as well as quantitative (amount) information of a sample from a thermogram (Figure 2.5). Thermograms show stable regions and locations of weight changes which are usually specific to various components of the sample undergoing thermal events. The size of the weight change can be used to obtain quantitative analysis of the thermal event such as organic content of a sample.¹⁴²

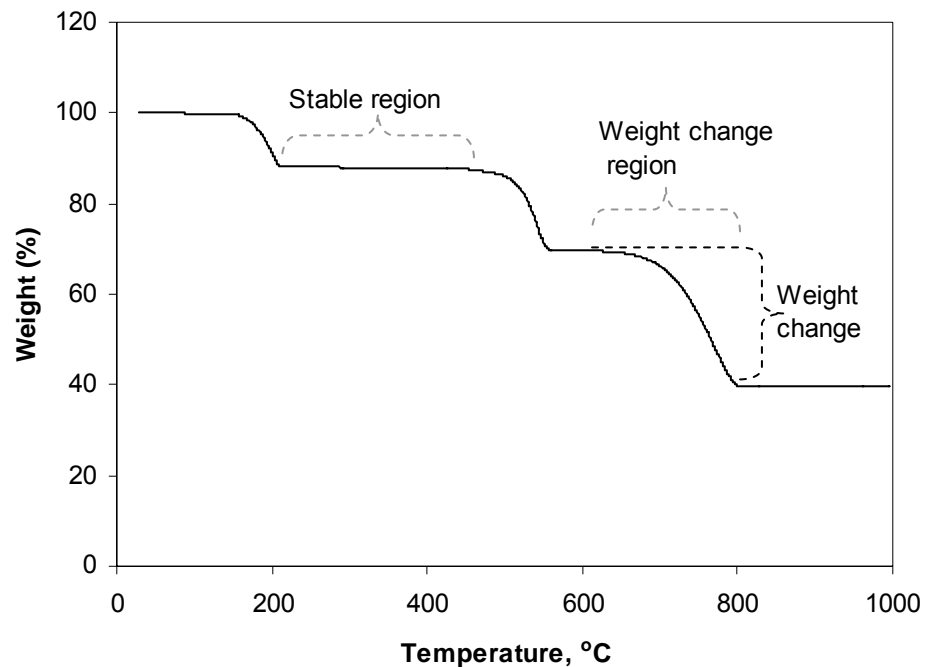


Figure 2.5 Thermogram

2.4.3 X-Ray Diffraction (XRD)

X-ray diffraction occurs when x-rays and electrons of atoms interact. When the x-rays hit the electrons some are scattered (diffracted). Depending on the arrangement of atoms in a sample, interference of two diffracted rays can be constructive (i.e., their path difference equals an integral number of the incident wavelength).^{143,144} For example, Figure 2.6 shows a schematic of atomic planes of a crystal sample. In this schematic example, scattering ray 3 travels a distance AB longer than ray 1 before scattering. After scattering ray 3' travels a distance BC longer than 1'. The total path difference (δ) between rays 1 and 3 is $AB + BC$. If $\delta = n\lambda$, where λ is the wavelength, then at the exit wave front rays 1 and 3 are in phase, which is described by Bragg's Law :¹⁴⁴

$$2d_{hkl}\sin\theta = n\lambda \quad (2.2)$$

where d_{hkl} is the inter-planer spacing and θ the Bragg angle, which is half the angle between incident and diffracted beam.

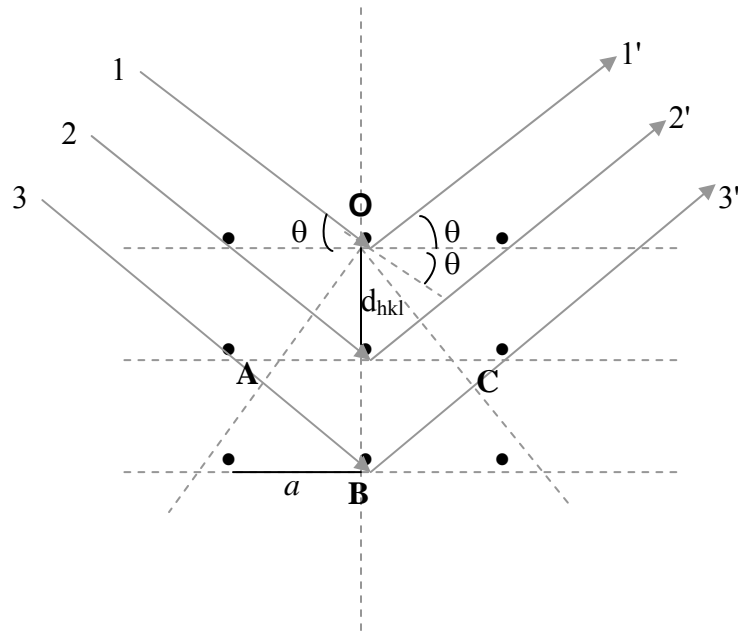


Figure 2.6 Incident rays on three parallel equidistant planes.¹⁴⁴

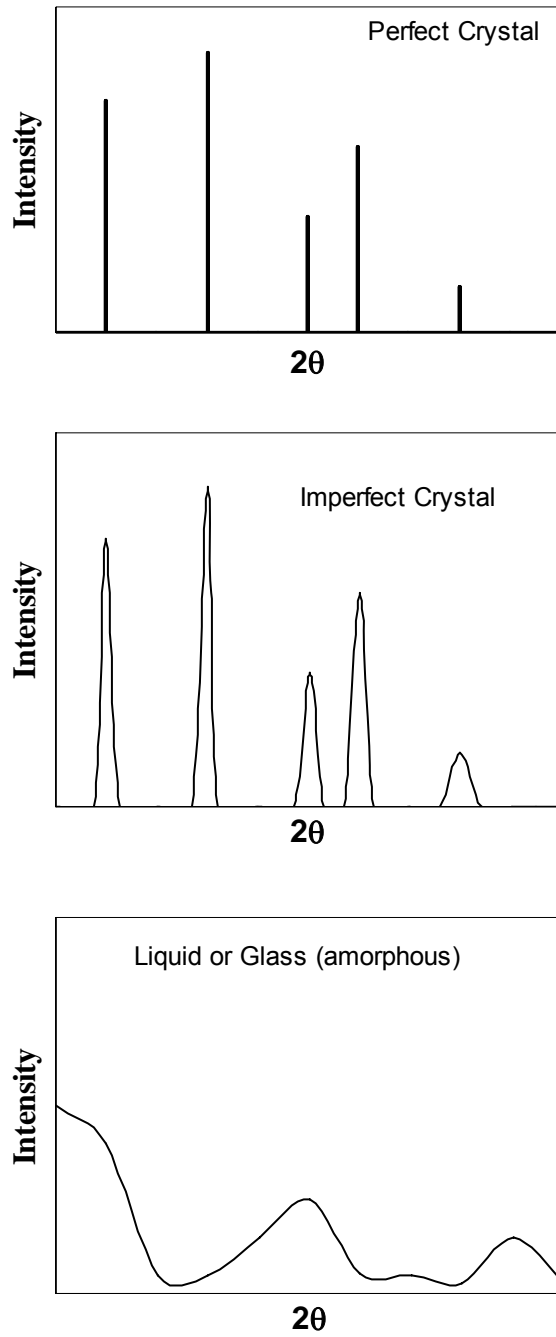


Figure 2.7 X-Ray Diffraction Patterns (Adapted from Heiney¹⁴⁶)

The degree of crystallinity of a single crystal or powder samples can be deduced from X-ray diffraction (XRD) patterns (Figure 2.7). The unit cell, structure, texture and size of the crystalline phase and chemical analysis of solid sample can also be obtained from XRD patterns. The widths (area) of the peaks in the XRD patterns determine the degree of crystallinity (Figure 2.7). The peaks broaden as the sample becomes more amorphous.

Mesoporous silica materials usually give patterns identical to imperfect crystals (Figure 2.7) since the silica itself is amorphous but the pore structure is ordered. Each peak in the pattern represents a different plane in the crystal. The patterns can be indexed based on combination of Bragg's law and plane-spacing equations to identify the type of pore structure. For example, for cubic structures the resultant equation of the combination of Bragg's law and the plane-spacing equation is:

$$\frac{\sin^2 \theta}{(h^2 + k^2 + l^2)} = \frac{\sin^2 \theta}{s} = \frac{\lambda^2}{4a^2} \quad (2.3)$$

For a particular pattern, $\frac{\lambda^2}{4a^2}$ is a constant and $s = h^2 + k^2 + l^2$ is always a set of integers.

The set of integers for a simple cubic structure follows the sequence 1,2,3,4,5,6,8,9,10,11,12,13,15,16,..... and the sequence 3, 8, 11, 16, for diamond cubic structures. The combination of Bragg's law and the plane-spacing equation for hexagonal structures is given by:

$$\sin^2 \theta = \frac{\lambda^2}{3a^2} (h^2 + hk + k^2) + \frac{\lambda^2}{4c^2} l^2 \quad (2.4)$$

$\frac{\lambda^2}{3a^2}, \frac{\lambda^2}{4c^2}$ are constants for any pattern. The integer set for h^2+hk+k^2 is 1, 3, 4, 7, 9....¹³³

The different sets of integers are consistent with the different atomic planes present in each structure. Based on the integer sets, each diffraction pattern can be indexed as to the type of crystal phase or phases present.

2.4.4 Transmission Electron Microscopy (TEM)

Transmission electron microscope (TEM) is used to greatly magnify specimens using a beam of electrons. The resolution of 100-keV electron is on the order of an atomic size (~ 0.3 nm) as compared to that of a light microscope (~ 300 nm).¹⁴⁷ The light microscope can only magnify images about 1000 times but images on an electron microscope can be highly magnified to see atomic details in the sample. This is because the resolving power (minimum distance between two distinct objects) is directly proportional to the wavelength of illumination.¹⁴⁸ The wavelength of electrons at 60 kV is about 5×10^{-3} nm compared to that of visible light (400 – 800 nm).¹⁴⁸ Images in TEM are magnified by electromagnetic lenses which control the electrons that pass through the sample to generate extremely fine structural detail of the sample.¹⁴⁷ Based on the thickness of the sample, some of the electrons are scattered. However, at the bottom of the microscope column electrons that pass through the electron transparent sections of the sample are focused on a viewing screen. A range of signals are detected in transmission electron microscopes to obtain images, diffraction patterns, chemical information and other kinds of spectra.¹⁴⁷

TEM analysis of nanoporous silica is used to generate fine structural image and diffraction pattern of the pores. The structural image can be used to confirm patterns observed in X-ray diffraction and the pore size obtained from nitrogen adsorption analysis.

2.4.5 Nitrogen Adsorption Analysis

The physical adsorption (physisorption) of gases on porous solid surfaces is useful in the characterization of porous solid materials, among other applications.¹⁴⁹ A gas (e.g. nitrogen) adsorption isotherm, a plot of relative pressure against volume of gas adsorbed, is used to estimate the type of pores in the solid material, the size of the pores, the total surface area of the solid material and the pore volume. Adsorption isotherms have been classified by IUPAC into six different types, as shown in Figure 2.8. Type I is observed for adsorption in microporous solids, type II isotherm is obtained from adsorption in non-porous or macroporous materials with unrestricted monolayer-multilayer adsorption. Adsorption on non-porous or macroporous materials with weak adsorbent-adsorbate interaction is given by type III isotherm. Adsorption in mesoporous materials gives type IV isotherms. A type V isotherm results from adsorption on porous materials with weak adsorbent-adsorbate interaction. Finally, type VI isotherm is due to stepwise multilayer adsorption on uniform non-porous surface.¹⁵⁰

The Brunauer-Emmett-Teller (BET) isotherm¹⁵¹ (Equation 2.5) is the standard method for obtaining the total surface area, S_{total} , of the sample (Equation 2.6) from the adsorption isotherm. A plot of $1/v[(P_o/P)-1]$ against P/P_o is a straight line with y-axis intercept equal to $1/v_m$, based on Equation 2.5. v_m is used to estimate the total surface area (S_{total}) from Equation 2.6.

$$\frac{1}{v[(P_o/P)-1]} = \frac{1}{v_m c} \left(\frac{P}{P_o} \right) + \frac{1}{v_m} \quad (2.5)$$

where v is the volume of gas adsorbed, P/P_0 is the relative pressure, v_m is the amount of gas adsorbed for monolayer formation and c is the BET constant. The BET constant is expressed by Equation 2.7.

$$S_{total} = \frac{(v_m N s)}{\rho M}; \quad (2.6)$$

where N is Avogadro's number, s is the adsorption cross sectional area, and M is the molecular weight of adsorbate, and ρ is the density of adsorbed gas. The surface area per weight of sample (specific surface area) can be determined by normalizing the total surface area by a , the weight of solid sample.

$$c = \exp\left(\frac{E_1 - E_L}{RT}\right) \quad (2.7)$$

where E_1 is the heat of adsorption of the first layer of gas and E_L is the heat of adsorption of the subsequent layers, termed the heat of liquefaction. R is the universal gas constant and T is the adsorption temperature.

The pore volume of the porous material is obtained from the data at relative pressure (P/P_0) close to 1. For mesoporous materials, the pore size is estimated based on Kelvin equation (Equation 2.8).

$$\ln\left(\frac{P}{P_0}\right) = -\frac{2\gamma V_m}{rRT} \quad (2.8)$$

where P/P_0 is the relative pressure, γ is the surface tension, V_m is the molar volume, R is the universal gas constant, T is the adsorption temperature, and r is the the pore radius.

More recently, the Barrett-Joyner-Halenda (BJH) pore size model,¹⁵² which is based on the Kelvin equation with a correction for multilayer adsorption, is used in obtaining the pore size of mesoporous and some macroporous materials.¹⁵³ Additional methods used in

analyzing adsorption data for pore size and surface area properties are the Kruk-Jaroniec-Sayari (KJS)¹⁵⁴ method, Horvath–Kawazoe (HK) method,¹⁵⁵ molecular simulations¹⁵⁶ and adsorption potential method.¹⁴⁶ Details of the KJS and adsorption potential methods are outlined in Appendix A.

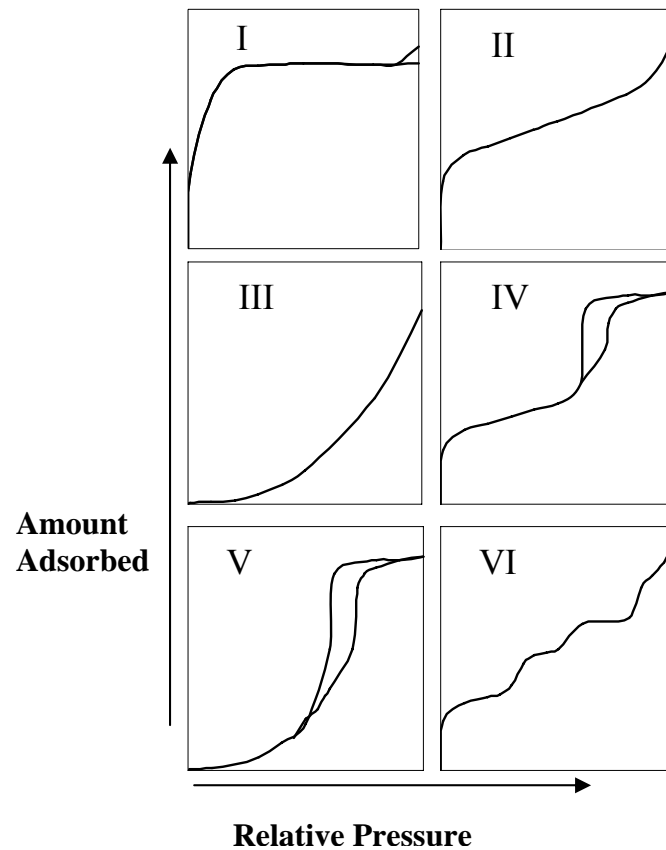


Figure 2.8 Types of physisorption isotherms (adapted from Sing et al¹⁵⁰)

CHAPTER 3

FLUORINATED SURFACTANT TEMPLATING OF VINYL-FUNCTIONALIZED NANOPOROUS SILICA

This chapter is based on work published as:

Osei-Prempeh, G.; Lehmler, J.H.; Knutson, B.L.; Rankin, S.E.; *Micropor. Mesopor. Mater.* **2005**, 85, 16. Copyright 2005 Elsevier.

3.1 SUMMARY

Ordered nanoporous vinyl-functionalized silica materials are synthesized by the ‘one-pot’ (direct) synthesis method using three cationic fluorinated surfactants ($C_6F_{13}C_2H_4NC_5H_5Cl$, $C_8F_{17}C_2H_4NC_5H_5Cl$ and $C_{10}F_{21}C_2H_4NC_5H_5Cl$) as templates in basic medium under ambient conditions. The materials obtained possess lower degrees of 2D hexagonal closed packed ordering of the pores when compared to CTAB templated materials. Increases in vinyl content lead to reductions in pore size as well as material order. In spite of having smaller pores, bromination experiments suggest that the vinyl groups are more accessible in the fluoro-surfactant templated materials. Although confinement of the vinyl groups to the palisade region of the fluorinated micelle templates may contribute to this increase in accessibility, reduced pore order in the fluorinated templated materials may also improve the accessibility, as observed here for intentionally disordered CTAB-templated materials. Cationic fluorocarbon surfactants not only have the potential to be templating agents, but also present the possibility of re-

organizing the alignment of organic functional groups in the pores of organic-inorganic hybrids obtained by direct synthesis.

3.2 INTRODUCTION

The discovery of ordered mesoporous silica prepared by surfactant templating in the 1990's⁵ has led to the investigation of different templating agents (cationic, anionic and non-ionic surfactants, and block-copolymers)^{158,159} and functional group incorporation. Tailoring the surface of mesoporous silica materials has a wide range of applications including catalysis, separation and sensing. Functional groups such as metals^{18,160-162}, organic compounds¹⁶³⁻¹⁶⁶, and biomolecules^{110,167} have been incorporated into these ordered porous silicas for applications ranging from heavy metal removal^{113,115,163} to drug delivery¹¹⁷.

The incorporation of organic functional groups into porous silica to form organic-inorganic hybrid materials can be achieved by several methods. Post-synthesis grafting techniques involve adsorption of the organic precursor species into the pores of the porous silica followed by covalent bond attachment of the functional group to the silica support. Alternative incorporation methods are the ship-in-bottle technique (piece-by-piece construction of the organic material within the pores of the silica)²¹ and the 'one-pot' synthesis technique, which involves the direct co-condensation of the silica precursor and a functionalized precursor.^{21,22,168,169} In contrast to post-synthesis grafting, the direct synthesis method results in a high functional group loading.²² However, a less ordered pore structure is usually observed in the materials as the functional group loading increases.^{22,23} Vinyl group incorporation into MCM-41 (2D hexagonal ordered

mesoporous silica) templated with cetyltrimethylammonium bromide (CTAB) has been investigated as a model system for direct synthesis.^{22,23}

Conventional surfactants for the synthesis of mesoporous silica are hydrocarbon based.^{79,170} The effect of the template structure has been explored, and well-ordered materials with pore sizes in the mesoporous range (2.7 nm and greater) have been obtained using these templates.⁷⁹ Only recently, researchers have begun to also investigate the use of fluorinated surfactants for the templating of structured nanoporous silica. Blin and colleagues¹¹ have investigated the use of the nonionic fluorinated surfactant $F(CF_2)_8C_2H_4(OC_2H_4)_9OH$ in the preparation of silica with an ordered 2D hexagonal pore structure. Our group has demonstrated the base-catalyzed precipitation of silica particles, using cationic fluorinated surfactants, 1H,1H,2H,2H-perfluoroalkylpyridinium chlorides, as templates.^{10,12,13} 2D hexagonal cylindrical structures with narrow pore size distributions (2.6 nm pores) were obtained using 1H,1H,2H,2H-perfluorooctylpyridinium chloride ($C_6F_{13}C_2H_4NC_5H_5Cl$) as the templating agent.¹⁰ A similar surfactant with two more fluorocarbon units in the tail ($C_8F_{17}C_2H_4NC_5H_5Cl$) was found to form elongated nanoparticles with mesh-phase slit pores oriented normal to the long axis of the particles.¹² An increase in surfactant tail length produces an increase in pore size analogous to that observed for hydrocarbon templates. In addition, pore structure changes are also observed from wormhole-like to hexagonal close packed cylinders to a mesh phase.

These studies have confirmed some of the advantages of fluorinated surfactants over their hydrocarbon analogs for the tailoring of mesoporous silica. The replacement of the hydrogen atoms in the surfactant tail by larger, more electronegative fluorine atoms

increases the volume of the surfactant chain due to the larger area occupied by the $-\text{CF}_2-$ group. The increased hydrophobicity of the fluorinated surfactants results in lower surface tensions and critical micelle concentrations⁵³, indicative of their ease of self-assembly. These properties allow micelle templating of unusually small pores in materials.¹³ The fluorinated surfactants generally form a broader range of nanoscale structures than their hydrocarbon analogues.^{55,172} These mesophases are more stable, better organized and rigid.¹⁷³

This work extends the use of fluorinated surfactant as pore templates to organically modified ceramic materials formed by ‘one-pot’ synthesis. The successful synthesis of vinyl-functionalized ordered porous silica using fluorinated surfactants ($\text{C}_6\text{F}_{13}\text{C}_2\text{H}_4\text{NC}_5\text{H}_5\text{Cl}$ (HFOPC), $\text{C}_8\text{F}_{17}\text{C}_2\text{H}_4\text{NC}_5\text{H}_5\text{Cl}$ (HFDePC) and $\text{C}_{10}\text{F}_{21}\text{C}_2\text{H}_4\text{NC}_5\text{H}_5\text{Cl}$ (HFDoDePC)) as templates is reported. The structure and textural properties of the materials are analyzed and compared to those of CTAB templated materials. The ability of the lipophobic fluorocarbon templates to alter the accessibility of the vinyl functional group is examined by means of a simple bromination reaction.

3.3 MATERIALS AND METHODS

3.3.1 Surfactant synthesis

Vinyl-functionalized porous silica materials were synthesized using the three partially fluorinated surfactant templates and, for comparison, CTAB, a hydrocarbon analogue. CTAB was obtained from Sigma with 99% purity. The fluorinated surfactants differ in the alkyl chain associated with the fluorine and have the general formula $\text{C}_n\text{F}_{2n+1}\text{C}_2\text{H}_4\text{NC}_5\text{H}_5\text{Cl}$ (1H,1H,2H,2H-perfluoroalkylpyridinium chloride). The

surfactants are labeled HFOPC, HFDePC and HFDoDePC for $n = 6, 8$ and 10 , respectively. The synthesis procedure of the surfactants is given elsewhere.^{13,173}

3.3.2 Materials synthesis

Tetraethoxysilane (TEOS, 99% purity) was obtained from Fluka Chemika and vinyltriethoxysilane (VTES, 97% purity) was purchased from Sigma-Aldrich. Non-functionalized materials are labeled as their surfactant template. The vinyl-modified CTAB template samples were labeled v4-CTAB and v6-CTAB, where the number following the “v” in the prefix indicates the TEOS:VTES ratio (4:1 and 6:1, respectively). The synthesis procedure is based on the room-temperature synthesis of Kumar et al.⁸² The work of Stein et al.²² suggested a TEOS:VTES ratio of 4:1 as the limit for obtaining ordered materials. A less ordered material v4-CTAB-d was synthesized with CTAB:TEOS ratio of 0.12, based on investigations by Bore et al.¹⁷⁴, where a CTAB:TEOS ratio approaching a limit of 0.09 (in a non-functionalized material) gives disordered materials. The partially fluorinated surfactant templates were used to synthesize v4-HFOPC, v6-HFOPC; v4-HFDePC, v6-HFDePC; v4-HFDoDePC, v6-HFDoDePC, v4 and v6 have the same meaning as previously stated. The HFDePC and HFDoDePC templated materials were synthesized in homogeneous ethanol/water synthesis medium to obtain ordered pore structures. 200 proof ethanol (Aaper Alcohol and Chemical Company) was used as solvent and de-ionized ultra-filtered water (DIUFW) was obtained from Fisher Scientific. The molar ratios of the reactants used in the synthesis of all the materials are given in Table 3.1. The molar ratio of vinyl to Si in the synthesis solution is 0.20 for v4 samples and 0.14 for v6 samples.

The samples were synthesized by first adding the surfactant to DIUFW (or DIUFW/ethanol homogeneous solution) and stirring the mixture for 5 minutes. NH₄OH (catalyst, 28-30% solution from Malinckrodt) was then added with continuous stirring. After 10 minutes of stirring, TEOS or a mixture of TEOS and VTES, in the desired proportions, was slowly added. The mixture was left to age under stirring at room temperature for 24 hours (2 hours for synthesis in homogenous medium to match the conditions used previously by Tan et al.¹³). The mixture was vacuum-filtered after the aging period and left to air-dry for 24 hours. An ethanol/HCl solution of 150 ml ethanol and 5 g aqueous HCl was used for the extraction of the surfactant, which was accomplished by stirring the sample in solution for 24 hours. This extraction process was repeated once. Concentrated HCl of 37.3% assay (Fisher Scientific) was used for the extraction.

Table 3.1: Molar ratios of reactants used in material synthesis

Material	DIUFW*	Ethanol	Surfactant	NH ₄ OH	TEOS*	VTES*
CTAB	149		0.15	5.1	1	
v4-CTAB	186		0.21	6.37	1	0.25
v4-CTAB-d	186		0.12	6.37	1	0.25
v6-CTAB	186		0.21	6.37	1	0.17
HFOPC	149		0.058	5.1	1	
v4-HFOPC	186		0.073	6.37	1	0.25
v6-HFOPC	197		0.077	6.73	1	0.17
HFDDePC	137	64	0.28	18.6	1	
v4-HFDDePC	137	64	0.28	18.6	1	0.25
v6-HFDDePC	137	64	0.28	18.6	1	0.17
HFDDoDePC	137	64	0.07	18.6	1	
v4-HFDDoDePC	137	64	0.07	18.6	1	0.25
v6-HFDDoDePC	137	64	0.07	18.6	1	0.17

*DIUFW: de-ionized ultra filtered water, TEOS: tetraethoxysilane, VTES: vinyl-triethoxysilane,

3.3.3 Materials characterization

Nitrogen adsorption measurements were carried out using a Micromeritics Tristar 3000 for the materials determined to be mesoporous, and a Micromeritics ASAP 2010 for those samples that were microporous. The materials were degassed at 150°C using flowing nitrogen gas for 4 hours before performing the adsorption analysis.

Fourier Transform Infrared (FTIR) analysis was performed to verify surfactant removal and vinyl incorporation. A small amount (approximately 1 wt%) of the sample was pressed with KBr matrix and analyzed using a Thermo Nicolet Nexus 470 FT-IR analyzer.

Powder X-ray diffraction patterns were obtained using Siemens 5000 diffractometer operating with CuK_α radiation of wavelength 1.54098 Å and a graphite monochromator.

Sample TEM images of the materials, after surfactant extraction, were observed and recorded with a JEOL 2000FX transmission electron microscope. The TEM samples were mounted on lacey carbon TEM grids (Ted Pella Inc) from an acetone suspension.

Accessibility of the vinyl group was analyzed by means of a bromination reaction ($\equiv\text{Si}-\text{CH}=\text{CH}_2 + \text{Br}_2 \rightarrow \equiv\text{Si}-\text{CHBr}-\text{CH}_2\text{Br}$). As the reaction proceeds, the UV absorbance at 412 nm is reduced due to the consumption of Br_2 . Following the method of Stein's group²², 5 mg of material was added to 2.5 ml of bromine solution (bromine in dichloromethane). The solution in a 3 ml cuvette had an initial UV absorbance of 1 at the wavelength of 412nm. The solution with the sample was shaken and allowed to sit for 15 to 30 minutes after which it was centrifuged for 15 minutes for the particles to settle, and the absorbance of the solution measured. This was done for a period of 4.5 hours, taking

absorbance readings about every 45 minutes. Duplicate bromination experiments were conducted for each sample.

3.4 RESULTS AND DISCUSSION

3.4.1 FTIR analysis

FTIR analysis confirms the presence of vinyl group in the materials after extraction of the surfactant. Complete surfactant extraction was observed by the disappearance of the surfactant peaks at 2854 cm^{-1} and 2924 cm^{-1} (for CTAB template materials, due to C-H vibrations in the CTAB chain¹⁷⁷) and 1493 cm^{-1} (fluoro-surfactant template materials), and a reduction in the peak at 1416 cm^{-1} for all materials (results not shown). The peak at 1493 cm^{-1} is attributed to the presence of pyridinium moiety in the fluorinated surfactants.¹⁷⁸ The presence of $-\text{CH}=\text{CH}_2$ in the vinyl functionalized materials contributes to the peak observed at 1416 cm^{-1} , due to the symmetric deformation of the $=\text{CH}_2$ group.¹⁷⁶ This peak was also present in non-functionalized materials prior to extraction of either surfactant, but it was observed to have a higher absorbance value in the vinyl-functionalized materials. This suggests a contribution from $-\text{CH}-$ stretching to the peak. This peak disappeared from the non-functionalized samples after extraction, so its presence after surfactant extraction in the functionalized materials indicates successful incorporation of the vinyl group.

3.4.2 Powder X-ray diffraction analysis

The pore order of the materials was investigated by performing powder X-ray diffraction (Figure 3.1). Most of the non-functionalized materials display x-ray patterns suggesting a 2-D hexagonal structure by the presence of at least three reflecting planes

that can be indexed to this structure, (100), (110), and (200). The hexagonal structure observed in the XRD reflections is consistent with the observation of Stein's and Ozin's groups for the incorporation of vinyl into CTAB template silica.^{22,23} The fluorinated surfactant templated materials display a (100) reflection that is broader when compared to the CTAB templated materials. The samples not showing evidence of significant long-range ordering (Figure 1D) are the non-functionalized material (HFDoDePC) and functionalized material (v6-HFDoDePC) templated by the longest chain fluorinated surfactant. In addition to broad (100) reflections, the XRD patterns of several of the vinyl functionalized materials (v4-HFOPC, v6-HFOPC, v6-HFDePC, v4-HFDoDePC) exhibit only faint traces of the (110) and the (200) reflections. The broad (100) reflection and missing higher order reflections show that the fluorinated surfactant templated samples have lower degrees of order as compared to the CTAB template materials. This could be due to smaller ordered domains in these materials.

The (100) reflection for all the fluorinated surfactant template materials occurred at higher $2\text{-}\theta$ values with corresponding smaller d_{100} -spacing, indicating pore sizes which are smaller than the CTAB template materials. This is attributed to the longer chain length of CTAB relative to the fluorinated templates, leading to larger pores. Non-functionalized fluorinated surfactant template materials, labeled HFOPC and HFDePC, display more order than their corresponding vinyl-functionalized samples, and the order decreases with increasing vinyl content (Figures 3.1B and 3.1C). These observations are consistent with previous evidence that an increase in vinyl functionalization reduces long-range pore order in CTAB template silica.^{22,23} In contrast, the materials obtained from the longest chain fluorinated surfactant (the 12-carbon chain surfactant,

HFDoDePC) display evidence of order in the materials synthesized at highest vinyl content (v4-HFDoDePC), but not in the non-functionalized material (HFDoDePC) or in the presence of a reduced ratio of the vinyl precursor (v6-HFDoDePC). This unexpected observation may be due to a structure transition towards a more-curved aggregate (cylindrical structure), creating a more stable pore structure, but we were unable to directly test this hypothesis.

To aid in the interpretation of accessibility studies, a less ordered version of v4-CTAB was synthesized. v4-CTAB-d (where d denotes disordered) has similar degree of pore order as the fluorinated surfactant template functionalized materials (Figure 3.1).

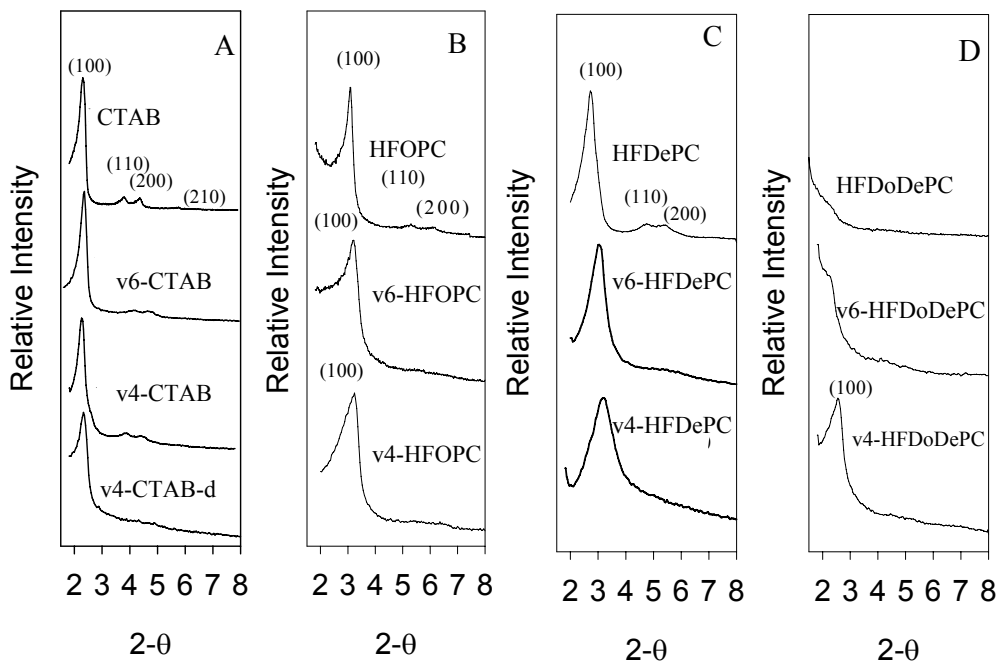


Figure 3.1 Powder X-ray diffraction patterns of A) CTAB template materials, B) HFOPC template materials, C) HFDePC template materials and D) HFDoDePC template materials. The plots have been offset vertically

3.4.3 Transmission Electron Microscopy

Examples of transmission electron microscopy (TEM) images of the vinyl-functionalized materials are presented in Figure 3.2, for the systems v4-CTAB, v6-HFOPC with inverse FFT (fast Fourier transform), v6-HFDePC and v4-HFDoDePC. The images are consistent with the XRD results. The TEM image of v4-CTAB (Figure 3.2A) shows very well ordered 2-D hexagonal pore structure whilst the images for the fluorosurfactant templated materials display partially ordered 2-D hexagonal structure. In most of the samples, the pores are randomly oriented in small close-packed domains, but in sample v6-HFDePC (Fig. 3.2C) the pores are oriented radially towards the edges of spherical particles. This morphology and pore orientation is consistent with what was observed in the non-functionalized materials templated by this fluorinated surfactant in aqueous ethanol.¹³

3.4.4 Nitrogen Adsorption analysis

Analysis of the pore size, specific surface area and pore volume of the materials was performed by means of nitrogen adsorption analysis. All the CTAB template materials display type IV isotherms (mesoporous materials) (Figure 3.3), consistent with previous observations for CTAB templated non-functionalized⁵ and functionalized^{22,23} materials. Fluorinated surfactant templated silica labeled HFOPC, HFDePC and v6-HFDePC, also display type IV isotherms (Figure 3.3). The inflection point on the type IV isotherms indicates mesopore filling, which occurred at lower relative pressures in the fluorinated surfactant-templated materials suggesting smaller pores. Functionalized and non-functionalized samples prepared with the 12-carbon chain surfactant (HFDoDePC, v6-HFDoDePC and v4-HFDoDePC) have type IV isotherms with maximum sorption

capacities at about $150 \text{ cm}^3/\text{g}$ STP, which is much lower when compared to all the other mesoporous materials synthesized in this study (results not shown). This is consistent with the absence of long range order observed by XRD. The isotherms display large hysteresis at relative pressures above 0.5 due to adsorption between particles or in macropores.

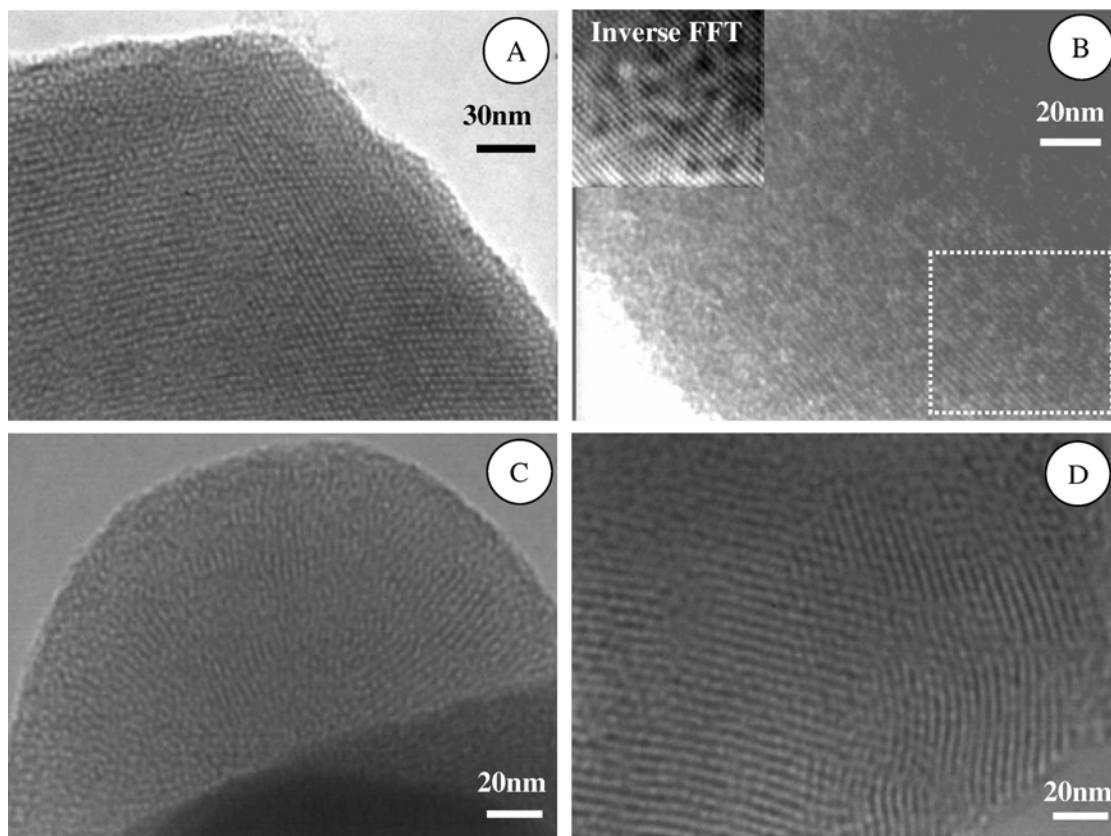


Figure 3.2: TEM images of A) v4-CTAB B) v6-HFOPC C) v6-HFDePC and D) v4-HFDoDePC.

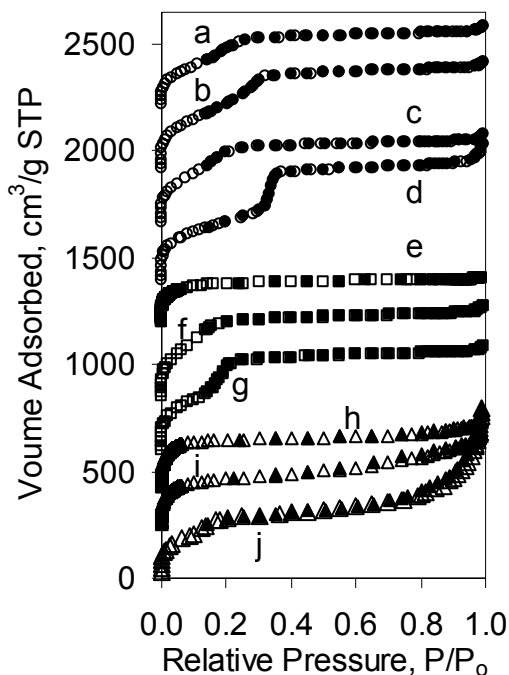


Figure 3.3 Nitrogen adsorption isotherms of a) v4-CTAB-d b) v4-CTAB c) v6-CTAB d) CTAB e) v4-HFDePC f) v6-HFDePC, g) HFDePC h) v4-HFOPC i) v6-HFOPC, j) HFOPC Open symbols are for adsorption and filled symbols are for desorption

The adsorption data for the mesoporous samples were analyzed by the KJS method (BJH method with a modified Kelvin equation)^{154,179,180} which makes use of the high resolution α_s -plot method. The resulting pore size distributions of the mesoporous materials, based on the modified Kelvin equation¹⁸⁰, are shown in Figure 3.4. A summary of the textural properties of all synthesized materials is given in Table 3.2.

Type I isotherms, characteristic of microporous materials¹⁹⁹, were observed for the vinyl functionalized material synthesized from the 8-carbon fluorinated surfactant (v4-HFOPC and v6-HFOPC) and the functionalized material synthesized at the highest vinyl content (v4-HFDePC) from the 10-carbon fluorinated surfactant. Physical

properties reported of the microporous materials, v6-HFOPC, v4-HFOPC and v4-HFDePC, are based on the methods of Dubinin and Kaganer¹⁷⁸ (Table 3.2). The pore size of v4-HFDePC may not be well-represented by this analysis. The d_{100} -spacing obtained for v4-HFDePC suggests that (if the wall thicknesses are similar in these materials) the pore size should have been close to that of v6-HFOPC, which is between 1.8 – 1.9 nm. The small pore size of v4-HFDePC determined from the Dubinin-Kaganer method may be the result of an apparent overestimation of the surface area and a concomitant underestimation of the pore volume.

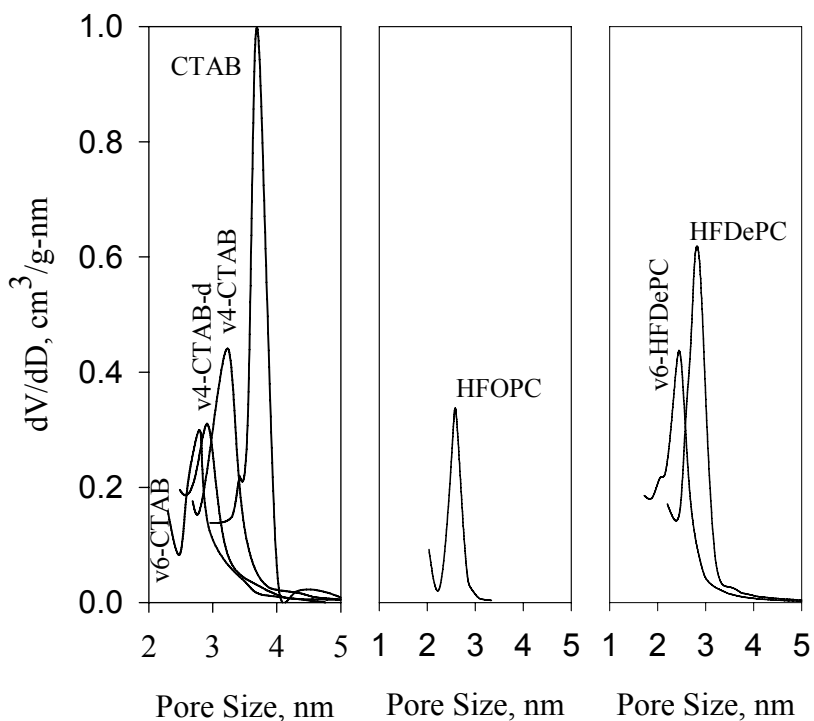


Figure 3.4 Pore size distributions calculated using the BJH method with a modified Kelvin equation.¹⁷⁷

Table 3.2: Summary of the textural properties of all the materials

SAMPLE	d_{100} (nm)	S_t (m ² /g)	v_m (cm ³ /g)	d_p (nm)	a_o (nm)
CTAB	3.84	995	0.76	3.66	4.43
v6-CTAB	3.74	450	0.2	2.58	4.32
v4-CTAB	3.87	997	0.69	3.25	4.47
v4-CTAB-d	3.8	752	0.5	2.91	4.39
HFOPC	2.87	811	0.28	2.6	3.31
v6-HFOPC	2.76	865	0.31	1.86	3.19
v4-HFOPC	2.72	943	0.33	1.66	3.14
HFDDePC	3.2	739	0.4	2.78	3.7
v6-HFDDePC	2.86	717	0.38	2.44	3.3
v4-HFDDePC	2.78	834	0.3	1.45	3.21
HFDDePC	--	286	0.14	3.22	--
v6-HFDDePC	--	524	0.19	2.96	--
v4-HFDDePC	3.46	635	0.27	2.69	4

S_t is the specific surface area, v_m is the mesopore/micropore volume and d_p is the pore diameter (size) measured using the BJH method with a modified Kelvin equation for mesopores and the Dubinin-Kaganer method for micropore. a_o is hexagonal cell parameter ($2d_{100}/3^{1/2}$)⁵

As summarized in Table 3.2, the incorporation of vinyl in the samples obtained using the 8-carbon chain fluorinated surfactant (HFOPC) shifts the pore size from 2.56 nm (mesopore) for non-functionalized silica to 1.86 nm (micropore) for v6-HFOPC (lower vinyl content; TEOS:VTES of 6:1) and 1.66 nm (micropore) for v4-HFOPC (higher vinyl content; TEOS:VTES of 4:1). The reduction in pore size with increasing vinyl content is consistent with the observation of Jaroniec and Ozin's group²³ who showed that increase in vinyl content for CTAB template materials reduces the pores from mesopores to micropores. Similarly, the 10-carbon chain fluoro-surfactant (HFDDePC) template materials exhibit a pore size trend of 2.78 nm, 2.34 nm to 1.45 nm for non-functionalized silica, v6-HFDDePC and v4-HFDDePC respectively.

3.4.5 Vinyl Accessibility Analysis

Bromination reactions were performed on the vinyl functionalized materials to investigate the accessibility of vinyl group within the pores of the materials.²² The accessibility correlates with the decreased absorbance of the reactant bromine in solution with respect to time, as measured for v4- (TEOS:VTES of 4:1) functionalized samples (Figure 3.5A) and the v6- (TEOS:VTES of 6:1) functionalized samples (Figure 3.5B). The absorbance values are normalized with the weight of material added to the bromine solution. A control experiment (not shown) was performed on non-functionalized CTAB and HFOPC templated silica, to investigate if other factors such as adsorption of bromine atoms on the surface contribute to accessibility measurement. The absorbance of the solutions in the control experiments was unchanged over 4 hours. In the functionalized materials, absorbance drops significantly over the first 50 minutes of the reaction due to the bromination of the most accessible vinyl groups, those outside the pores and near the pore openings. After the first 50 minutes there is a gradual decrease in absorbance due to bromination of the vinyl groups inside the pores. After approximately 150 minutes, the absorbance approaches a constant value in the functionalized materials.

The accessibility of the vinyl groups in the CTAB-templated material (v4-CTAB), based on the final values, is lower than that for all the other v4-samples which were synthesized with fluorinated surfactants (Figure 3.5A). v4-HFDePC (radial pore structure) and v4-HFDoDePC show similar accessibilities, which was greater than the accessibility in v4-HFOPC (Figure 3.5A). The results for the v6-samples also suggest that there are fewer accessible vinyl groups in v6-CTAB relative to the fluorinated samples synthesized at an identical ratio of functionalized precursor (Figure 3.5B). Surprisingly,

v6-HFDePC displays the highest accessibility, followed by v6-HFOPC (Figure 3.5B) in spite of the lower vinyl content during the synthesis relative to the v4-materials.

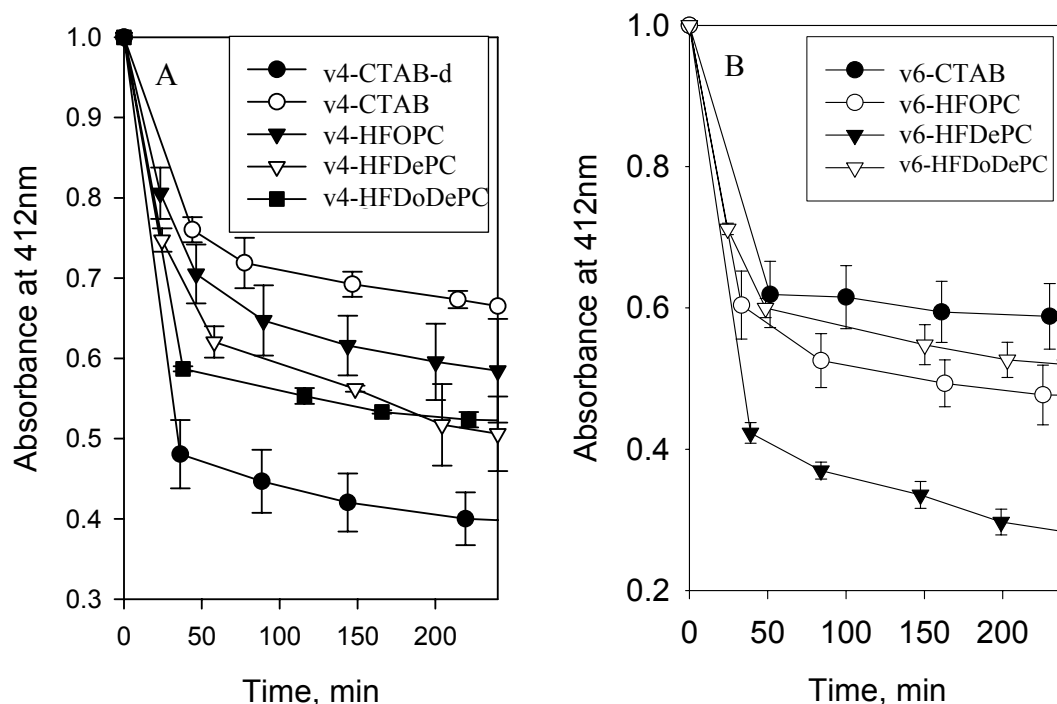


Figure 3.5 Bromination reaction plots of A) samples prepared with 4 TEOS: 1 VTES and B) samples prepared with 6 TEOS: 1 VTES.

The high accessibilities observed in the fluorinated surfactant template materials may be due to the increased attraction of the vinyl pendant group to the surface of the micelles during the synthesis of the fluorinated surfactant template materials. Alternatively, the accessibility of the vinyl-functionalized group may be improved by a lower degree of long-range order in the fluorinated surfactant-templated materials. Accessibility within disordered materials has been observed to be higher than in ordered materials.⁸² In the case of well-ordered materials, accessibility may be reduced by steric hindrance of attached groups at the pore openings. This possibility was further investigated by synthesizing a less-ordered CTAB-templated material (v4-CTAB-d) with

pore order similar to the fluorinated template materials. The accessibility within this material is about 100% greater than in the ordered v4-CTAB after 200 minutes of bromination (absorbance approaching a constant value; Figure 3.5A). Thus higher accessibilities in v4-HFDePC and v6-HFDePC could be due to their decreased ordered pore structure when compared to v4-HFOPC, v6-HFOPC and v4-HFDoDePC.

3.5 CONCLUSIONS

Partially fluorinated cationic surfactants have been successfully used in preparing ordered mesoporous silica functionalized with organic vinyl. This is the first demonstration of fluorinated surfactant templating to produce organic functionalized silica by direct synthesis. Adsorption data indicates that the pore sizes decrease with an increase in vinyl content irrespective of the surfactant chain length. However, the size of the pores in all fluorinated surfactant-templated materials was smaller than that of the CTAB-templated material, for a given level of functionalization. From the powder x-ray diffraction analysis, the order of the pores in the materials obtained from $C_6F_{13}C_2H_4C_5H_5NCl$ and $C_8F_{17}C_2H_4C_5H_5NCl$ templates decreases as the vinyl content increases, while the opposite effect was observed in the $C_{10}F_{21}C_2H_4C_5H_5NCl$ template materials. In spite of a decrease in pore size of the fluorinated surfactant-templated materials (some even being microporous), the vinyl accessibility was shown to be higher than in ordered CTAB template materials. The greater accessibility in v4-CTAB-d, relative to the more ordered v4-CTAB, shows that the long-range pore order strongly affects the accessibility of the functional groups within the pores. This study begins to address the unusual potential to alter the accessibility of the organic functional group on

the basis of the high hydrophobicity and lipophobicity of the tail of the fluoro-surfactant template.

CHAPTER 4

FLUOROCARBON AND HYDROCARBON FUNCTIONAL GROUP INCORPORATION INTO NANOPOROUS SILICA EMPLOYING FLUORINATED AND HYDROCARBON SURFACTANTS AS TEMPLATES

4.1 SUMMARY

Ordered mesoporous fluorocarbon-functionalized (heptadecafluoro-1,1,2,2-tetrahydro-decyl) silica and its hydrocarbon functionalized analogue (n-decyl) are synthesized by the ‘one-pot’ (direct) synthesis method using two cationic fluorinated surfactants, $C_6F_{13}C_2H_2NC_5H_5Cl$ (HFOPC) and $C_8F_{17}C_2H_2NC_5H_5Cl$ (HFDePC), and a typical hydrocarbon surfactant, $C_{16}H_{33}N(CH_3)_3Br$ (CTAB), as templates. The properties of the resulting materials are determined for the following combinations of surfactant/functional groups: hydrocarbon/hydrocarbon, hydrocarbon/fluorocarbon, fluorocarbon/hydrocarbon and fluorocarbon/fluorocarbon. Synthesis using the longer chain fluoro-surfactant (HFDePC) template results in the highest incorporation of both n-decyl and the fluorocarbon functional group, with a corresponding loss of material order in the fluorinated material. The decyl-functionalized materials synthesized using the HFOPC template possess very low levels of incorporation of the decyl group (0.18 mmol/g) compared to the HFDePC templated materials (1.12 mmol/g). CTAB templated materials display greater long-range pore order than the fluorocarbon templated materials. The incorporation of the fluorocarbon functional precursor is more efficient (on a percent yield basis) than the hydrocarbon functional precursor for silica material synthesized

using CTAB. Similarly, the use of fluorocarbon templates enhances fluorocarbon incorporation relative to hydrocarbon incorporation in the mesoporous material. Solubility of the precursors (n-decyl triethoxysilane and heptadecafluoro-1,1,2,2-tetrahydrodecyl triethoxysilane) in the synthesis medium and favorable hydrophobic interaction between the surfactant tail and the alkane/fluoro-alkane functional group improves the incorporation of the functional group.

4.2 INTRODUCTION

Synthesis of organic functionalized nanoporous silica is an active research area because of the broad range of potential applications of these high surface area materials in sensing, catalysis and separation. Surfactant templating of sol-gel derived silica results in large surface areas, large pore volumes and narrow pore size distributions. Also, the pore size and structure can be tailored for specific applications by using surfactants with different hydrophobic tails and varying the synthesis conditions. Since the discovery of the M41S family of nanostructured materials,⁵ various organic functional groups have been incorporated into mesoporous silica by means of post-synthesis grafting or direct co-condensation.²¹

Synthesis of functionalized mesoporous silica by co-condensation results in high functional group incorporation.²² Lim and Stein²² and Kruk et al.²³ investigated vinyl incorporation by co-condensation in the presence of cetyltrimethylammonium bromide (CTAB) as a pore template. An increase in vinyl content decreases the pore size (moving from mesoporous to microporous materials), pore volume and order of the materials. This is consistent with our observations of reduced material order, pore size, surface area and

pore volume with increasing vinyl content when partially fluorinated surfactants were used as templates in synthesizing vinyl functionalized nanoporous silica.¹⁸¹ Primary amines and secondary amines have also been incorporated in mesoporous silica by employing cationic surfactants (e.g., CTAB)⁶, anionic surfactants (e.g., sodium dodecylsulfate, SDS)⁷, nonionic surfactants⁸ and block co-polymers⁹ as templates. In addition, other functional groups, such as thiol groups (mainly mercaptopropyl functionalization)¹⁸²⁻¹⁸⁵ and, more recently, organic bridging groups^{186,187} have been incorporated into mesoporous silica through co-condensation of their corresponding silica precursors. Bi-functionalized nanoporous silica (e.g., ureidopropyl with 3-[2-(2-aminoethylamino) ethylamino]-propyl¹⁸⁸, sulfonic acid-amino groups¹⁸² and carboxyl-amino groups¹⁸⁹) has also been prepared by co-condensation synthesis. Post-synthesis attachment to reactive organic sites in these organic/inorganic composites has been used to further functionalize mesoporous silica, for example, with biomolecules.^{190,191}

Numerous investigations have examined hydrocarbon-based templates^{21,192-194} and, more recently, fluorocarbon surfactant templates^{10-15,195,196} for the synthesis of mesoporous silica. However, organic functionalization has focused primarily on the incorporation of hydrocarbon, not fluorocarbon, functional groups. The hydrocarbon-hydrocarbon interaction of traditional surfactant templates and organic functional groups, as well as the hydrophobic or hydrophilic nature of the functional group, determine the alignment of the group within the pores during direct synthesis of organic functionalized mesoporous silica.^{24,197,198} The interaction of organic functional groups with the surfactant can be compared to alcohol interaction with cationic surfactants. For example, the role of alcohol in the formation of C_nTAB (alkyltrimethylammonium bromide)

aggregates changes from co-solvent to co-aggregate to co-surfactant with increasing alcohol chain length.¹⁹⁹ Matching the chain length and chemical nature of a hydrophobic group and the surfactant hydrophobic tail promotes the incorporation of the hydrophobic group in surfactant micelles, improving solubilization and stability of the aggregate.²⁰⁰

In contrast to hydrocarbon functionalization, there are limited examples of fluorocarbon incorporation into mesoporous silica.^{69,201-203} Fluorocarbon functionalization of silica results in a surface with increased hydrophobicity and lipophobicity.²⁰⁴ The applications of fluorinated surfaces, which are “solvent responsive” include their use in chromatographic purification and separation of fluorinated compounds²⁰⁵, in fluorous biphasic catalysis^{206,207} and as hydrophobic surface coatings.^{204,208} Low-surface tension mobile phases such as fluorocarbon solvents and supercritical carbon dioxide effectively wet the surfaces of fluorocarbon functionalized silica, allowing for their effective use for separation processes. Fluorocarbon incorporated porous silica can also be used as low-k dielectric in the manufacture of semiconductors.²⁰⁹

Post-synthesis attachment has been the primary method to prepare fluorocarbon-functionalized silica.²¹⁰ When extending direct synthesis approaches to fluorocarbon functionalized material, the nature of the surfactant/organic precursor interactions (e.g., hydrocarbon surfactant template/fluorinated silica precursor) is expected to influence the self assembly process. Mixtures of hydrocarbon and fluorocarbon surfactants may form uniformly mixed aggregates or segregated hydrocarbon rich and fluorocarbon rich micelles or mixed micelles with de-mixed hydrocarbon and fluorocarbon regions.^{65,211} Aggregation behavior of hydrocarbon and fluorocarbon surfactant mixtures is a function

of the surfactant chain lengths, hydrophobic chain structure (e.g. aromaticity, branching), concentration, and temperature.^{66,211}

Lebeau et al²⁰² have successfully demonstrated the incorporation of 2-pentafluorophenyl functionality into hexagonally ordered mesoporous silica by direct synthesis using CTAB as a template. The role of perfluoroalkyl chain length in surfactant assembly and its effect on the silica mesostructure was investigated in the synthesis of fluorinated organosilicate films by solvent evaporation using CTAC as template.²⁰⁴ The fluorocarbon functionalized silica films display both hexagonal and cubic mesostructure for short chain functional group ($\text{CF}_3(\text{CH}_2)_2-$ or FH_2-) and only hexagonal structure for the long chain functional groups (F_6H_2- and F_8H_2-). An increase in the hexagonal cell parameter and pore wall thickness with increasing perfluoroalkyl chain length is attributed to the extension of fluorocarbon groups in the pore channel.²⁰¹ Porcherie et al²⁰⁵ have also examined templating with hydrocarbon and fluorocarbon surfactants in the synthesis of fluorocarbon functionalized silica, thus providing the first investigation of the effect of fluorocarbon surfactant/fluorocarbon functional group combination on silica materials properties. The use of cationic fluorinated surfactant template resulted in disordered porous silica with low fluorocarbon incorporation for a long chain fluorinated functional group (F_6H_2-), even at a high TEOS to functional precursor ratio of 19:1. Improved fluorocarbon incorporation and material order were observed when a short chain fluorocarbon (FH_2-) functionalized silica was synthesized, suggesting that incorporation of the long chain functional group disrupts the self assembly of the cationic fluorinated surfactant micelles.

This work examines the effect of combinations of hydrocarbon and fluorocarbon templates and functionalized silica precursors on the material textural properties, pore structure, long-range order and functional group loading of functionalized silica formed by direct synthesis. The incorporation of fluorocarbon functional group (heptadecafluoro-1,1,2,2-tetrahydro-decyl; perfluoro-decyl) and its hydrocarbon analogue (n-decyl) is investigated using CTAB (cetyltrimethylammonium bromide), HFOPC (tridecafluoro-1,1,2,2-tetrahydro-octylpyridinium chloride) and HFDePC (heptadecafluoro-1,1,2,2-tetrahydro-decylpyridinium chloride) as templates. In this work we demonstrate the incorporation of a longer chain fluorinated group with a much higher ratio of the functionalized precursor to tetraethoxysilane than has been examined previously.²⁰⁵ The influence of hydrocarbon/fluorocarbon surfactant/template interactions on functional group incorporation, mesostructure and physical properties of the silica is examined. .

4.3 MATERIALS AND METHODS

Tetraethoxysilane (TEOS; Figure 4.1) with a purity of 99% was obtained from Fluka Chemika. n-Decyltriethoxysilane ($H_{10}TES$, 95% purity; Figure 4.1) and heptadecafluoro(1,1,2,2-tetrahydro) decyltriethoxysilane (F_8H_2TES , 95% purity; Figure 1) were purchased from Gelest Inc. CTAB (99% purity; Figure 4.2) was obtained from Sigma. The fluorinated surfactants (Figure 4.2), $C_6F_{13}C_2H_4NC_5H_5Cl$ and $C_8F_{17}C_2H_4NC_5H_5Cl$, labeled HFOPC and HFDePC, respectively, were synthesized as previously described.¹⁸¹

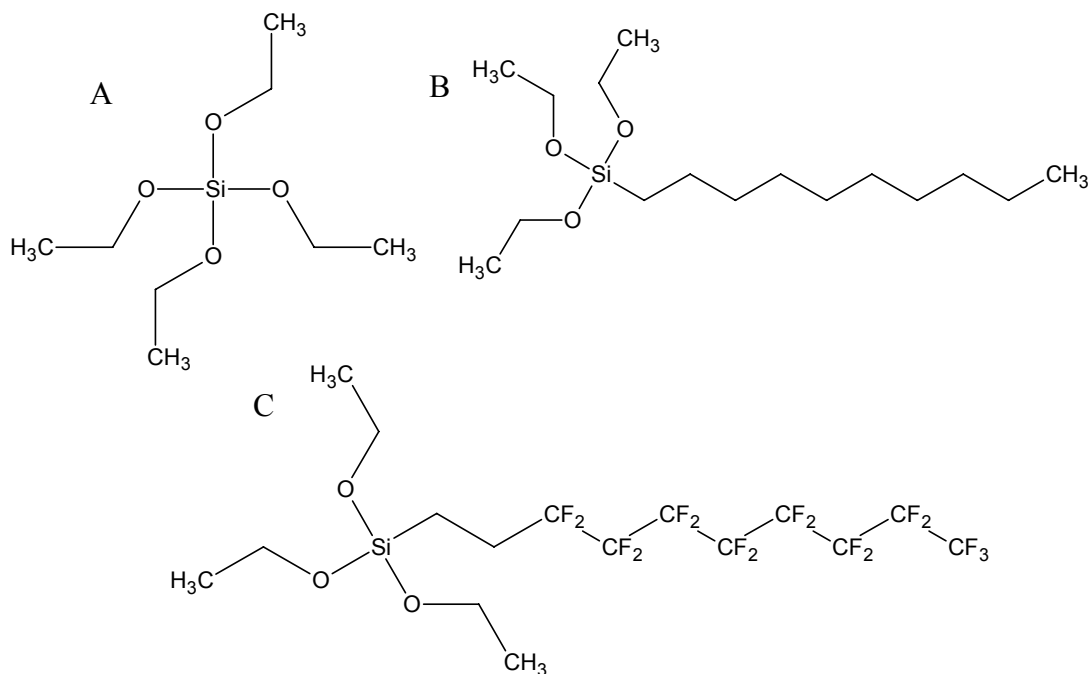


Figure 4.1 Structures of precursors: A) tetraethoxysilane (TEOS) B) n-decyl triethoxysilane (H₁₀TES) and C) heptadecafluoro-1,1,2,2-tetrahydrodecyl triethoxysilane (F₈H₂TES)

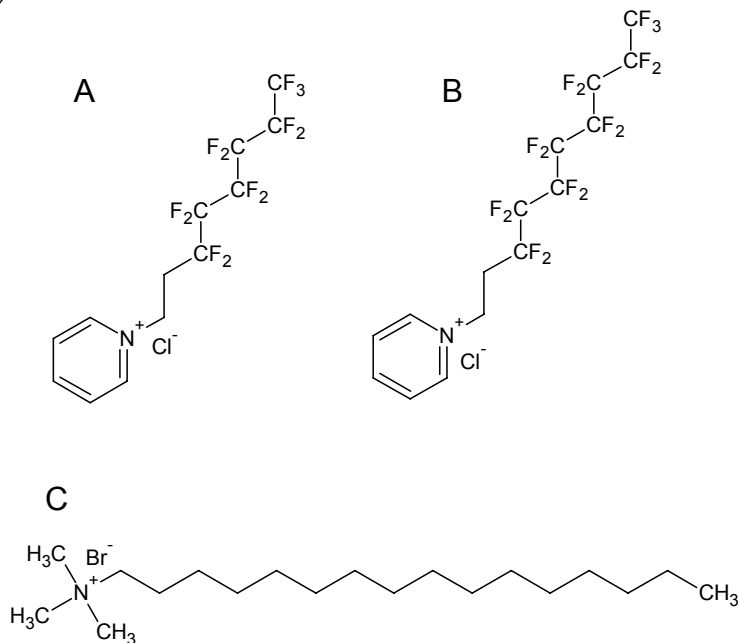


Figure 4.2: Structures of surfactants: A) tridecafluoro-1,1,2,2-tetrahydro-octyl pyridinium chloride (HFOPC) B) heptadecafluoro-1,1,2,2-tetrahydro-decyl pyridinium chloride (HFDePC) and C) cetyltrimethylammonium bromide (CTAB)

4.3.1 Synthesis of Mesoporous Silica

Functionalized mesoporous silica was synthesized by utilizing a 4:1 molar ratio of TEOS to F₈H₂TES or H₁₀TES in aqueous solutions for CTAB and HFOPC templated materials. HFDePC templated materials were synthesized in 4:1 molar ratio of TEOS to F₈H₂TES or H₁₀TES dissolved in a homogeneous water/ethanol solution, where the addition of ethanol was required to obtain ordered structures. Non-functionalized materials were synthesized as previously described in chapter 3.

Materials synthesis began by adding the surfactant to de-ionized ultra-filtered water (DIUFW) and stirring the mixture for 5 minutes. Concentrated ammonia (catalyst, 28 - 30% solution from Malinckrodt) was then added with continuous stirring of the mixture for an additional 10 minutes, after which TEOS or a mixture of TEOS and F₈H₂TES (or H₁₀TES), in the desired proportions, was slowly added. The mixture was aged with stirring at room temperature for 24 hours. The molar ratios of the reactants used in the syntheses were 186 DIUFW: 0.184 CTAB (or 0.082 HFOPC): 3.31 NH₃: 1 TEOS: 0.25 H₁₀TES (or F₈H₂TES) and 136 DIUFW: 64 ethanol: 0.197 HFDePC: 10.6 NH₃: 1 TEOS: 0.25 H₁₀TES (or F₈H₂TES). The synthesis procedure is based on the room-temperature synthesis of unmodified silica reported by Kumar et al.⁸¹ The mixture was vacuum-filtered after the aging period and left to air-dry for 24 hours. An ethanol/HCl solution of 150 ml ethanol and 5 g concentrated aqueous HCl was used for the extraction of the surfactant. Extraction was accomplished by stirring the dried sample in acidic ethanol for 24 hours. This extraction process was repeated once.

Synthesized materials were labeled H₁₀-CTAB and F₈H₂-CTAB; H₁₀-HFOPC and F₈H₂-HFOPC; and H₁₀-HFDePC and F₈H₂-HFDePC. The naming convention for the

functionalized silica is the functional group incorporated followed by the template used. In tables and figures, non-functionalized materials were labeled simply as their surfactant templates (i.e., CTAB, HFOPC, and HFDePC).

4.3.2 Materials Characterization

Nitrogen adsorption measurements were performed using a Micromeritics Tristar 3000 automated gas adsorption instrument. The materials were degassed at 150 °C using flowing nitrogen gas for 4 hours before performing the adsorption analysis. Data from nitrogen sorption analysis were analyzed to obtain material total surface area (S_t), pore volume (v_p) and pore size distribution (d_p) using α_s -plot and the modified BJH method proposed by Kruk, Jaroniec and Sayari (KJS).^{154,179,180}

Fourier transform infrared spectroscopy (FTIR) analysis was performed to verify surfactant removal and functional group incorporation. A small amount (approximately 1 wt %) of the silica sample was pressed into a pellet with KBr matrix and analyzed using a Thermo Nicolet Nexus 470 FT-IR analyzer.

Thermogravimetric analysis (TGA) was carried out using a Universal V2.5H TA instrument to quantify organic group incorporation. The materials were analyzed with nitrogen purge with a starting temperature of 35 °C and heated at 10 °C/min up to 750 °C.

Powder X-ray diffraction (XRD) patterns were obtained using a Siemens 5000 diffractometer operating with CuK_α radiation of wavelength 0.154098 nm and a graphite monochromator.

Transmission electron micrograph (TEM) images of the materials, after surfactant extraction, were recorded with a JEOL 2000FX transmission electron microscope. The

TEM samples were prepared by grinding the sample and mixing with a small amount of acetone. The solution was allowed to settle and lacey carbon TEM grids (Ted Pella Inc) were used to scoop some of the clear liquid and then allowed to dry. This was done so that the smallest particles could be mounted on the grid for better TEM analysis.

4.4 RESULTS AND DISCUSSION

The incorporation of fluorocarbon and hydrocarbon functionality in mesoporous silica by direct synthesis is demonstrated for CTAB, HFOPC, and HFDePC templated materials. FTIR provides qualitative evidence for organic functionalization, while incorporation is quantified using TGA, which is interpreted as a function of the fluorocarbon/hydrocarbon template and precursor combinations. The effect of fluorocarbon incorporation on pore size, pore order, and surface area is determined using XRD and N₂ adsorption analysis. Changes in the surface hydrophobicity are observed with hydrocarbon and fluorocarbon functionalization.

4.4.1 Functional Group Incorporation

Fourier transform infrared spectroscopy (FTIR) analysis of the materials demonstrates successful removal of surfactant templates and also provides evidence of functional group incorporation. Peaks at 2856 cm⁻¹ and 2925 cm⁻¹ in the as-synthesized (unextracted, denoted with the suffix A) CTAB-templated materials as well as the n-decyl functionalized materials (H₁₀-CTAB, H₁₀-HFOPC, H₁₀-HFDePC) correspond to the characteristic stretching of C-H in the hydrocarbon functional group and the hydrocarbon surfactant template (Figure 4.3). The magnitude of the peak is reduced in H₁₀-CTAB, for example, after surfactant extraction. A significant reduction of the peak at 1473 cm⁻¹ (C-H bending) and disappearance of the 1493 cm⁻¹ peak (N-C stretching; attributed to the

presence of CTAB surfactant) is also observed for H₁₀-CTAB. The as-synthesized decyl functionalized materials templated with the fluorosurfactants (H₁₀-HFOPC-A (Figure 4.3B) and H₁₀-HFDePC-A (Figure 4.3C)) display peaks corresponding to the n-decyl functional group (1473 cm⁻¹, 2856 cm⁻¹ and 2925cm⁻¹) as well as additional peaks which disappear after surfactant extraction (1502 cm⁻¹, due to the pyridinium head group; and 1217 cm⁻¹ and 1155 cm⁻¹, due to C-F stretching of surfactant). The low peak intensities at 2856 cm⁻¹ and 2925 cm⁻¹ following surfactant extraction suggest low n-decyl incorporation in H₁₀-HFOPC relative to H₁₀-HFDePC and H₁₀-CTAB.

The FTIR of the perfluoro-decyl functionalized silica templated with CTAB, as synthesized (F₈H₂-CTAB-A), displays peaks at 2856 cm⁻¹ and 2925 cm⁻¹ (Figure 4.3A) that disappear after surfactant extraction, suggesting complete surfactant removal. Complete surfactant extraction in the fluorocarbon functionalized materials made with fluorosurfactant templates (F₈H₂-HFOPC and F₈H₂-HFDePC) is confirmed by the disappearance of the peaks at 1502 cm⁻¹ and 1454 cm⁻¹, which are attributed to the presence of pyridine and C-H bending, respectively.²¹³ Peaks at 1217 cm⁻¹ and 1155 cm⁻¹, characteristic of -CF₂- vibrations in the fluorocarbon functional group,²¹³ are present in all of the as-synthesized fluoro-functionalized materials (F₈H₂-CTAB-A, F₈H₂-HFOPC-A and F₈H₂-HFDePC-A). A significant reduction of peaks characteristic of -CF₂- vibrations is observed for F₈H₂-CTAB (Figure 4.3A) and F₈H₂-HFOPC (Figure 4.3B) after surfactant extraction, while F₈H₂-HFDePC (Figure 4.3C) shows only a slight decrease in the intensity of the peaks. The loss of unincorporated fluoro-functional groups may contribute to the reduction of these peaks.

The prominent peaks observed in all the materials at 1100 cm^{-1} and the shoulder at 1200 cm^{-1} are typical of silica. The broad band below 3200 cm^{-1} is due to adsorbed water and silanols.²¹⁶

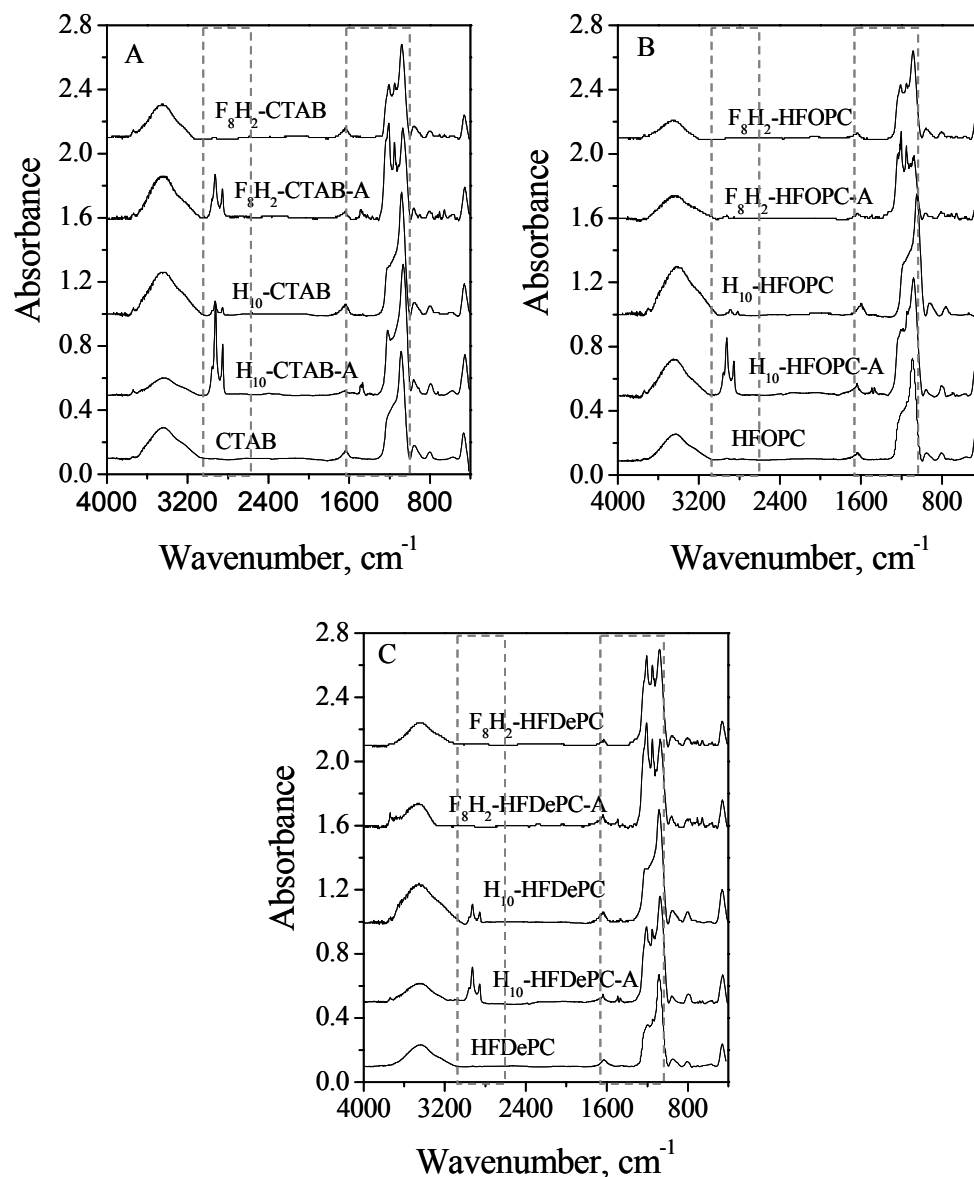


Figure 4.3 FTIR plots of as-synthesized and extracted A) CTAB templated, B) HFOPC templated, and C) HFDePC templated silica. The thin boxes outline the surfactant and organic bands discussed in the text.

TGA was used to quantify the extent of organic incorporation in the synthesized materials. TGA analyses of all the materials show an initial weight loss at temperatures less than 100 °C, due to the loss of water and solvent from the materials (Figure 4.4). Further weight loss is observed between 190 °C and 240 °C, which could be due to the loss of residual surfactants in the materials^{200,201} and condensation of available silanols.²¹² The largest weight loss is observed between 450 °C and 600 °C for all samples except F₈H₂- HFDePC, which has a significant weight decline starting at about 400 °C. The weight loss in the region between 400 °C and 600 °C indicates the decomposition of the organic functional group,²¹⁶ giving the percentage of organic functional group in the silica material (Table 4.1). The theoretical organic content, assuming complete hydrolysis and siloxane bond formation during synthesis (i.e 100% yield), is also presented in Table 4.1. The organic content measured by TGA is less than the theoretical values, which suggests incomplete hydrolysis of the precursors or the formation of unattached, soluble silsesquioxanes which are removed during surfactant extraction. Alternatively, possible carbon re-deposition after decomposition of the organic functional group during TGA analysis could lower the measured organic content of the functionalized silica.

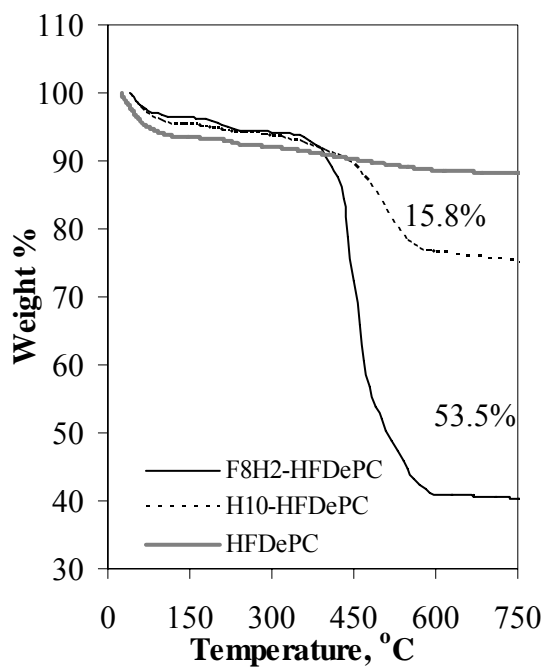


Figure 4.4 Sample TGA plots of HFDePC, H₁₀-HFDePC and F₈H₂-HFDePC.

Table 4.1 Organic content of functionalized materials

Material	Organic Content by TGA, mmol/g*	Theoretical Organic Content, mmol/g ⁺
F ₈ H ₂ -CTAB	0.57 (42%)	
F ₈ H ₂ -HFOPC	0.56 (42%)	1.35
F ₈ H ₂ -HFDePC	1.20 (89%)	
H ₁₀ -CTAB	0.67 (29%)	
H ₁₀ -HFOPC	0.18 (8%)	2.31
H ₁₀ -HFDePC	1.12 (48%)	

⁺Theoretical organic content is based on complete hydrolysis and siloxane bond formation (i.e. 100% yield). *Percentage of organic content relative to theoretical yield is in parenthesis.

The incorporation of the fluoro-functional group is greatest in F₈H₂-HFDePC relative to F₈H₂-HFOPC and F₈H₂-CTAB, as measured from TGA analysis (Table 4.1). This higher degree of fluorocarbon incorporation in F₈H₂-HFDePC may be due to favorable interaction between functional group and the surfactant tail, which have the same molecular structure (-C₂H₂C₈F₁₇). Surprisingly, the greatest extent of hydrocarbon functionalization is also achieved using this fluoro-surfactant template (H₁₀-HFDePC), although the extent of incorporation (48% on a basis of the theoretical yield) is significantly less than that of the fluorocarbon functional group (F₈H₂-HFDePC; 89%). This high degree of n-decyl incorporation may be due to matching the number of carbon atoms in the precursor/template for H₁₀-HFDePC. While hydrocarbons are more soluble in hydrocarbons than fluorocarbons, matching fluorinated chain length and hydrocarbon chain length has been demonstrated to significantly increase the miscibility range.⁶⁰ Alternatively, solubilization of both the fluorocarbon and hydrocarbon precursors may be enhanced in the micelle aggregates of the ethanol/water media used to template the HFDePC materials, leading to a high degree of functional group incorporation.

In the absence of added ethanol, the extent of fluorocarbon functionalization is similar (0.56 mmol/g) for both the CTAB-templated and HFOPC-templated materials (F₈H₂-CTAB and F₈H₂-HFOPC, respectively). The incorporation of the hydrocarbon precursor is minimal in HFOPC (H₁₀-HFOPC, 8% of theoretical maximum). In addition, efficiency of hydrocarbon incorporation in the hydrocarbon templated material (H₁₀-CTAB) is reduced relative to fluorocarbon incorporation (29 and 42 % theoretical yields, respectively) at a TEOS to functional precursor ratio of 4:1. Fluorocarbon groups are more hydrophobic than hydrocarbons, which may promote the incorporation of the

fluorocarbon precursor within the micelles of the hydrocarbon surfactant template in spite of its dissimilar chemical nature.

4.4.2 Hydrophobicity of functionalized silica materials

The functionalization of silica, which is hydrophilic due to the presence of surface hydroxyl groups, can result in dramatically different surface properties. The hydrophobicity of the functionalized materials due to the incorporation of the hydrocarbon and fluorocarbon groups is confirmed by observing wetting properties of the functionalized and non-functionalized silica powder. Sample images of a water droplet on the surface of powder silica (HFDePC, H₁₀-HFDePC and F₈H₂-HFDePC) spread on glass are presented in Fig. 4.5. The images show the droplets on the functionalized silica possess very large contact angles ($\theta > 90^\circ$), which suggest the materials are highly hydrophobic. Hydrocarbon functionalized silica particles are able to disperse on the outer surface of the water droplet (Figure 4.5B), but in the presence of the more hydrophobic fluorocarbon functionalized silica the water droplet sitting on the silica surface remains clear (Figure 4.5C). In contrast, water droplets are immediately absorbed into the non-functionalized silica material (Fig 4.5A). The dramatic change in surface properties of the silica powders not only indicates functionalization, but also suggests the potential application of fluorofunctionalized materials. Fluorocarbon functionalized materials usually possess high lipophobicity and hydrophobicity, in addition to high chemical and thermal stability.^{204,208}

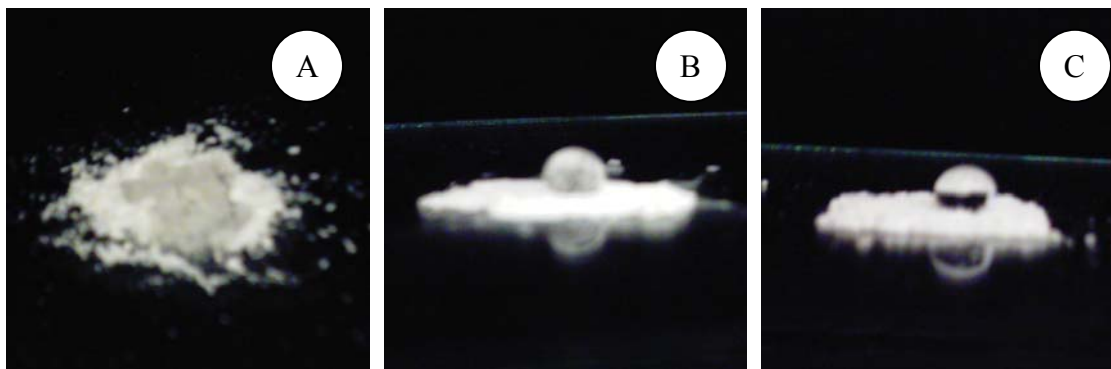


Figure 4.5 Images of water droplet on A) HFDePC templated silica, B) H₁₀-HFDePC and C) F₈H₂-HFDePC.

4.4.3 Structural Properties of Functionalized Silica

The pore structure and order of the silica material after surfactant extraction was examined by powder X-ray diffraction (Figure 4.6). For the decyl functionalized silica, 2-D hexagonal pore structure is observed for the CTAB templated material (H₁₀-CTAB), as interpreted from the presence of (100), (110), (200) and (210) reflections in the XRD profile. Silica templated with the fluorinated surfactants (H₁₀-HFOPC and H₁₀-HFDePC) is characterized by only the first three reflections, which also correspond to a 2-D hexagonal pore structure. These reflections are of lower intensity than the hydrocarbon-templated material, suggesting better long range order in the CTAB templated material. TEM images (Figure 4.7) obtained for these materials confirm the 2-D hexagonal pore structure inferred from the XRD patterns. However, the image of H₁₀-HFDePC (Figure 4.7E) shows particles of spherical morphology with radial pores, which is characteristic of materials synthesized in homogeneous water/ethanol solution.¹⁹⁷

Similar to the trend observed in hydrocarbon functionalized silica, hydrocarbon surfactant templating results in fluoro-functionalized materials with greater order than fluoro-surfactant templated materials. While both F₈H₂-CTAB and F₈H₂-HFOPC display

XRD peaks characteristic of hexagonal pore structure, the intensities of the reflections are much higher in the CTAB templated material. The single broad peak in the XRD pattern for F₈H₂-HFDePC suggests materials of low order. The peak width could also be due to low electron density contrast because of the high incorporation of the fluorocarbon functional group in this material (Table 4.1). Increasing the incorporation of functional groups in mesoporous silica results in decreased pore order.^{22,23,219} Spherical particles are also observed for the fluorofunctionalized silica synthesized in a homogenous water/ethanol solution (F₈H₂-HFDePC; Fig. 4.7F). Pores are not observable in F₈H₂-HFDePC at a higher magnification, possibly due the low contrast in the presence of fluorocarbons in the pores.

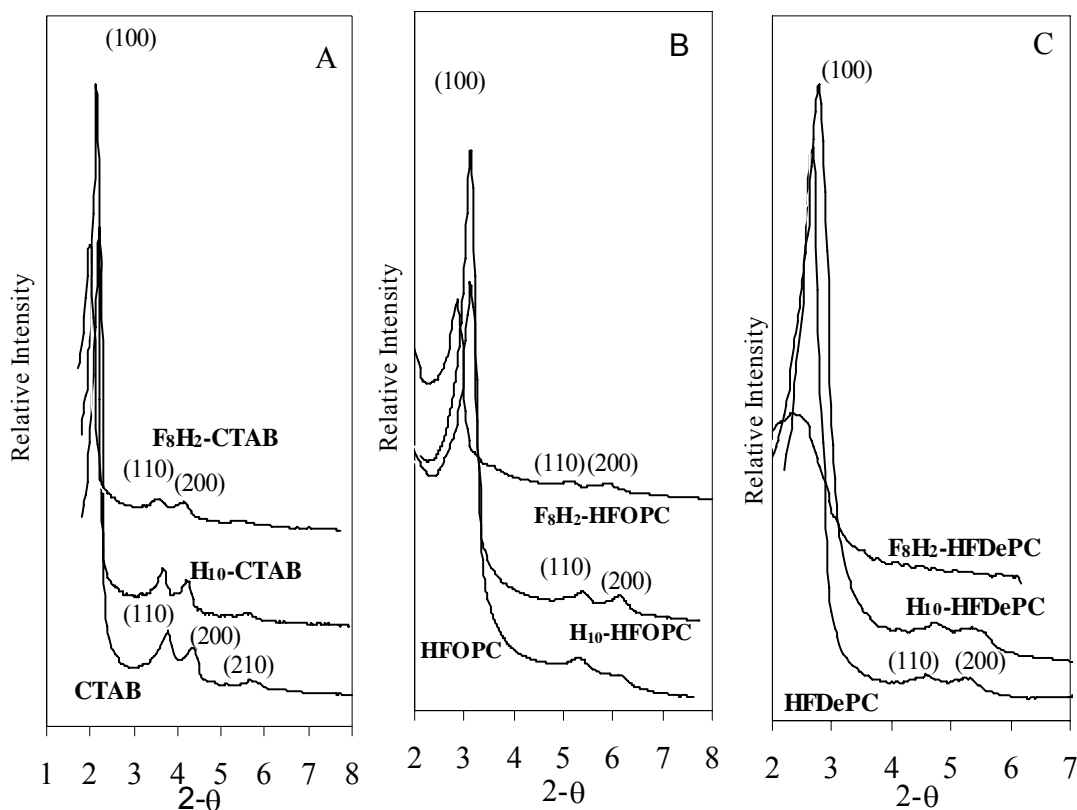


Figure 4.6 Powder X-ray diffraction plots of A) CTAB templated, B) HFOPC templated, and C) HFDePC templated silica materials.

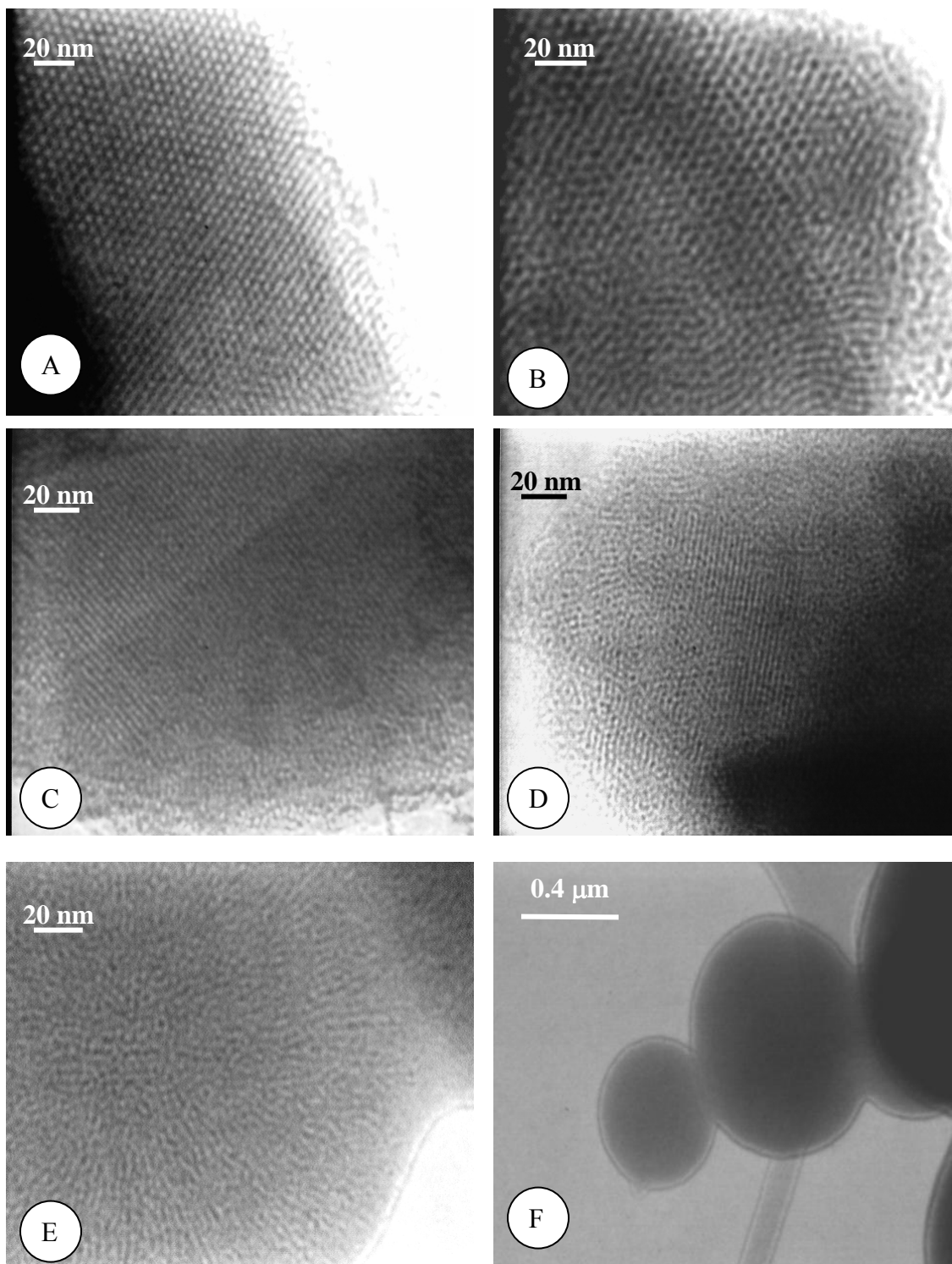


Figure 4.7 Representative TEM images of A) H₁₀-CTAB, B) F₈H₂-CTAB, C) H₁₀-HFOPC, D) F₈H₂-HFOPC, E) H₁₀-HFDePC, and F) F₈H₂-HFDePC.

The physical properties (pore size; d_p , total surface area; S_t and pore volume; v_p) of the silica materials were analyzed by means of nitrogen adsorption. All the materials display type IV adsorption isotherms (Figure 4.8), characteristic of mesoporous materials.¹⁷⁸ The n-decyl functionalized materials possess higher sorption capacity than the corresponding fluoro-functionalized materials owing to the more ordered pore structure of the decyl materials. For both the hydrocarbon and fluorocarbon functionalized materials, the HFOPC-templated silica materials display a large hysteresis in the adsorption isotherm and large adsorption values at relative pressures close to 1. This large hysteresis is due to non-uniformity in the pores and the presence of a large number of macropores.

Pore size distributions (Figure 4.8) in the synthesized silica were determined from the adsorption isotherms using the KJS method.^{154,179,180} A unimodal pore size distribution was observed in the range of 1.5 nm to 10 nm for mixed surfactant/functional group systems (hydrocarbon/fluorocarbon and fluorocarbon/hydrocarbon surfactants and precursors). A single pore size is consistent with no de-mixing into hydrocarbon rich and fluorocarbon rich micelles during the synthesis of the materials. The similar pore sizes (Table 4.2) for H₁₀-HFOPC and F₈H₂-HFOPC (2.44 nm) suggest that the functional group chain length, rather than the type of functional group, controls the micelle size captured in the synthesis process. Functionalization results in a slight reduction in pore size as compared to non-functionalized HFOPC (2.60 nm). In contrast to the slight reduction of pore size observed with functionalization of HFOPC templated material, we previously observed that the direct synthesis of vinyl functionalized silica using HFOPC (4:1, TEOS:vinyl triethoxysilane synthesis conditions) resulted in marked reduction of

pore size from 2.60 nm (HFOPC) to 1.66 nm (v4-HFOPC).¹⁸¹ The vinyl chain may act as a co-aggregate during micellar formation due to its much shorter chain length relative to the surfactant templates, whereas the longer F₈H₂- will act as a co-surfactant.

Table 4.2 Structural properties of fluorocarbon and hydrocarbon functionalized materials

Material	d ₁₀₀ (nm)	S _t (m ² /g)	*S _{external} (m ² /g)	V _p (cm ³ /g)	d _p (nm)	*a _o (nm)	*t _{pw} (nm)
CTAB	4.01	995	106	0.76	3.67	4.63	0.96
HFOPC	2.87	811	323	0.28	2.60	3.31	0.71
HFDePC	3.29	739	41	0.40	2.77	3.80	1.03
F ₈ H ₂ -CTAB	4.5	819	45.7	0.34	2.58	5.20	2.62
F ₈ H ₂ -HFOPC	3.07	444	192	0.10	2.44	3.54	1.10
F ₈ H ₂ -HFDePC	3.87	370	9.48	0.12	2.32	4.47	2.15
H ₁₀ -CTAB	4.14	947	98.6	0.45	2.76	4.78	2.02
H ₁₀ -HFOPC	2.88	618	234	0.13	2.44	3.33	0.89
H ₁₀ -HFDePC	3.23	899	24.4	0.32	2.16	3.73	1.57

* S_{external} is the external specific surface area, a_o hexagonal cell parameter ($2d_{100}/3^{1/2}$) and t_{pw} is the pore wall thickness (a_o – d_p).

The 10-carbon chain hydrocarbon and fluorocarbon functional groups (H₁₀ and F₈H₂, respectively) are not expected to fully extend into the hydrophobic core of the CTAB (16-carbon hydrophobic tail) aggregate. However, for HFDePC (10-carbon hydrophobic tail) the functional groups will be able to replace some of the surfactant molecules during aggregation. The bulky fluorocarbon group occupies more volume than the hydrocarbon group. This is consistent with the larger pore size of H₁₀-CTAB (2.76 nm) relative to F₈H₂-CTAB (2.58 nm). On the other hand, functionalization of HFDePC templated silica results in a hydrocarbon functionalized material (H₁₀- HFDePC) with a smaller pore size (2.12 nm) than the corresponding fluoro-functionalized material (F₈H₂- HFDePC, 2.32 nm). The functional groups in the more ordered H₁₀-HFDePC compared

to F₈H₂-HFDePC might have caused decrease in the effective pore size. The smaller pore sizes obtained for the HFDePC templated materials as compared to the HFOPC materials may be due to the combined effect of high functional group incorporation in the HFDePC templated materials and synthesis in homogeneous water/ethanol medium.^{222,223} High additive (e.g. alcohol) incorporation in micelles leads to reduced micellar size due to reduction in headgroup repulsion.¹⁹⁹

Pore wall thickness is observed to increase after functional group incorporation (Table 2). The increase in pore wall thickness is due to the covalent attachment of the functional groups to the silica walls.²⁰⁴ Because of the relative size of the functional groups, the fluorocarbon functionalized silica materials have larger pore walls than the hydrocarbon functionalized materials. Comparing pore wall thickness across surfactants templates, CTAB (hydrocarbon) templated materials possess the largest increase in pore wall thickness relative to non-functionalized silica, while the increase in pore wall thickness is less in HFOPC templated silica, possibly due to low functional group incorporation. The incorporation of the functional groups in the silica walls generally decreases the total surface area and pore volume (Table 4.2). Across all surfactants, the largest decrease is observed for the fluorocarbon functionalized silica materials which are less ordered than the hydrocarbon functionalized silica.

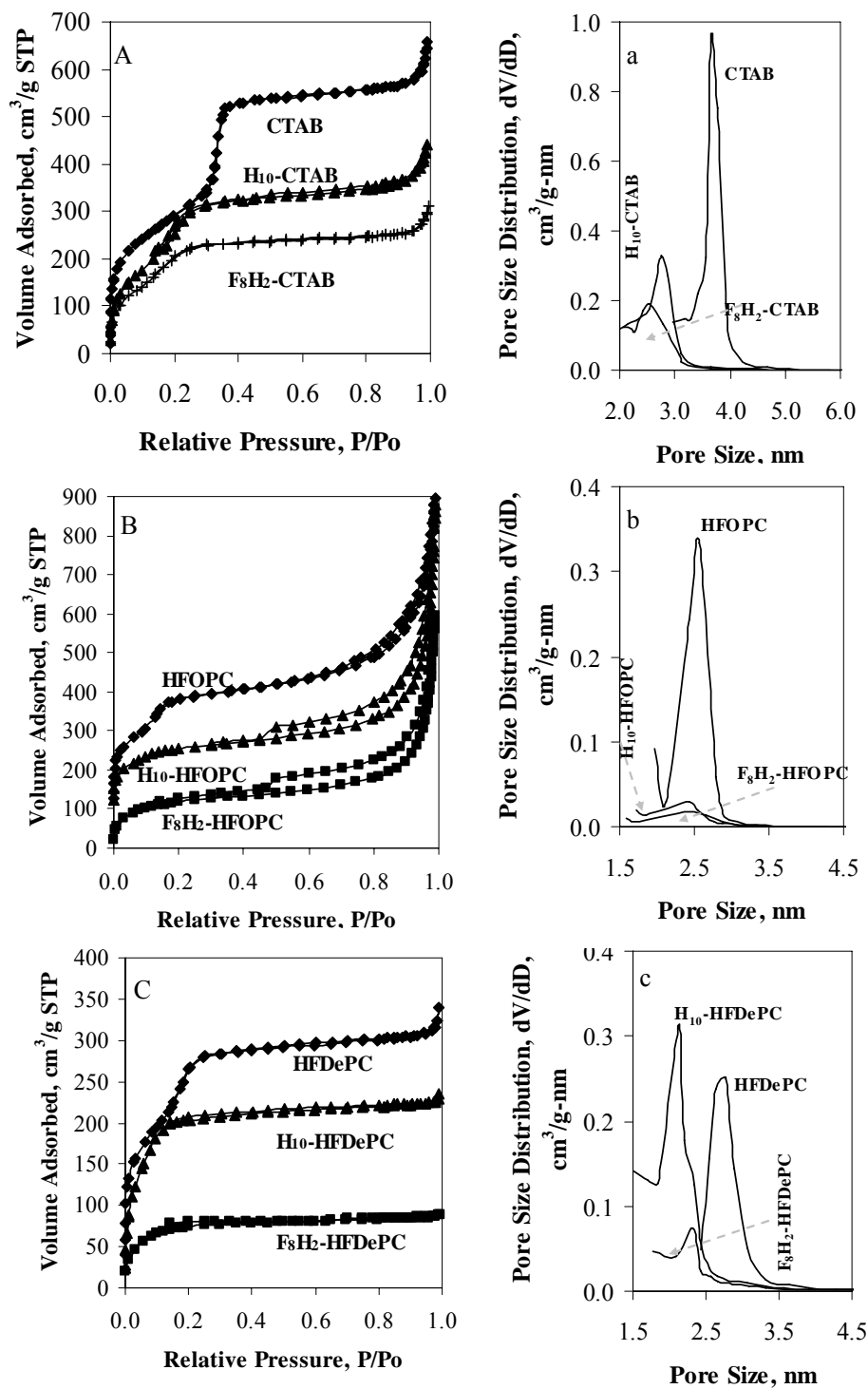


Figure 4.8 Nitrogen adsorption isotherm and pore size distribution of A) CTAB templated, B) HFOPC templated, and C) HFDePC templated silica materials.

4.5 CONCLUSIONS

Cationic fluorocarbon surfactants with two chain lengths (tridecafluoro-1,1,2,2-tetrahydro-octylpyridinium chloride (HFOPC) and heptadecafluoro-1,1,2,2-tetrahydro-decylpyridinium chloride (HFDePC)) and a hydrocarbon surfactant (CTAB) are demonstrated as templates for the synthesis of 2-D hexagonal or disordered pore structured, fluorocarbon (perfluoro-decyl) functionalized mesoporous silica by direct ('one-pot') synthesis. Corresponding hydrocarbon functional group (n-decyl) incorporation is also investigated. For all surfactant/n-decyl precursor combinations, n-decyl functionalized silica with 2-D hexagonal pore structure is obtained. Synthesis in homogeneous water/ethanol medium leads to high degree of functional group incorporation, and results in disordered pore structure for the fluorocarbon functionalized HFDePC templated silica. Higher yield of fluorocarbon functional group incorporation than the hydrocarbon group was obtained for all surfactants. The dramatic increase in surface hydrophobicity of the silica after functional group incorporation, particularly for the fluorocarbon functionalized silica, is consistent with the analysis by FTIR and TGA that demonstrated functional group incorporation. Based on the unimodal pore size distributions achieved for combinations of fluorinated and hydrocarbon precursors and templates, there is no evidence of segregation of hydrocarbon-rich and fluorocarbon-rich aggregates during synthesis.

The length of the functional group relative to the surfactant tail and the type of incorporated functional group affect pore size. Structural order, pore size and surface area generally decrease with functionalization. The increase in pore wall thickness for functionalized materials, greater for fluorocarbon functionalized materials relative to

hydrocarbon functionalized materials, is consistent with the attachment of the functional group to the silica pore walls. The degree of fluorocarbon incorporation and the silica surface areas are considerably higher than reported previously for fluorofunctionalized silica formed by direct synthesis.²⁰⁵

CHAPTER 5

APPLICATION OF FLUORO-FUNCTIONALIZED MESOPOROUS SILICA TO FLUOROUS SEPARATIONS

This work is submitted to Industrial & Engineering Chemistry Research for publication.

5.1 SUMMARY

Two types of fluorocarbon-functionalized (F_6H_2 and F_8H_2) mesoporous silica were synthesized by the 'one-pot' (direct) synthesis method using cationic fluorocarbon surfactants, $C_6F_{13}C_2H_2NC_5H_5Cl$ (HFOPC) and $C_8F_{17}C_2H_2NC_5H_5Cl$ (HFDePC), and a traditional hydrocarbon surfactant, $C_{16}H_{33}N(CH_3)_3Br$ (cetyltrimethylammonium bromide, CTAB), as templates. The effect of the chain length of the fluorocarbon functional precursor and the surfactant template on the pore order, materials textural properties, and fluorocarbon incorporation was examined. Fluorocarbon functionalization decreased the silica pore order, pore size and surface area. Matching surfactant type (hydrocarbon surfactant or fluorocarbon) with the functional functional group (a fluorocarbon) did not improve functional group incorporation; the incorporation of the perfluoro-octyl functional group (F_6H_2 -) was greater in the CTAB templated silica (1.13 mmol/g) relative to the HFOPC templated silica (0.83 mmol/g). The application of these mesoporous silica powders to fluororous solid phase extraction (F-SPE) was investigated. Hydrocarbon and fluorocarbon-tagged anthraquinones (HC-dye and FC-dye, respectively) were separated by gradient elution using an increasingly fluorophilic solvent system. Although higher incorporation of the perfluoro-octyl functional group (F_6H_2 -) was observed relative to the

perfluoro-decyl group (F_8H_2-) for all surfactant templates, the perfluoro-decyl functionalized silica materials provided higher fluorocarbon dye recovery in the separation. The yield of FC-dye was 87.8 (± 5.8)% for F_8H_2 -HFDePC packed column compared to 76.7 (± 1.1)% for F_6H_2 -HFDePC packing materials of the same weight. Dye elution through a packed column of mesoporous silica occurs in a narrower band than for fluorocarbon functionalized silica gel, consistent with the high fluorocarbon content, and smaller pore and particle size of the mesoporous material.

5.2 INTRODUCTION

Combinatorial chemistry and parallel synthesis approaches have resulted in procedures to readily synthesize a library of potential pharmaceuticals in the same reaction vessel and at the same conditions.^{222,223} The post-synthesis challenge is separating the mixture of compounds into functionally resolved fractions. To promote the separation processes, reactants and substrates are sometimes tagged.²²⁴⁻²²⁷ Fluorous tagged molecules contain at least one highly fluorinated carbon chain, which can be permanently or temporarily attached to the organic compound of interest. This fluorous tag provides for the separation by liquid-liquid extraction or solid-liquid extraction. Fluorous compounds with varied fluorinated chain lengths can also be separated based on fluorous chromatography. The separation of fluorous tagged compounds on fluorocarbon functionalized solid surface is based on similar interactions among fluorocarbons.²⁰⁷ The high electronegativity of the fluorine atom, when replacing a hydrogen atom in a carbon bond, results in strong intramolecular and weak intermolecular forces. As a result, fluorocarbons are lipophobic, and also are more hydrophobic than hydrocarbons.²²⁸

The limited examples of fluorocarbon functionalized solid materials²²⁹ are primarily formed through the post synthesis attachment of the fluorocarbon group to porous silica particles. The covalent attachment of fluorocarbon functionalized silanes via the surface OH groups of silica results in silica-O-Si(R)₂(CH₂)_nR_f, where R_f denotes the fluorocarbon group. Commercially available fluorosilica include FluoroFlash silica gel (Fluorous Technologies, Inc.; R_f = C₈F₁₇) and SiliaBond Tridecafluoro silica gel (Silicycle; R_f = C₆F₁₃). Of the two materials, FluoroFlash silica gel has been suggested to provide a more “fluorophilic” surface for solid phase extraction (SPE) and flash chromatography; the tridecafluoro silica gel requires higher water content for fluorosilica molecules to be retained.²⁰⁶

Direct synthesis of fluorocarbon functionalized surfactant-templated mesoporous silica is an alternative route to making fluorocarbon functionalized solid material for use as packing for solid phase extraction, chromatography and solid phase synthesis. Ordered silica material is synthesized through the co-assembly of surfactant micelles with hydrolyzed alkoxy silane precursors. Polymerization of the precursor via sol-gel chemistry (the liquid-phase reactions of alkoxy silane precursors to generate silica) and subsequent surfactant removal results in pore structures that mimic surfactant liquid crystal mesophases. Nanostructured silica synthesized by surfactant templating is characterized by ordered pore structures, narrow pore size distributions and large surface areas (>700m²/g) relative to silica gels.⁸¹ Direct (‘one-pot’) synthesis describes the co-condensation of a mixture of tetraalkoxy silane and organic functionalized alkoxy silane (including materials formed in the presence of a pore templating agent) resulting in functionalized mesoporous silica. Direct synthesis generates materials with high

functional group loading and uniform distribution relative to post synthesis attachment.^{22,23} Few studies have investigated the formation of fluorocarbon functionalized silica by direct synthesis,^{199,201-205} and only one previous investigation examines the use of fluorinated templates to enhance the incorporation of fluorinated precursors in direct synthesis.²⁰⁵ Porcherie et al²⁰⁵ synthesized fluoro-functionalized silica by direct synthesis using a neutral fluorinated surfactant ($n\text{-C}_8\text{F}_{17}\text{C}_2\text{H}_4\text{NH}_2$), a fluorinated cationic surfactant ($n\text{-C}_8\text{F}_{17}\text{C}_2\text{H}_4\text{N}(\text{CH}_3)_3^+\text{I}^-$) analogous to CTAB, as well as CTAB, as pore forming agents. In the case of the cationic fluorinated template, disordered porous silica with low fluorocarbon incorporation was obtained for a long chain fluorinated functional group (F_6H_2 -), even at a low TEOS to functional precursor ratio of 19:1. These results are consistent with the disruption of micelle formation of the cationic fluorinated surfactant by the long chain functional group, an explanation supported by the improved fluorocarbon incorporation and material order when functionalizing the silica using a short chain fluorinated group ($\text{CF}_3(\text{CH}_2)_2$ -).

Surfactant templating is influenced by numerous factors that drive co-assembly: precursor, surfactant type (cationic, anionic, or non-ionic), surfactant functionality and chain length, the pH of the synthesis medium (acidic or basic) and temperature.^{82,230} The effect of an organic functionalized precursor on self assembly is expected to be analogous to the solubilization of hydrophobic molecules in the hydrophobic portion of surfactant aggregates in aqueous solutions.^{68,69} Matching the chain length and chemical nature of the hydrophobic molecule and the surfactant hydrophobic tails will maximize hydrophobic interactions. This results in improved solubilization of hydrophobic molecules in the surfactant aggregate and stability of the aggregate.²⁰² For example, the role of alcohol in

the formation of C_n TAB (alkyltrimethylammonium bromide) aggregates changes from co-solvent to co-aggregate to co-surfactant with increasing alcohol chain length.⁷⁰ The segregation of mixtures of hydrocarbon and fluorocarbons into fluorocarbon-rich and hydrocarbon-rich phases suggests that a fluorocarbon surfactant may be better suited than a traditional hydrocarbon surfactant for the incorporation of fluorocarbon functional groups by direct synthesis.⁵⁴ Therefore, we expect that the combination of surfactant template-fluorocarbon functional group will affect the degree and uniformity of functional group incorporation in mesoporous silica and the performance of these silica powders in fluorous separations.

This chapter describes the synthesis and characterization of fluorocarbon-functionalized silica and its application as packing material for the fluorous-solid phase extraction (F-SPE) of hydrocarbon and fluorocarbon tagged anthraquinones. Two relatively long chain fluorocarbon functional groups (tridecafluoro-1,1,2,2-tetrahydro-octyl (F_6H_2) and heptadecafluoro-1,1,2,2-tetrahydro-decyl (F_8H_2)) are incorporated into mesoporous silica. Fluoro-functionalization is achieved by direct synthesis at a TEOS to functional precursor ratio of 4:1 using a traditional cationic hydrocarbon surfactant, CTAB, and two cationic fluorocarbon surfactants, HFOPC (tridecafluoro(1,1,2,2-tetrahydro)octylpyridinium chloride) and HFDePC (heptadecafluoro(1,1,2,2-tetrahydro)decylpyridinium chloride), as templates. The materials are analyzed for pore structure and order, degree of functional group incorporation and texture properties. The separation performance of the fluorocarbon functionalized mesoporous silica is compared to a commercial fluorocarbon functionalized silica gel (*FluoroFlash*).

5.3 MATERIALS AND METHODS

5.3.1 Materials

Tetraethoxysilane (TEOS, with purity of 99%), tridecafluoro-1,1,2,2-tetrahydro-octyltriethoxysilane (F_6H_2TES , 95% purity), and heptadecafluoro-1,1,2,2-tetrahydro-decyltriethoxysilane (F_8H_2TES , 95% purity) were purchased from Gelest Inc. CTAB (Figure 4.2) was obtained from Sigma with 99% purity. The fluorinated surfactants $C_6F_{13}C_2H_4NC_5H_5Cl$ and $C_8F_{17}C_2H_4NC_5H_5Cl$ (Figure 4.2), labeled HFOPC and HFDePC, respectively, were synthesized as previously described.¹⁷⁸ The perfluorinated dye (1-fluoro, 4-pentadecafluoro-1,1-dihydro-octylamino-anthraquinone) was synthesized following published procedures²³¹ by the reaction of 1,4-difluoro-9,10-anthracendione with the appropriate amine in dimethyl sulfoxide at 60°C. The hydrocarbon tagged dye [Sudan blue II; (Bis(butylamino)anthraquinone)] was purchased from Sigma-Aldrich (analytical grade). Structures of the dyes are given in Figure 5.1. FluoroFlash silica gel (silica bonded phase of $Si(CH_2CH_2C_8F_{17})$)²⁰⁶ was obtained from Fluorous Technologies, Inc. De-ionized ultra-filtered water (DIUFW) was purchased from Fisher Scientific. All solvents were of analytical grade.

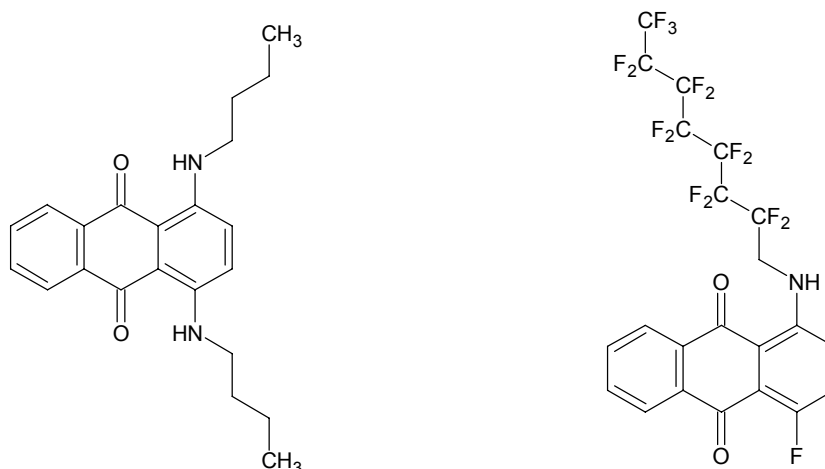


Figure 5.1 Hydrocarbon-tagged anthraquinone (Sudan blue II [Bis(butylamino)anthraquinone]) (left); and fluorocarbon-tagged anthraquinone dye (1-fluoro, 4-pentadecafluoro-1,1-dihydro-octylamino-anthraquinone) (right).

5.3.2 Synthesis of Mesoporous Silica

Functionalized mesoporous silica was synthesized by utilizing a 4:1 molar ratio of TEOS to F_6H_2TES or F_8H_2TES in aqueous solutions for CTAB and HFOPC templated materials. Non-functionalized materials were synthesized as previously described in chapter 3. HFDePC templated materials were synthesized with a 4:1 molar ratio of TEOS to F_6H_2TES or F_8H_2TES dissolved in a homogeneous ethanol/water solution, where the addition of ethanol was used to promote complete dissolution of the fluorinated surfactant (HFDePC). Materials synthesis began by first adding the surfactant to de-ionized ultra-filtered water (DIUFW) or a mixture of DIUFW/ethanol and stirring for 5 minutes. Concentrated aqueous ammonia (catalyst, 28 - 30% solution) was then added with continuous stirring of the mixture for 10 minutes, after which TEOS or a mixture of TEOS and F_6H_2TES or F_8H_2TES , in the desired proportions, was slowly added. The mixture was aged with stirring at room temperature for 24 hours. The molar ratios of the

reactants used in the syntheses were 186 DIUFW: 0.184 CTAB (or 0.082 HFOPC): 3.31 NH₃: 1 TEOS: 0.25 F₆H₂TES (or F₈H₂TES) and 136 DIUFW: 64 Ethanol: 0.197 HFDePC: 10.6 NH₃: 1 TEOS: 0.25 F₆H₂TES (or F₈H₂TES). The mixture was vacuum-filtered after the aging period and dried at 40 °C for 24 hours. An ethanol/HCl solution of 150 mL ethanol and 5 g concentrated aqueous HCl was used for the extraction of the surfactant. Extraction was accomplished by stirring the dried sample in acidic ethanol for 24 hours. This extraction process was repeated once. The synthesis procedure is based on the room-temperature synthesis of unmodified silica reported by Kumar et al.⁸¹

Synthesized materials were labeled F₆H₂-CTAB and F₈H₂-CTAB; F₆H₂-HFOPC and F₈H₂-HFOPC; and F₆H₂-HFDePC and F₈H₂-HFDePC. The naming convention for the functionalized silica is the functional group incorporated followed by the template used. The prefixes F₆H₂ and F₈H₂ correspond to tridecafluoro-1,1,2,2-tetrahydro-octyl and heptadecafluoro-1,1,2,2-tetrahydro-decyl functional groups, respectively. In tables and figures, non-functionalized materials were labeled simply as their surfactant templates (i.e., CTAB, HFOPC, and HFDePC).

5.3.3 Materials Characterization

Nitrogen adsorption measurements were performed using a Micromeritics Tristar 3000 automated gas adsorption instrument. The materials were degassed at 150 °C using flowing nitrogen gas for 4 hours before performing the adsorption analysis. Data from nitrogen sorption analysis were analyzed to obtain material surface area, pore volume and pore size distribution using α_s -plot and the modified BJH method proposed by Kruk, Jaroniec and Sayari (KJS).^{154,179,180}

Fourier Transform Infrared (FTIR) analysis was performed to verify surfactant removal and functional group incorporation. A small amount of synthesized material (approximately 1 weight %) was pressed into a pellet with KBr matrix and analyzed using a Thermo Nicolet Nexus 470 FT-IR spectrometer.

Thermogravimetric analysis (TGA) was carried out using a Universal V2.5H TA instrument. The materials were analyzed under nitrogen purge with a starting temperature of 35 °C and a ramp rate of 10 °C/min to 800 °C.

Powder X-ray diffraction (XRD) patterns were obtained using a Siemens 5000 diffractometer operating with $\text{CuK}\alpha$ radiation of wavelength 0.154098 nm and a graphite monochromator.

Transmission electron micrograph (TEM) images of the materials, after surfactant extraction, were recorded with a JEOL 2000FX transmission electron microscope. The TEM samples were prepared by moving lacey carbon TEM grids (Ted Pella Inc) through a powder sample, thereby allowing the smallest particles to be mounted on the grid.

Morphology of the particles was determined by scanning electron microscopy (SEM). Samples were dispersed in ethanol, sonicated for about 15 minutes and mounted on the SEM stage. After evaporating the ethanol, the samples were coated with gold by sputtering to provide a conductive coating. The samples were analyzed using a Hitachi S3200 scanning electron microscope.

Particle size analysis was performed by dynamic light scattering at 90° using a Brookhaven 90Plus particle analyzer. Agglomerated particles, which were larger than the limit (3 μm) of the Brookhaven 90Plus instrument, were analyzed by laser diffraction using a Horiba Partica LA-950 particle size analyzer. The samples were dispersed in

ethanol and sonicated for 15 minutes before analysis. Internal sonication and agitation was used during particle analysis with the Partica LA-950.

5.3.4 Partitioning of anthraquinone dyes onto functionalized mesoporous silica

Partitioning of the anthraquinone dyes was measured between the silica materials and standard F-SPE solvents (80 vol% methanol-20 vol% water solution (the fluorophobic solvent system) and 100% methanol (a more fluorophilic solvent)). Initial dye solution concentrations in the two solvent systems, provided in Table 5.2, range from 4.27×10^{-5} mol/L to 1.10×10^{-4} mol/L. An advantage of the anthraquinone dyes is the ability to quantify their concentration in dilute solutions and sparingly soluble solvent systems. Initial solution concentrations were selected based on the solubility limit of the dyes in the specific solvent systems. For the partition analysis, 0.1 g of functionalized silica was added to 2 ml of the dye solution. The adsorption of the dye on the silica materials was monitored by the depletion of the dye from solution. Dye concentration in solution was determined from the measured UV-vis absorbance of the FC-dye (475 nm) or the HC-dye (595 nm). Equilibrium partitioning behavior is reported at 96 hours. Partitioning behavior from dilute solutions is reported as a partition coefficient, K , calculated in units of g/L as $C_{\text{solid}}/C_{\text{liquid}}$, where C_{solid} = mols adsorbed/g solid and C_{liquid} = mols/L in solution.

5.3.5 Fluorous-solid phase extraction (F-SPE)

F-SPE cartridges were prepared by packing 0.2 g or 0.4 g of sample in a 1 ml syringe. Whatman filter paper, placed on the bottom of the syringe prior to loading the material, was used as a frit. The packed columns were conditioned with 1 ml of 80 % methanol-20 % water solution.

The elution of the dyes through a 0.4 g packed column of F₈H₂ functionalized mesoporous silica or commercial silica gel was measured as a function of the solvent volume eluted, an approach which resembles a chromatographic separation. A mixture of the FC- and HC-tagged dyes was prepared by adding 5 mg of each dye to 2 mL of N,N-dimethyl formamide. 20 µL of the dye mixture was loaded onto the conditioned columns. The dyes were separated by gradient elution. The HC-dye (blue dye) was eluted with 80% methanol-20% water, followed by 100% methanol to elute the FC-dye (orange dye). Fractions of 0.1 mL were taken as the eluent was pushed through the column. Each of these 0.1 mL fractions was combined with 1.9 mL of methanol and the concentration of the individual dyes in the eluent was determined by UV-vis spectroscopy. The elution solvent was switched to methanol when the recovery of the hydrocarbon-tagged dye with additional 80% methanol-20% water solution was not observable by UV-vis.

The separation performance (yield and purity) of fluoro-functionalized mesoporous silica and commercially-available silica gel for solid phase extraction was determined using vacuum (20 in Hg (67.7 kPa) to 25 in Hg (84.7 kPa)) to draw the eluent through the SPE columns. Standard SPE columns are designed such that samples are either pulled by vacuum or pushed through the column;²³⁴ however, most recent SPE columns are mounted on vacuum manifolds and samples drawn by vacuum. 20 µL of the dye mixture was loaded onto 0.2 g of the packed material in the conditioned columns. Gradient elution of the dyes employed an 80% methanol-20% water solution followed by 100% methanol. The elution solvent was switched to methanol when the recovery of additional HC-dye in 80% methanol-20% water solution was not observable by UV-vis.

Solvent volumes of 1.2 mL to 2 mL were used to elute each dye, depending on the solid adsorbent. Each of the two eluted fractions (hydrocarbon phase and fluorocarbon phase) was diluted with methanol to a volume of 2 mL for compositional analysis of the dyes by UV-vis spectroscopy.

5.4 RESULTS AND DISCUSSION

Mesoporous materials were synthesized as a function of surfactant template (CTAB, HFOPC, or HFDePC) and fluorinated chain length of the silica precursor (F_6H_2 or F_8H_2) using a “one pot” synthesis approach. Fourier transform infrared spectroscopy (FTIR) provides evidence of functional group incorporation and complete surfactant removal in the surfactant templated materials (Figure 5.2). Mesoporous silica displays peaks characteristic of silica at 466 cm^{-1} , 802 cm^{-1} , 956 cm^{-1} , 1085 cm^{-1} , shoulders at 1220 cm^{-1} , 1641 cm^{-1} (-Si-OH stretch) and a broad band peaking at 3451 cm^{-1} due to attached water and silanols.^{216,235} The peaks at 2856 cm^{-1} and 2925 cm^{-1} in the as-synthesized (unextracted) CTAB template material are due to the characteristic stretching of C-H of the hydrocarbon surfactant template. The disappearance of these peaks (Figure 5.2A), in addition to the disappearance of peaks at 1473 cm^{-1} (C-H bending) and 1493 cm^{-1} (N-C stretching), confirms the complete removal of CTAB.

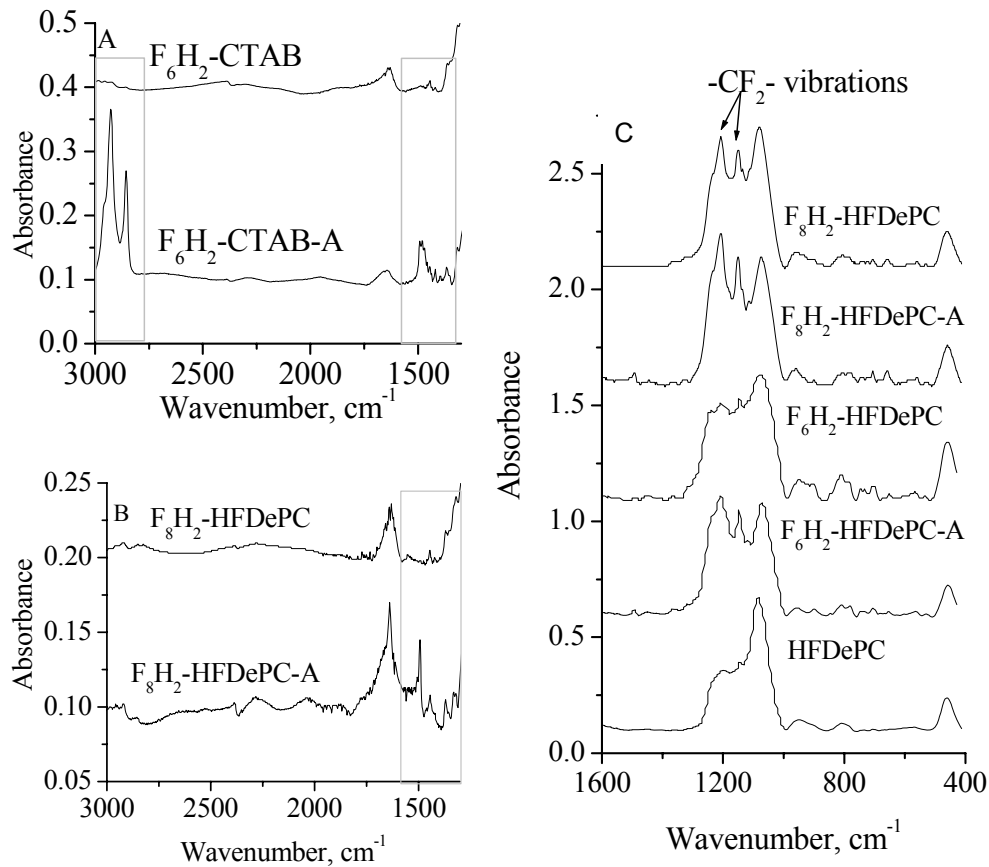


Figure 5.2 FTIR profile of A) F_6H_2 -CTAB template before and after extraction; B) F_8H_2 -HFDePC before and after extraction; and C) HFDePC templated materials. The letter ‘A’ denotes a materials sample before extraction of the surfactant.

Fluorocarbon functional group incorporation is indicated by the presence of the peaks at 1145 cm^{-1} and 1211 cm^{-1} , which are due to $-CF_2-$ vibrations.²¹³ In addition to these peaks due to fluorocarbons, the as-synthesized fluoro-surfactant templated materials display peaks at 1493 cm^{-1} and 1416 cm^{-1} , which correspond to pyridine and $-CH_2-$ bending, respectively.²¹³ These peaks, attributed to the fluorocarbon surfactant, disappear after surfactant extraction. There is also a significant decrease in the characteristic fluorocarbon peak in all fluorocarbon-functionalized materials after extraction. The exception is F_8H_2 -HFDePC, which shows only a slight decrease in the intensity of the

characteristic fluorocarbon peaks. The reduction in the peaks at 1211 cm^{-1} and 1145 cm^{-1} is due to extraction of surfactants in the fluorocarbon template materials and possibly the loss of unincorporated fluorous functional precursor.

TGA was used to quantify the extent of fluorocarbon incorporation in the synthesized materials. The weight loss in the region between $300\text{ }^{\circ}\text{C}$ and $600\text{ }^{\circ}\text{C}$ indicates the decomposition of the organic functional group,²¹⁸ giving the percentage of fluorocarbon functional group in the silica material, as illustrated in Figure 5.3. The incorporation of fluorocarbon groups (in mmol/g solid) is reported in Table 5.1. The temperature range for loss of the fluorocarbon group differs with the fluorocarbon chain length. For example, F_6H_2 -HFDePC loses organic functional groups between 300 to $600\text{ }^{\circ}\text{C}$, while the decomposition range for F_8H_2 -HFDePC is 400 to $600\text{ }^{\circ}\text{C}$ (Figure 5.3). The trend of increased thermal stability of the longer chain fluorocarbon functionalized materials (F_8H_2 relative to F_6H_2) was observed for all surfactant templates.

Increased incorporation of fluorocarbon groups was observed for perfluoro-octyl (F_6H_2) functionalized materials relative to the perfluorodecyl (F_8H_2) functionalized materials for all three surfactant templates. The highest functional group incorporation was observed for F_8H_2 -HFDePC (1.20 mmol/g) and F_6H_2 -HFDePC (1.50 mmol/g) (Table 5.1). The increased incorporation of the fluoro-functional group in the HFDePC templated materials may be due to the improved dispersion of precursors in the ethanol/water homogeneous solution and possibly better solubilization of functional groups in the surfactant micelle core. Although the HFOPC surfactant has a fluorinated tail and its chain length is identical to that of the perfluoro-octyl (F_6H_2) functional group, F_6H_2 -HFOPC had the lowest organic content (0.83 mmol/g) in the F_6H_2 functionalized

set of materials. Thus, matching the fluorinated chain length of the surfactant template and the functional group did not appear to improve incorporation of the functional group in these systems.

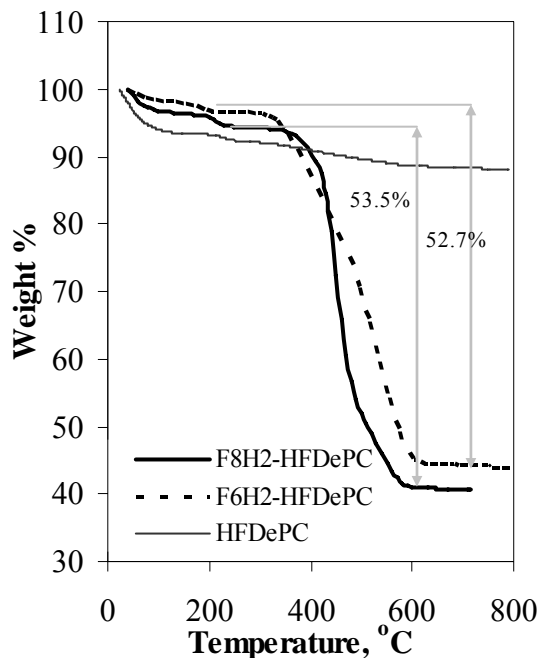


Figure 5.3: Sample TGA plot of HFDePC, F₈H₂-HFDePC and F₆H₂-HFDePC

A comparison of fluoro-functional group incorporation with CTAB and the fluorinated surfactant templates suggests that matching the nature of the functional group-surfactant tail is not sufficient to predict degree of fluorinated group incorporation. The incorporation of fluorinated groups using a hydrocarbon surfactant template, CTAB, was similar to or greater than that of HFOPC templated materials. The mechanism of the fluorinated group incorporation may have been the co-aggregation of the fluorinated functional precursors in the CTAB micelle. Due to the much longer chain length of the CTAB surfactant template, the functional precursors can only act as co-aggregates for

CTAB,¹⁹⁹ which may have resulted in higher functional group incorporation. Similarly, higher incorporation of F₆H₂- was achieved in CTAB templated silica relative to n-C₈F₁₇C₂H₄N(CH₃)₃⁺I⁻ templated silica at identical direct synthesis conditions.²⁰⁵

Pore structure, pore order, materials textural properties (e.g., surface area, pore size) and particle morphology will directly impact the application of these functionalized materials to fluorinated separations. The pore structure and order of the synthesized silica material was examined by powder X-ray diffraction. All CTAB and HFOPC template materials have a 2-D hexagonal pore structure, as interpreted from the presence of the (100), (110), (200) reflections in the XRD profiles (sample profiles provided in Figure 5.4). TEM images (not shown) confirm the hexagonal pore structure of the CTAB and HFOPC template materials. For functionalized materials synthesized with HFDePC only one broad reflection is observed in the XRD profile, which suggests the materials have disordered pore structure. High incorporation of a functional group by direct synthesis may result in less order in the templated material.²³ Thus, the disordered pore structure is consistent with the high functional group incorporation for HFDePC templated materials, as observed from FTIR and TGA analysis. TEM images of the pore structure obtained for HFDePC templated materials reveals particles with spherical morphology but no observable pore structure. However, low contrast due to high fluorocarbon incorporation may mask the pore structure.

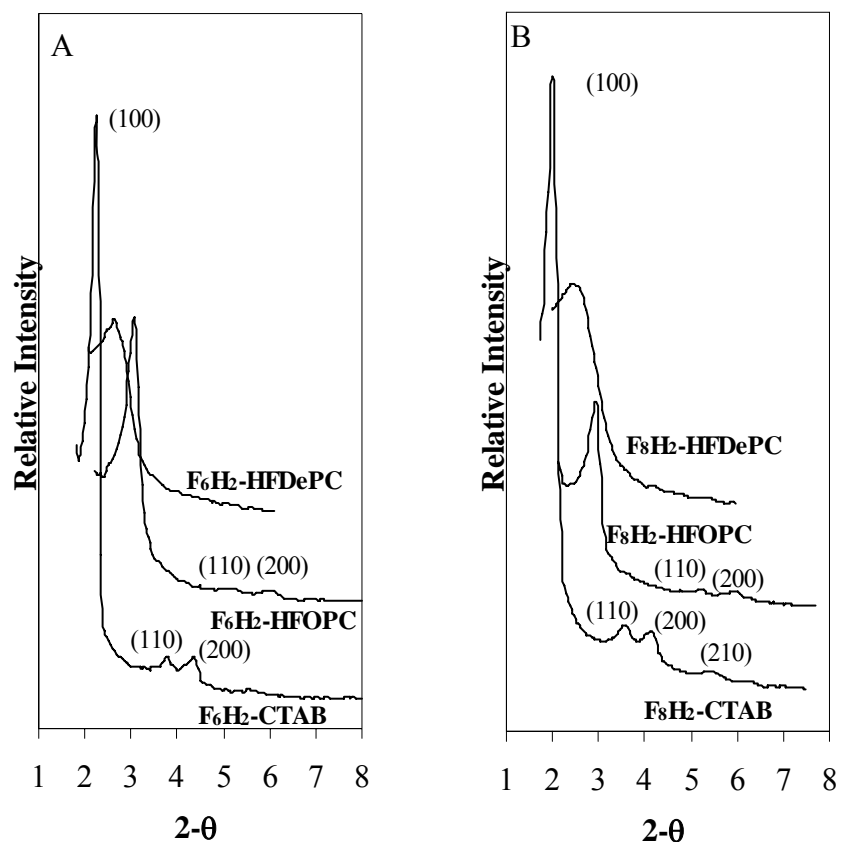


Figure 5.4 Powder X-ray diffraction plots of A) F₆H₂ functionalized B) F₈H₂ functionalized silica materials.

Nitrogen adsorption analysis provides material total surface area (S_t) and pore size (d_p) as a function of the surfactant template / fluoro-functional precursor pair (Table 5.1). For all templates, fluorocarbon functionalization decreases the specific surface area relative to the non-functionalized materials, consistent with an expected decrease in long-range pore order. A decrease in pore size (d_p) upon functionalization was also observed. This effect is expected, and is attributed to the addition of a bulky functional group in the pores and the possible reduction in micellar aggregate size (decrease in headgroup repulsion)²⁰⁰ due to functional group incorporation during self-assembly. The pore size

of CTAB and HFOPC templated materials is similar with the incorporation of F₆H₂ and F₈H₂. In contrast, the difference in pore size of functionalized materials templated with HFDePC (2.03 nm for F₆H₂; 2.32 nm for F₈H₂) is significant. The presence of a unimodal pore size distribution in CTAB template materials suggests that hydrocarbon and fluorocarbon aggregates do not segregate during the templating process.

Table 5.1 Organic content and textural properties of functionalized and non-functionalized materials

Material	Organic Content by TGA, mmol/g (% Theoretical ^{**})	S _t m ² /g	d _p nm	D _p μm
CTAB	-	995	3.67	-
F ₆ H ₂ -CTAB	1.13 (71%)	568	2.57	1.86 (±0.08)
F ₈ H ₂ -CTAB	0.57 (40%)	819	2.58	1.45 (±0.07)
HFOPC	-	811	2.60	-
F ₆ H ₂ -HFOPC	0.83 (52%)	675	2.41	0.77 (±0.10)
F ₈ H ₂ -HFOPC	0.56 (39%)	444	2.44	1.26 (±0.19)
HFDePC	-	739	2.77	-
F ₆ H ₂ -HFDePC	1.50 (94%)	803	2.03	2.58 (±0.18)
F ₈ H ₂ -HFDePC	1.20 (84%)	370	2.32	*22.9(±2.3)
⁺ FluoroFlash	0.83	525	6.00	40.0-63.0

*Agglomerated particle size was obtained by laser diffraction. ⁺Data was provided by Fluorous Technologies Inc, where organic content was given as 10% carbon loading. ^{**}Theoretical organic content is based on complete hydrolysis and siloxane bond formation (i.e. 100% yield); 1.60 mmol/g for F₆H₂ and 1.43 mmol/g for F₈H₂.

Aqueous synthesis (CTAB and HFOPC templated materials) results in irregular particle morphology (Figure 5.5). The connectivity of the particles formed by HFOPC templating is foam-like and broken (Figure 5.5B). In contrast, spherical particles are observed for synthesis in water/ethanol homogeneous medium (HFDePC templated materials) (Figure 5.5C). TEM images confirm the spherical shape of HFDePC

templated silica and the irregular shapes of CTAB and HFOPC templated mesoporous silica (not shown).

The spherical particle morphology of F₈H₂-HFDePC is comparable to other silica particles synthesized in ethanol-containing ammonia solutions.^{91,92} Particle sizes determined by dynamic light scattering are consistent with SEM (less than 2 μm) for CTAB and HFOPC templated silica (Table 5.1). The particle size of F₈H₂-HFDePC is between 1 μm – 2 μm from the SEM image. Effective hydrodynamic diameters of HFDePC templated silica particles are higher than observed by SEM, approximately by an order of magnitude for F₈H₂-HFDePC, meaning that the particles remain agglomerated in ethanol solution after 15 minutes of sonication.

5.4.1 Silica materials as packing for dyes separation

The potential to use fluoro-functionalized mesoporous materials for solid phase extraction was examined based on the separation of two dyes derived from anthraquinone, one containing a fluorinated tail (1-fluoro, 4-pentadecafluoro-1,1-dihydro-octylamino-anthraquinone (orange dye)) and one containing a hydrocarbon tail (Bis(butylamino)anthraquinone (sudan blue II dye)) (Figure 5.1). Anthraquinones are drug components with anti-inflammatory properties and potent anticancer activity,²³³ and represent model fluorous and hydrocarbon tagged systems. This pair of dyes, as well as the elution solvent systems, was previously employed to demonstrate F-SPE using fluorous-functionalized silica gel.²³⁶

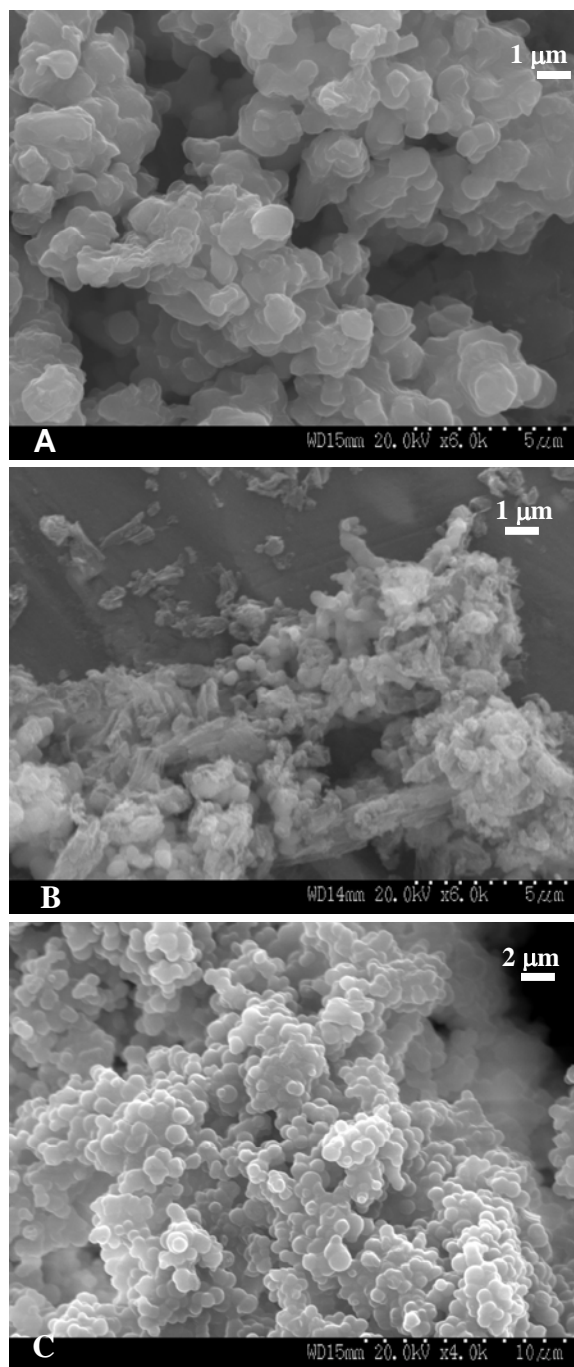


Figure 5.5 SEM image of A) $\text{F}_8\text{H}_2\text{-CTAB}$ B) $\text{F}_8\text{H}_2\text{-HFOPC}$ and C) $\text{F}_8\text{H}_2\text{-HFDePC}$

The separation of the fluorocarbon- and hydrocarbon-tagged dyes on fluoro-functionalized silica is illustrated in Figure 5.6, which shows the elution of the dyes from a column using 80% methanol-20% water (the “fluorophobic” solvent), which elutes the

HC-dye (blue) followed by 100% methanol (a more “fluorophilic” solvent), which elutes the FC-dye (orange). A narrower elution band is observed for the functionalized mesoporous silica (Figure 5.6C) relative to the commercially available silica particles (Figure 5.6B). The narrow elution band observed for the mesoporous silica materials is in agreement with high column efficiencies usually obtained for columns packed with less than 5 μm sized monodispersed particles.²³⁵ All fluoro-functionalized materials were capable of separating the dyes; non-functionalized materials did not provide a separation.

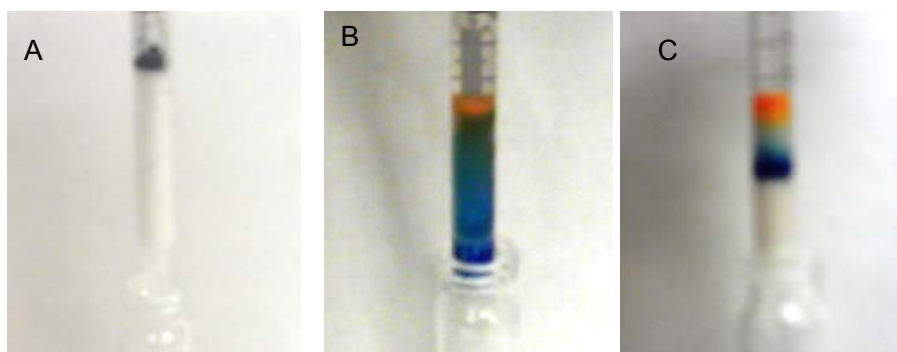


Figure 5.6 A) Mixture of HC- and FC-tagged anthraquinones loaded on column. Elution behavior of HC- and FC-tagged anthraquinone (blue and orange dyes, respectively) on B) fluoroflash fluoro-functionalized silica gel and, C) F_8H_2 - HFDePC column.

Elution profiles on 0.4 g packed columns were used to quantify the enhanced potential of fluorinated-functionalized mesoporous silica for the separation of fluorinated-tagged molecules, as suggested by the narrow elution bands observed in Figure 5.6. Elution profiles of the dyes (measured as the dye absorbance relative to the cumulative solvent elution volume) are shown in Figure 5.7 for elution with an 80% methanol-20% water solution followed by pure methanol. The peak width at half height (w_h), calculated based on Gaussian distribution, is used to quantify the broadness of the elution band.

Narrow elution peaks were observed for the F₈H₂-HFDePC packed column, while peaks observed for F₈H₂-CTAB materials were slightly wider. For both dyes, the largest values of w_h were measured for the functionalized silica gel. In particular, significant tailing in the hydrocarbon dye peak was observed. The small pore size and particle size of the mesoporous silica is expected to contribute to the narrowness of these elution bands.²³⁷ In addition to particle morphology, the degree of fluoro-functionalization, the accessibility of these functional groups to the dyes, and the surface area of the sorbent materials are expected to contribute to differences in elution behavior for the functionalized silica packing material.

The relative affinity of the dyes for the fluoro-functionalized mesoporous materials and the commercial fluoro-functionalized silica gel can be described by their equilibrium partitioning in the elution solvent systems (Table 5.2). Fluorophilic interactions, which are more lipophobic and hydrophobic than hydrocarbon interactions, are evident from the partition behavior between the FC-dye and the FC-functionalized material. Both dyes are relatively soluble in 100% methanol, resulting in low partition values. However, the FC-dye has more affinity for the fluoro-functionalized surface than the HC-dye. The longer chain functional group (F₈H₂-) results in increased fluorophilic behavior (increased FC-dye partition coefficients) relative to the shorter chain fluorinated functionalized (F₆H₂-) mesoporous materials for both hydrocarbon and fluorocarbon templated mesoporous materials.

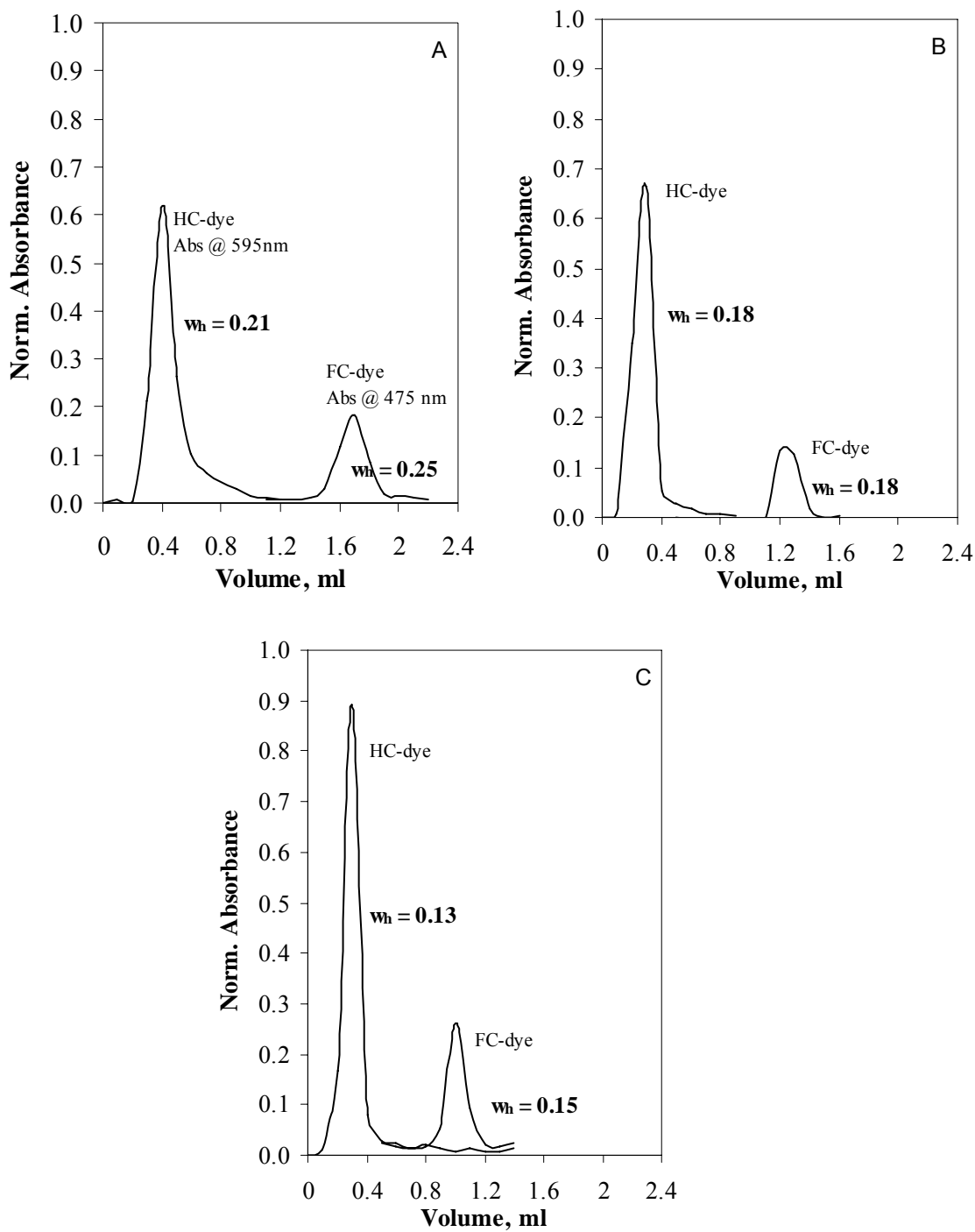


Figure 5.7: Dye elution plots of hydrocarbon-tagged anthraquinone (HC-dye) and fluorocarbon-tagged anthraquinone (FC-dye) on A) Fluoroflash silica gel, B) F_8H_2 -CTAB, and C) F_8H_2 -HFDePC

Pore size or pore blocking may play a role in the increased FC-dye affinity for F₆H₂-CTAB (2.57 nm pore size) relative to F₆H₂-HFDePC (2.03 nm pore size), which has a significantly higher FC-content. The largest dimension of the FC-dye is estimated to be 1.6 nm (estimated using Molecular Modeling Pro Plus). The high partition values observed for commercial silica gel may be attributed to its much larger pore size (6 nm); its surface area and FC content are comparable to those of the synthesized mesoporous materials.

Table 5.2 Partition behavior of HC- and FC- dyes in eluent solvents

Solvent	HC-dye 100% MeOH	HC-dye 80% methanol- 20% water	FC-dye 100% MeOH	FC-dye 80% methanol- 20% water
Initial Dye Concentration	5.86×10 ⁻⁵ mol/L	5.32×10 ⁻⁵ mol/L	1.10×10 ⁻⁴ mol/L	4.27×10 ⁻⁵ mol/L
Material	Partition Coefficient, K, (mol/g)/(mol/L)			
F ₆ H ₂ -CTAB	0.65 (±0.03)	1.10 (±0.39)	0.72 (±0.19)	10.5 (±0.2)
F ₈ H ₂ -CTAB	0.43 (±0.03)	0.75 (±0.09)	1.64 (±0.38)	13.6 (±3.2)
F ₆ H ₂ -HFOPC	0.44 (±0.05)	0.73 (±0.27)	0.80 (±0.09)	6.00 (±0.31)
F ₈ H ₂ -HFOPC	0.61 (±0.05)	0.92 (±0.26)	1.80 (±0.59)	10.1 (±3.3)
F ₆ H ₂ -HFDePC	0.85 (±0.08)	0.74 (±0.03)	0.43 (±0.15)	5.30 (±0.49)
F ₈ H ₂ -HFDePC	0.42 (±0.07)	0.74 (±0.12)	1.10 (±0.32)	14.9 (±0.6)
FluoroFlash	1.70 (±0.33)	1.20 (±0.10)	1.70 (±0.10)	17.2 (±2.1)

Sorbent materials used for solid phase extraction typically have particle size ranges of 40 – 60 µm, a pore size of 5 – 50 nm and surface area of 50 – 500 m²/g.²³² The particle size and pore sizes of all the synthesized materials fall below the usual range of sorbent properties for SPE. Vacuum (approximately 20 mm Hg for 75 mm × 5 mm i.d. column with 12 to 20 mm packing height, depending on material) was required to elute the solvents through the mesoporous silica packing material. The HFOPC template functionalized silica was not an appropriate SPE packing material because of the large

pressure drop required to elute solvent through the column. The irregular particle structure of materials templated with HFOPC (Figure 5.5B) may have contributed to the increased pressure drop.

The F-SPE separation performance (yield and purity) using mesoporous silica was analyzed using 0.2 g of materials packed in syringe cartridges (Table 5.3). The performance of the fluoro-functionalized silica templated with CTAB and HFDePC templates was comparable to the commercial fluorocarbon functionalized silica gel (Table 5.3). FC-dye yields for F₈H₂-HFDePC, F₈H₂-CTAB and FluoroFlash silica gel were greater than 80%. All FC-dye eluents had purities greater than 98%. The affinity of the functionalized silica materials for fluoro-tagged species may hinder its recovery, where methanol may not be sufficiently “fluorophilic” to efficiently remove the FC-tagged molecule. In contrast, the HC-dye has minimal affinity for the fluoro-functionalized silica and is essentially washed off the column, resulting in high yields.

Table 5.3 Anthraquinone dye separation by fluorosolid phase extraction (F-SPE) using a 0.2 g packed column

Sample	Elution of FC-Dye		Elution of HC-Dye	
	Yield	Purity	Yield	Purity
F ₆ H ₂ -CTAB	79.2(± 0.4)	99.6(± 0.3)	89.9(± 3.2)	85.0(± 3.3)
F ₈ H ₂ -CTAB	82.4(± 3.0)	98.3(± 0.3)	97.3(± 1.2)	90.6(± 4.3)
F ₆ H ₂ -HFDePC	76.7(± 1.1)	98.9(± 1.1)	93.0(± 0.6)	91.7(± 2.8)
F ₈ H ₂ -HFDePC	87.8(± 5.8)	99.3(± 0.4)	97.0(± 2.8)	97.4(± 1.1)
Fluoroflash Silica Gel	81.4(± 5.4)	98.9(± 0.3)	93.2(± 1.9)	85.7(± 0.8)

The lower yield of the FC-dye and the associated lower purity of the HC-dye eluent on F₆H₂ functionalized mesoporous silica are consistent with its lower affinity for the FC-dye. Separation using the functionalized silica gel resulted in lower purity of the HC-dye

eluent relative to the F₈H₂-HFDePC silica packing material, and comparable to that of F₈H₂-CTAB and F₆H₂ silica materials.

5.5 CONCLUSIONS

The ability to use fluorinated surfactant templating to synthesize ordered silica with a high degree of long chain fluorocarbon incorporation, appropriate for fluorous separations, was demonstrated. Fluorocarbon functionalized mesoporous silica materials have been synthesized by direct ('one-pot') synthesis using a hydrocarbon surfactant template, CTAB, and cationic fluorocarbon surfactant templates, HFOPC and HFDePC. Matching the fluorinated functional precursor with a fluorinated surfactant did not result in improved incorporation. Also, there was no evidence of the segregation of the hydrocarbon surfactant and the fluorinated precursors during the synthesis of fluoro-functionalized CTAB templated mesoporous silica. Similarly, a match between the FC-chain length of the precursor and the surfactant (i.e., F₆H₂-HFOPC material) was not necessary to achieve high fluorocarbon incorporation. The highest degree of fluorocarbon incorporation in the mesoporous material was achieved using a homogenous ethanol/water solution synthesis, which was required to achieve order in HFDePC templated materials. Synthesis in an ethanol/water medium also resulted in regularly-shaped spherical particles that were appropriate as packing materials for F-SPE. The partitioning behavior of the FC-dye and HC-dye in the elution solvent systems is consistent with the degree of functional group incorporation and the pore size of the functionalized silica materials. The separation yield and purity of HC-tagged and FC-tagged molecules obtained using mesoporous silica is comparable to that of commercially available fluoro-functionalized silica gel. However, the narrow separation band observed

in mesoporous silica, and the ability to tailor its pore size and functionality suggest that fluorocarbon functionalized nanoporous silica materials have great potential for application in F-SPE.

CHAPTER 6

DIRECT SYNTHESIS AND ACCESSIBILITY OF AMINE-FUNCTIONALIZED NANOPOROUS SILICA

6.1 SUMMARY

3-Aminopropyl (AP) functionalized silica is synthesized by the ‘one-pot’ (direct) synthesis method using cationic fluorinated surfactants ($C_6F_{13}C_2H_2NC_5H_5Cl$ (HFOPC) and $C_8F_{17}C_2H_2NC_5H_5Cl$ (HFDePC)) as templates. The degree of amine incorporation and material properties (pore structure and order, pore size and surface area) synthesized using a 10:1 molar ratio of tetraethoxysilane (TEOS) to amine functionalized silica precursor (3-aminopropyltriethoxysilane, APTES) are compared to silica synthesized with a traditional hydrocarbon surfactant template, $C_{16}H_{33}N(CH_3)_3Br$ (CTAB). 3-Aminopropyl silica synthesized with CTAB has 2-D hexagonal pore structure; the order and surface area decreases for the fluorinated surfactant templated material. Greater amine incorporation is also achieved in the CTAB templated material (1.44 mmol/g) relative to the fluorinated surfactant templates, where the lowest amine incorporation is measured for the longer chain fluorinated surfactant (0.92 mmol/g).

CO_2 sorption and fluorescein isothiocyanate incorporation are used to probe the accessibility and surface properties of the amine functionalized silica. Due to the significant reduction of total surface area with amine functionalization (reduction by as much as $635\text{ m}^2/\text{g}$ for HFOPC templated silica when compared to non-functionalized silica), similar levels of CO_2 sorption are observed per gram of material for

functionalized and non-functionalized material. However, the interaction of CO₂ with accessible amines results in higher CO₂ sorbed per surface area in amine functionalized silica than non-functionalized silica. For example, amine-functionalized silica templated with HFDePC captures 83.2 (± 2.3) μg/m² of pure CO₂ at 30 °C as compared to 32.0 (± 0.1) μg/m² for HFDePC templated silica. Although, amine-functionalized silica templated with HFDePC has the lowest amine incorporated, the material adsorbs more CO₂ per surface area than amine-functionalized silica templated with CTAB (despite higher amine incorporation). The role of the non-functionalized silica surface in CO₂ sorption is highlighted by extending the direct synthesis technique to “CO₂-philic” fluorocarbon and fluorocarbon-amine bi-functionalized silica material, which display reduced affinity for CO₂ adsorption compared to non-functionalized and 3-aminopropyl functionalized (AP-) silica.

6.2 INTRODUCTION

Synthesis of organic functionalized nanoporous silica is an active research area because of the widespread application of these high surface area materials in sensing, catalysis and separation. Nanoporous silica is characterized by very large surface areas, large pore volumes and narrow pore size distributions. The pore size and structure can be tailored for specific applications through the choice of pore template and synthesis conditions. Surfactant templated synthesis of porous silica is based on the sol-gel process, in which precursors such as alkoxysilanes are hydrolyzed and condensed in the presence of a structure directing agent (template). Based on the synthesis conditions, the porous

silica obtained can possess ordered pore structures such as hexagonal, cubic, and lamellar or may have disordered pore structure.⁷⁶

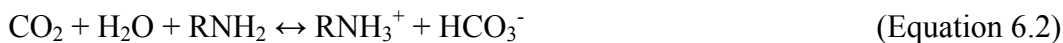
Since the discovery of the M41S family of materials⁵ various organic functional groups have been incorporated into nanoporous silica, by means of post-synthesis grafting and direct co-condensation²¹. Direct synthesis is the co-condensation of a mixture of tetraalkoxysilane and organic functionalized alkoxy silane, which yields functionalized mesoporous silica. Synthesis of functionalized nanoporous silica by co-condensation results in high functional group incorporation²² and uniform distribution of functional groups in the material.

Amine functionalized silica have been widely synthesized; the high reactivity of amines provide varied applications for these materials. Nanoporous silica functionalized with amine groups have been applied in metal removal from environmental waste^{182,233}, gas separation²³⁷⁻²³⁹, chromatography²⁴⁰ and as catalysts²⁴¹. Presently, the synthesis of amine functionalized mesoporous silica mainly utilizes traditional hydrocarbon cationic surfactants (e.g. CTAB)⁶, anionic surfactant (e.g. sodium dodecylsulfate, SDS)⁷ or non-ionic surfactants⁸ and block co-polymers⁹ as templates. Fluorinated surfactant templates for amine functionalized materials are yet to be investigated. Fluorinated surfactants possess higher hydrophobicity than hydrocarbon surfactants, which results in lower surface tensions and critical micelle concentrations.⁵¹ These properties allow for the formation of small micelles, and a broad range of nanoscale self assembled structures^{53,171} that are more stable, better organized and more rigid¹⁷² than their hydrocarbon analogues.

Cationic fluorinated surfactants (a series of perfluoroalkylpyridinium chloride) have recently been demonstrated as templates for the synthesis of nanoporous silica^{10,12-15} with varied particle morphology (irregular, spherical, elongated) and pore structures (disordered, hexagonal, mesh phase). The morphology and pore structure are a function of synthesis conditions, surfactant structure and chain length. The high hydrophobicity of fluorocarbon materials may allow better incorporation of hydrophobic functional groups during direct synthesis. Our research team has investigated the direct synthesis of vinyl¹⁸¹, perfluoro-octyl, n-octyl, perfluoro-decyl and n-decyl functionalized nanoporous silica using fluorinated surfactant templates (HFOPC and HFDePC).²⁴² The type of functional group (hydrocarbon or fluorocarbon) and functional group chain length affect pore size, order and surface area of the functionalized silica. The incorporation of a vinyl group, which is short and is therefore incorporated in the palisade region of the surfactant micelle, led to substantial decrease in pore size relative to the non-functionalized silica, while maintaining high surface area.¹⁸¹ In contrast, minimal pore size reduction was observed when fluorocarbon and hydrocarbon silica precursors were incorporated in templated silica in the presence of cationic fluorinated and hydrocarbon surfactants.²⁴¹ These longer chain tails (perfluoro-octyl, n-octyl, perfluoro-decyl, n-decyl) alkoxy silane precursors most likely acted as a co-surfactant, inserting directly into the micelle during self-assembly.⁶⁹ This study examines the incorporation of a hydrophilic reactive functional group (amine) during the templating of silica by fluorinated surfactants.

This study uses CO₂ sorption, as well as the reactivity of a fluorescent probe molecule, to determine the accessibility and surface properties of amine functionalized

silica. Amine groups react reversibly with CO₂, forming carbamate in the absence of water (Equation 6.1) and bicarbonate (or carbonate) if water is present (Equation 6.2).²⁴²



The reaction of CO₂ and amines favors CO₂ capture and storage, an approach used in industrial plants to clean flue gases and also by the natural gas industry for the removal of acidic gases (e.g., CO₂ and H₂S) from crude natural gas.²³⁸ Commercial CO₂ capture techniques employ liquid alkanolamines (i.e., monoethanolamine (MEA), diethanolamine (DEA), methyldiethanolamine (MDEA), and triethanolamine (TEA)) in absorption-stripping processes.²⁴⁴ The drawback to this process is the high energy cost required during solvent regeneration and equipment replacement due to corrosion.²⁴⁵⁻²⁴⁷ Use of solid adsorbents for CO₂ capture and storage may provide an efficient, cost effective alternative since the adsorbents are regenerated with minimal energy consumption. Nanoporous ceramics (e.g. silica) are of particular interest as an adsorbent for CO₂ capture because of their very large surface areas, large pore volumes, narrow pore size distributions and numerous adsorption/reactive sites that can be introduced by functionalization.²⁴⁸ Amine incorporated porous silicas have been investigated for CO₂ capture from gas streams of varied CO₂ compositions, a range of system temperatures, and in the presence and absence of moisture.^{238,249,250} Metal (e.g. Al, Fe and Cu) incorporated silica has also been proposed for CO₂ capture.²⁵² CO₂ separation utilizing ceramic membranes (e.g. TiO₂ and γ -Al₂O₃) functionalized with fluoro-silanes²⁵³ have been investigated. CO₂ exhibited a permeability greater than 20×10^{-14} mmol m⁻¹ sec⁻¹ Pa⁻¹ compared to 0.28×10^{-14} mmol m⁻¹ sec⁻¹ Pa⁻¹ for N₂.²⁵³ The high CO₂ permeability in the

fluoro-silane grafted TiO_2 is suggested to be due to solubility-diffusion transfer mechanism as a result of the CO_2 -philic property of fluorocarbons.²⁵²

In this chapter we describe the direct synthesis and accessibility evaluation (by fluorescent molecule (FITC) reaction and CO_2 capture) of 3-aminopropyl functionalized mesoporous silica. The degree of amine incorporation and materials properties are investigated as a function of type of surfactant template (hydrocarbon or fluorinated) and synthesis conditions (addition of ethanol). We also test the hypothesis that incorporating a hydrophobic functional group, a fluorocarbon, in addition to the reactive amine group in the silica will minimize non-specific surface interactions, isolating the effect of the amine in further application of the functionalized silica. Thus, the direct synthesis and amine accessibility of bi-functionalized (3-aminopropyl and tridecafluoro-1,1,2,2-tetrahydrooctyl) nanoporous silica is also investigated.

6.3 MATERIALS AND METHODS

Tetraethoxysilane (TEOS) with purity of 99%, 3-aminopropyltriethoxysilane (APTES, 95% purity) and tridecafluoro-1,1,2,2-tetrahydro-octyltriethoxysilane ($\text{F}_6\text{H}_2\text{TES}$, 95% purity) were purchased from Gelest Inc. CTAB (Figure 4.2) was obtained from Sigma with 99% purity. The cationic fluorinated surfactants templates used are $\text{C}_6\text{F}_{13}\text{C}_2\text{H}_4\text{C}_5\text{H}_5\text{NCl}$ (tridecafluoro-1,1,2,2-tetrahydro-octyl pyridinium chloride) and $\text{C}_8\text{F}_{17}\text{C}_2\text{H}_4\text{C}_5\text{H}_5\text{NCl}$ (heptadecafluoro-1,1,2,2-tetrahydro-decyl pyridinium chloride), labeled HFOPC and HFDePC, respectively (Figure 4.2). The surfactants were synthesized as previously described²⁶. De-ionized ultra-filtered water (DIUFW) was purchased from Fisher Scientific. All solvents were analytical grade.

In tables and figures, non-functionalized materials were labeled simply as their surfactant templates (i.e., CTAB, HFOPC, and HFDePC). CTAB-templated material is commonly referred to as MCM-41 for hexagonal pore structured silica. The 3-aminopropyl functionalized mesoporous silica was synthesized using a 10:1 molar ratio of TEOS to APTES. The 3-aminopropyl functional materials are labeled with the prefix AP and the surfactant used: AP-CTAB, AP-HFOPC and AP-HFDePC. HFDePC templated materials were synthesized in a homogeneous water/ethanol solution, where the addition of ethanol facilitated surfactant dissolution. The bi-functionalized silica materials were synthesized by utilizing a 10:2.5:1 molar ratio of TEOS: F₆H₂TES: APTES and labeled as AP-F₆H₂-CTAB, AP-F₆H₂-HFOPC and AP-F₆H₂-HFDePC.

The materials were prepared by first adding the surfactant to de-ionized ultra-filtered water and stirring the mixture for 5 minutes. NH₄OH (catalyst, 28 - 30% solution from Malinckrodt) was then added with continuous stirring of the mixture for another 10 minutes, after which TEOS (and F₆H₂TES) was slowly added. For aminopropyl functionalized silica, APTES was added to this mixture after 20 seconds. APTES hydrolyzes faster than TEOS and F₆H₂TES since it is more soluble in aqueous medium, thus a short delay time is required before adding APTES to the solution. The non-functionalized silica materials are synthesized using the identical procedure without addition of functionalized precursor. The mixture was left to age under stirring at room temperature for 24 hours. The molar ratio of the reactants used in the synthesis was 186 DIUFW: 0.184 CTAB (or 0.082 HFOPC): 5.73 NH₄OH:1 TEOS and 0.1 APTES or (0.1 APTES: 0.25 F₆H₂TES) (for functionalized silica) and 136 DIW: 64 Ethanol: 0.197 HFDePC: 18.4 NH₄OH:1 TEOS and 0.1 APTES or (0.1 APTES: 0.25 F₆H₂TES) (for

functionalized silica). The synthesis procedure is based on the room-temperature synthesis of Kumar et al.⁸¹ The mixture was vacuum-filtered after the aging period and left to dry in a vacuum oven at 40°C for 24 hours. An ethanol/HCl solution of 150 ml ethanol and 5 g aqueous HCl was used for the extraction of the surfactant for each batch of materials synthesized. Extraction was accomplished by stirring the dried sample in acidic ethanol for 24 hours. This extraction process was repeated once.

Materials Characterization

Nitrogen adsorption measurements were performed using a Micromeritics Tristar 3000. The materials were degassed at 150°C under flowing nitrogen for 4 hours before performing the adsorption analysis.

Fourier Transform Infrared (FTIR) analysis was performed to verify surfactant removal and functional group incorporation. A small amount (approximately 1 wt%) of the silica sample was pressed with KBr matrix and analyzed using a Thermo Nicolet Nexus 470 FT-IR.

Thermal stability analysis of the functionalized silica was performed by thermogravimetric analysis (TGA) using a Universal V2.5H TA instrument. The materials were analyzed under nitrogen purge with a starting temperature of 35 °C and 10 °C/min ramp rate to 800 °C. The corresponding carbon, hydrogen and nitrogen elemental analysis was performed using LECO CHN-2000 elemental analyzer under flowing oxygen.

Powder X-ray diffraction (XRD) patterns were obtained using a Siemens 5000 diffractometer operating with CuK_α radiation of wavelength 1.54098 Å and a graphite monochromator.

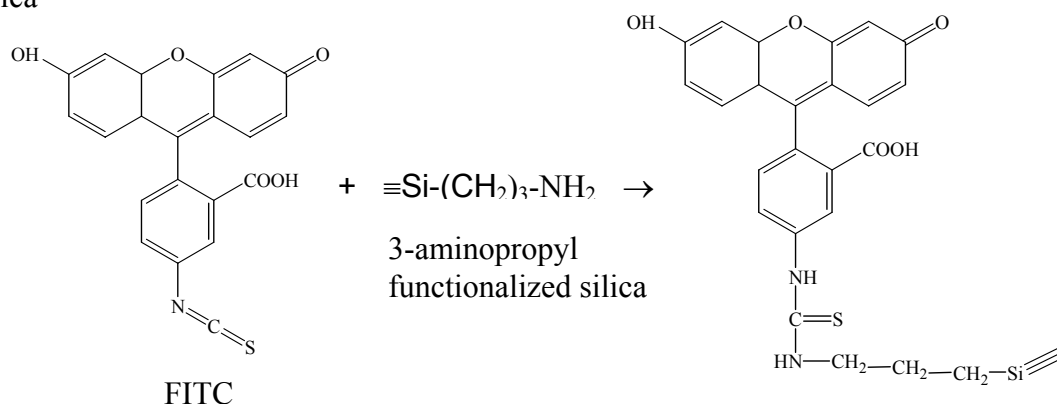
Transmission electron micrograph (TEM) images of the materials, after surfactant extraction, were observed and recorded with a JEOL 2000FX transmission electron microscope. The TEM samples were prepared by moving the lacey carbon TEM grid (Ted Pella Inc) through some of the dry powder sample thereby allowing the smallest particles to be mounted on the grid.

The accessibility of the aminopropyl groups was determined qualitatively through the attachment of fluorescein isothiocyanate (FITC) to the aminopropyl group (Scheme 6.1), resulting in a fluorescent material. The silica sample (0.2 g) was added to a 10 ml solution of FITC in an ethanol/NH₄OH mixture (6.89×10^{-3} mmol/L concentration of FITC) of pH 9. The mixture was stirred overnight, vacuum filtered and washed with more ethanol for 24 hours to remove unreacted FITC. The samples were mounted on glass slide and viewed with a Leica TCS NT SP Laser Scanning Confocal Microscope to confirm FITC incorporation by observing the fluorescence of FITC using an excitation wavelength range of 400 – 500 nm. An HP 8453 UV-vis spectrometer was used to quantify the rate of incorporation of FITC into the functionalized silica by observing the depletion of FITC in ethanol/NH₄OH solution. 10 mg of silica sample was added to 1 ml FITC/ethanol/NH₄OH solution, resulting in an initial absorbance of approximately 1 at a wavelength of 502 nm. The time dependent depletion of FITC from solution was observed over a 6 hour period. The solution was centrifuged for 15 to 20 min before each UV absorbance reading.

CO₂ sorption analysis was performed using a Hi-Res TGA 2950 thermogravimetric analyzer (TA Instruments). Silica samples of about 7 – 14 mg were placed in a platinum pan and loaded onto the TGA instrument. Initially, the temperature

was ramped to 110 °C in the presence of N₂ gas flowing at 120 ml/s to remove adsorbed moisture. The system was maintained at these conditions for 5 minutes and then ramped to the desired temperature (30 °C or 50 °C). The gas was then switched to CO₂ (99% purity) and the system temperature was maintained until CO₂ adsorption was constant (approximately 20 minutes).

Scheme 6.1: Reaction of fluorescein isothiocyanate (FITC) with 3-aminopropyl functionalized silica



FTIR analyses of the CO₂ adsorbed silica samples were performed following CO₂ adsorption to confirm the reaction of CO₂ with the amine group. Approximately 15 minutes after the samples were taken out of the TGA, a small amount (approximately 1 wt%) was pressed with KBr matrix and analyzed using a Thermo Nicolet Nexus 470 FT-IR.

6.4 RESULTS AND DISCUSSION

The incorporation of 3-aminopropyl functionality in mesoporous silica by direct synthesis is demonstrated for CTAB, HFOPC, and HFDePC templated materials.

Materials textural properties (i.e., pore order, pore size, pore volume and surface area) are compared for functionalized and non-functionalized materials using XRD and N₂ adsorption analysis. FTIR analysis provides a qualitative description of amine group incorporation, while CHN elemental analysis of the materials is used to quantify the degree of 3-aminopropyl incorporation. The accessibility of the incorporated amines is examined through the reaction of a fluorescent probe with the amine functional group. CO₂ sorption serves as both a probe of the accessibility of the amine groups and the surface properties of the materials, as well as an example of the potential application of these amine-functionalized materials to CO₂ capture. The materials properties of fluorocarbon (F₆H₂) functionalized silica are described elsewhere,²⁴² but the probing of their surface properties by CO₂ sorption is presented here with results for amine-functionalized and bi-functionalized (amine-fluorocarbon) mesoporous silica.

6.4.1 Chemical Analysis of Functional Group Incorporation

Fourier Transform Infrared Spectroscopy (FTIR) analysis, performed on the functionalized and non-functionalized materials, demonstrates successful removal of surfactant templates and also provides evidence of functional group incorporation (Figure 6.1). The unextracted CTAB templated material (AP-CTAB-A; suffix A denotes unextracted material) displays peaks at ~2850 cm⁻¹ (symmetric stretching of -CH₂-) and ~2920 cm⁻¹ (anti-symmetric stretching of -CH₂-), due to the presence of CTAB surfactant and the incorporated 3-aminopropyl group (Figure 6.1A). These peaks completely disappear in the FTIR profile of non-functionalized silica (CTAB) and are greatly reduced in that of AP-CTAB. In the fluorocarbon surfactant templated amine functionalized silica materials small peaks are evident at ~2850 cm⁻¹ and ~2920 cm⁻¹

before and after extraction (Figure 6.1B). The peak due to symmetric stretching of $-\text{CF}_2-$ observed at $\sim 1145\text{cm}^{-1}$ in unextracted silica (AP-HFOPC-A) is attributed to the presence of fluoro-surfactant template, and disappears after surfactant extraction (Figure 6.1B).

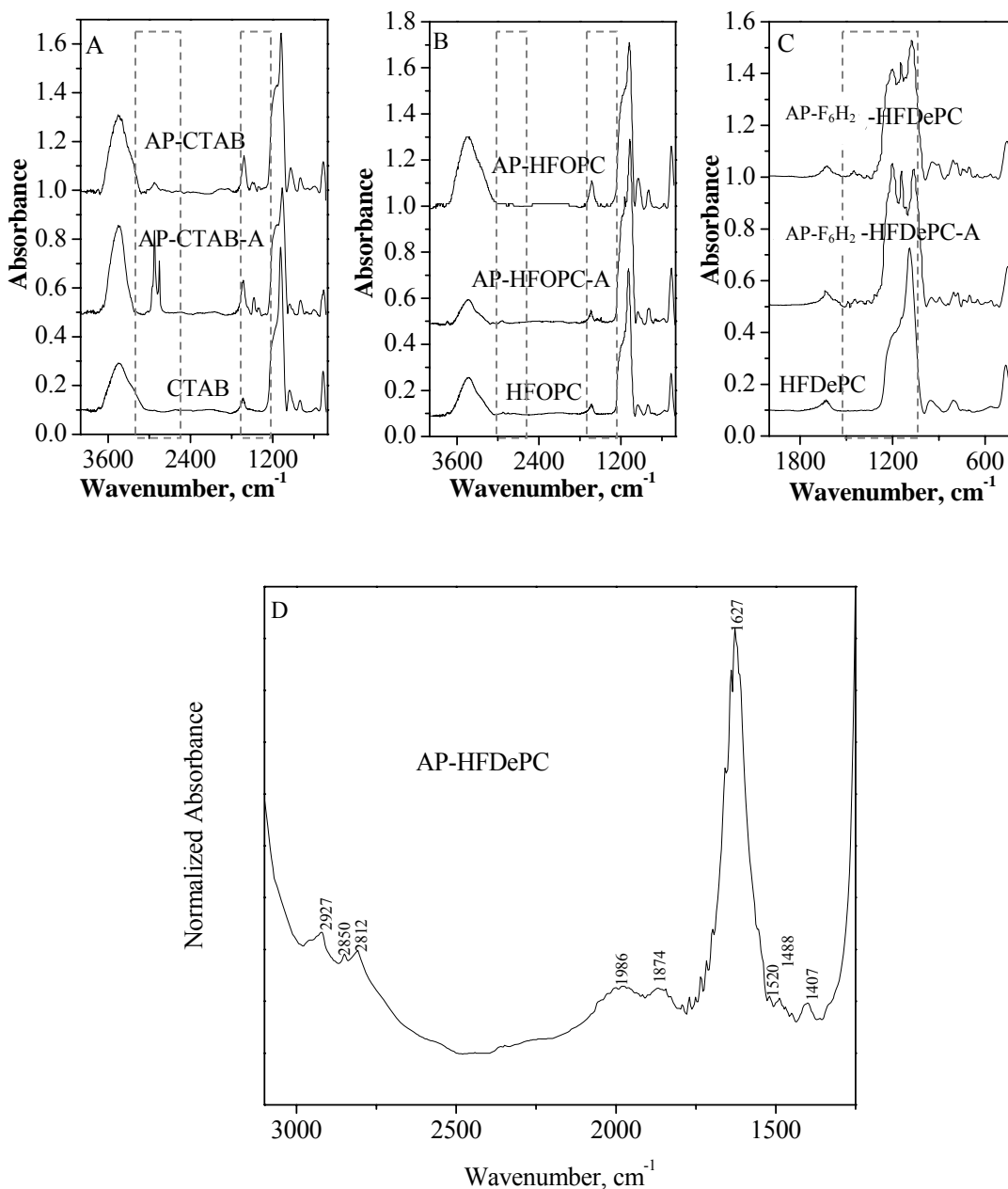


Figure 6.1: FTIR plots of A) CTAB templated AP- silica materials; B) HFOPC templated AP-silica materials; C) HFDePC templated AP-F₆H₂-silica and D) AP-

HFDePC. The suffix –A denotes unextracted samples (samples containing the surfactant template).

In the bi-functionalized silica the peaks at 1145 cm^{-1} and 1211 cm^{-1} (all due to $-\text{CF}_2-$ vibrations; Figure 6.1C) are still present after surfactant extraction and are assigned to the incorporated fluorocarbon functional group. A magnified image of the FTIR reflections observed for AP-HFDePC in the range of 1250 cm^{-1} to 3050 cm^{-1} is provided in Figure 6.1D. This figure highlights the peaks due to the presence of 3-aminopropyl group: the H–C–H scissoring vibration (1407 cm^{-1} , $\sim 1488\text{ cm}^{-1}$), the N-H or H-C-H bend (1520 cm^{-1}), and the H–C–H asymmetric and symmetric stretch (triple peaks observed at $\sim 2812\text{ cm}^{-1}$, 2850 cm^{-1} and $\sim 2927\text{ cm}^{-1}$). These peaks were also observed for AP-CTAB and AP-HFOPC. Characteristic silica peaks are observed in both the functionalized and non-functionalized materials (Figure 6.1). These peaks appear at 460 cm^{-1} , 1100 cm^{-1} and as a shoulder at 1200 cm^{-1} (Si-O-Si vibrations), at 950 cm^{-1} (Si-OH stretch), and as peaks due to adsorbed water (1650 cm^{-1}) and O-H stretching (due to silanols ($\equiv\text{Si-OH}$) and adsorbed water) at 3400 cm^{-1} .^{214,253}

The thermal stability of the 3-aminopropyl functionalized silica was determined by TGA. When increasing the temperature from $35\text{ }^\circ\text{C}$ to $800\text{ }^\circ\text{C}$ at $10\text{ }^\circ\text{C}/\text{min}$, all the materials show an initial weight loss at temperatures less than $150\text{ }^\circ\text{C}$ (shown in Figure 6.2 for AP-HFDePC and AP-F₆H₂-HFDePC). This is due to the loss of water and solvent in the materials. Further weight loss is observed between $150\text{ }^\circ\text{C}$ and $300\text{ }^\circ\text{C}$ and is attributed to the condensation of available silanols.²¹³ Loss of material in the temperature range of $300\text{ }^\circ\text{C}$ to $800\text{ }^\circ\text{C}$ corresponds to the degradation of the 3-aminopropyl group in

AP- materials or the combined decomposition of 3-aminopropyl and perfluoro-octyl groups in the bi-functionalized silica materials.²¹³

Elemental analyses of the samples suggest traces of nitrogen (N) present in the non-functionalized silica (Table 6.1). This contribution is most likely from residual surfactant, and is estimated to be 5 – 10% of the nitrogen observed in the amine-functionalized samples. Analyses of the 3-aminopropyl functionalized silica show that AP-CTAB has the highest incorporation of elemental N (i.e., 3-aminopropyl group; corresponding to a maximum incorporation of 1.44 mmol/g). Surprisingly, lower amine content is observed in AP-HFDePC (0.92 mmol/g), which was synthesized in homogeneous water/ethanol solution. Previous investigation have shown that fluorocarbon and hydrocarbon functionalized silica synthesized using HFDePC template in homogeneous water/ethanol solution has a higher functional group incorporation than CTAB and HFOPC templates.^{181,242} The amount of amine incorporation in AP-HFDePC (0.92 mmol/g) is similar to that of AP-HFOPC (1.04 mmol/g). In the amine functionalized silica, the measured amine contents are similar to (CTAB template) or lower than (fluorocarbon surfactant template) the theoretical aminopropyl content based on the ratio of TEOS:APTES used in the direct synthesis of the materials (1.39 mmol/g). This theoretical organic content is based on complete hydrolysis and siloxane bond formation (i.e., 100% yield).

The theoretical amine content in the bi-functionalized silica (0.58 mmol/g) is lower than the measured values for AP-F₆H₂-CTAB (0.63 mmol/g) and AP-F₆H₂-HFOPC (0.68 mmol/g). This is possibly due to residual surfactants. Bi-functionalized material synthesized in ethanol/water (AP-F₆H₂-HFDePC) has the lowest amine incorporation of

the bi-functional materials similar to the trend observed in the amine functionalized silica.

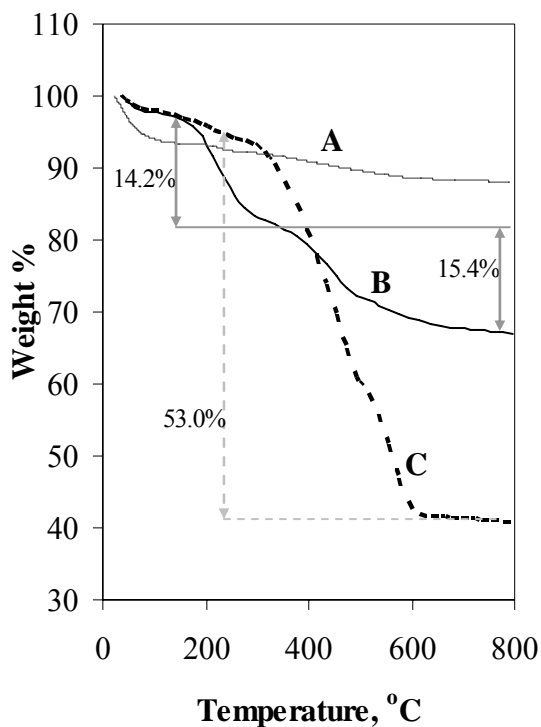


Figure 6.2: TGA plot of A) HFDePC B) AP-HFDePC and C) AP-F₆H₂-HFDePC

Table 6.1 Elemental nitrogen analysis of the non-functionalized and amine-functionalized material

Sample	Theoretical Nitrogen Content, mmol/g	Nitrogen content from Elemental Analysis mmol/g*
CTAB		0.11 (±0.01)
HFOPC	—	0.11 (±0.01)
HFDePC		0.05 (±0.01)
AP-CTAB		1.44 (±0.01)
AP-HFOPC	1.39	1.04 (±0.02)
AP-HFDePC		0.92 (±0.01)
AP-F ₆ H ₂ -CTAB		0.63 (±0.01)
AP- F ₆ H ₂ -HFOPC	0.58	0.68 (±0.02)
AP- F ₆ H ₂ -HFDePC		0.53 (±0.01)

*Standard deviations in parenthesis are based on duplicated analyses

6.4.2 Pore Structure, Size, and Order of Synthesized Materials.

Powder X-ray diffraction was performed to investigate the pore structure and order of the materials following surfactant extraction. 2-D hexagonal pore structure was observed for all the non-functionalized materials (CTAB, HFOPC and HFDePC), as interpreted from the presence of (100), (110) and (200) reflections (Figure 6.3). CTAB-templated materials maintain their well ordered 2-D structures during the incorporation of amines by direct synthesis, as indicated by the presence of the characteristic (100), (110) and (200) reflections (Figure 6.3A). Transmission electron microscopy (TEM) images of AP-CTAB confirm a 2-D hexagonal pore structure (observed as uniform channels in Figure 6.4A). In contrast, XRD of the 3-aminopropyl silica synthesized using the fluorinated templates (AP-HFOPC and AP-HFDePC) resulted in one broad (100) reflection. Corresponding TEM images (Figures 6.4B and 6.4C) show cylindrical pores with no apparent order. The pores in the TEM image appear interconnected and wormhole-like.

The XRD patterns and TEM images suggest differences in material properties due to synthesis in a water/ethanol solution. The XRD pattern of AP-HFDePC has a more intense (100) reflection than that of AP-HFOPC, hence AP-HFDePC could possess regions of worm-like pore structure and 2-D hexagonal ordered pore structure. The TEM image of AP-HFDePC (Figure 6.4C) displays particles of spherical morphology, which is characteristic of materials synthesized in homogeneous water/ethanol solution. The high solubility of the precursor in water/ethanol synthesis medium promotes good dispersion and controlled precipitation of small oligomers, which contributes to the formation of particles with spherical morphology.^{91,220}

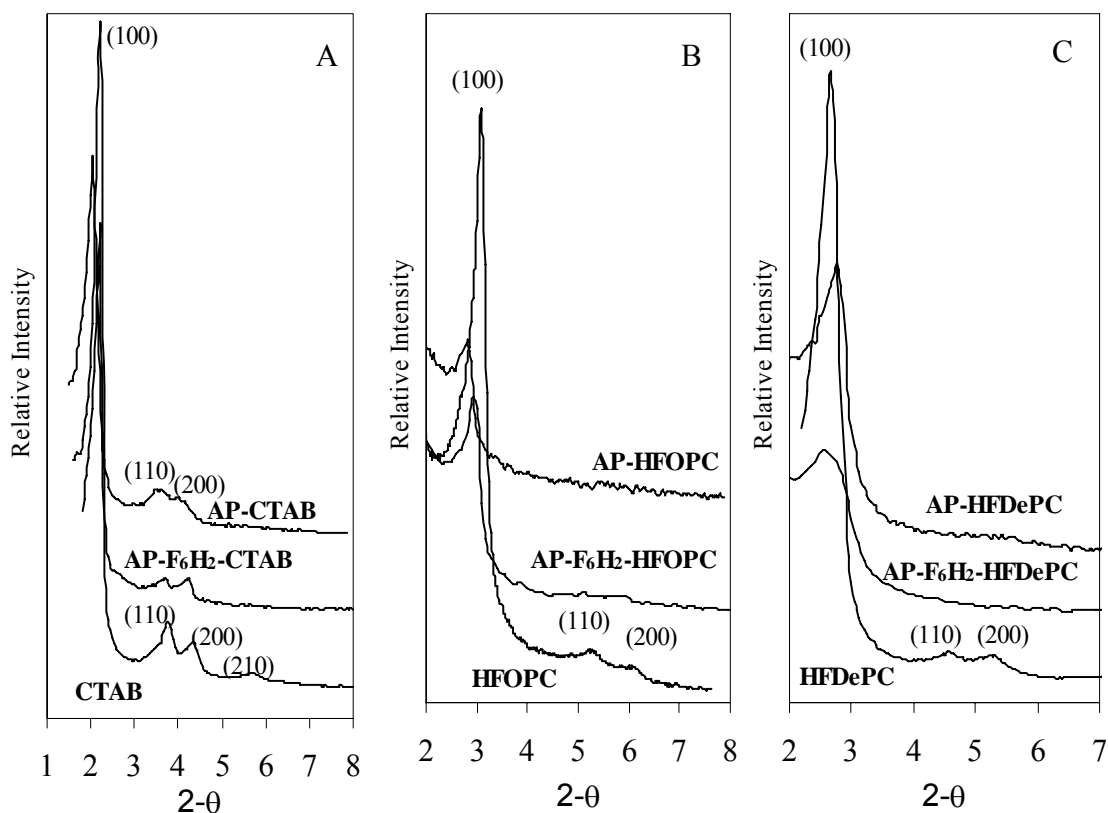


Figure 6.3 Powder X-ray diffraction plots of non-functionalized, amine-functionalized, and bi-functionalized (amine and fluorocarbon) silica materials templated with A) CTAB; B) HFOPC; and C) HFDePC.

The degree of order in the silica mesostructure is dependent on the effect of incorporated organic group on surfactant assembly and relative condensation of silica around micelles.²⁵⁴ The self assembly of the 3-aminopropyltriethoxysilane ($((\text{C}_2\text{H}_5\text{O})_3\text{Si}-\text{C}_3\text{H}_6-\text{NH}_2)$) with the cationic surfactants does not favor incorporation into the surfactant micelles²⁵⁵ as with hydrophobic functionalized silanes. However, the presence of the $-\text{NH}_2$ group (uncharged in basic medium)²⁵⁶ in the functionalized precursor can allow the 3-aminopropyl chain to be randomly oriented, even becoming part of the silica matrix²⁵⁴ which might lead to a reduction in long-range order.

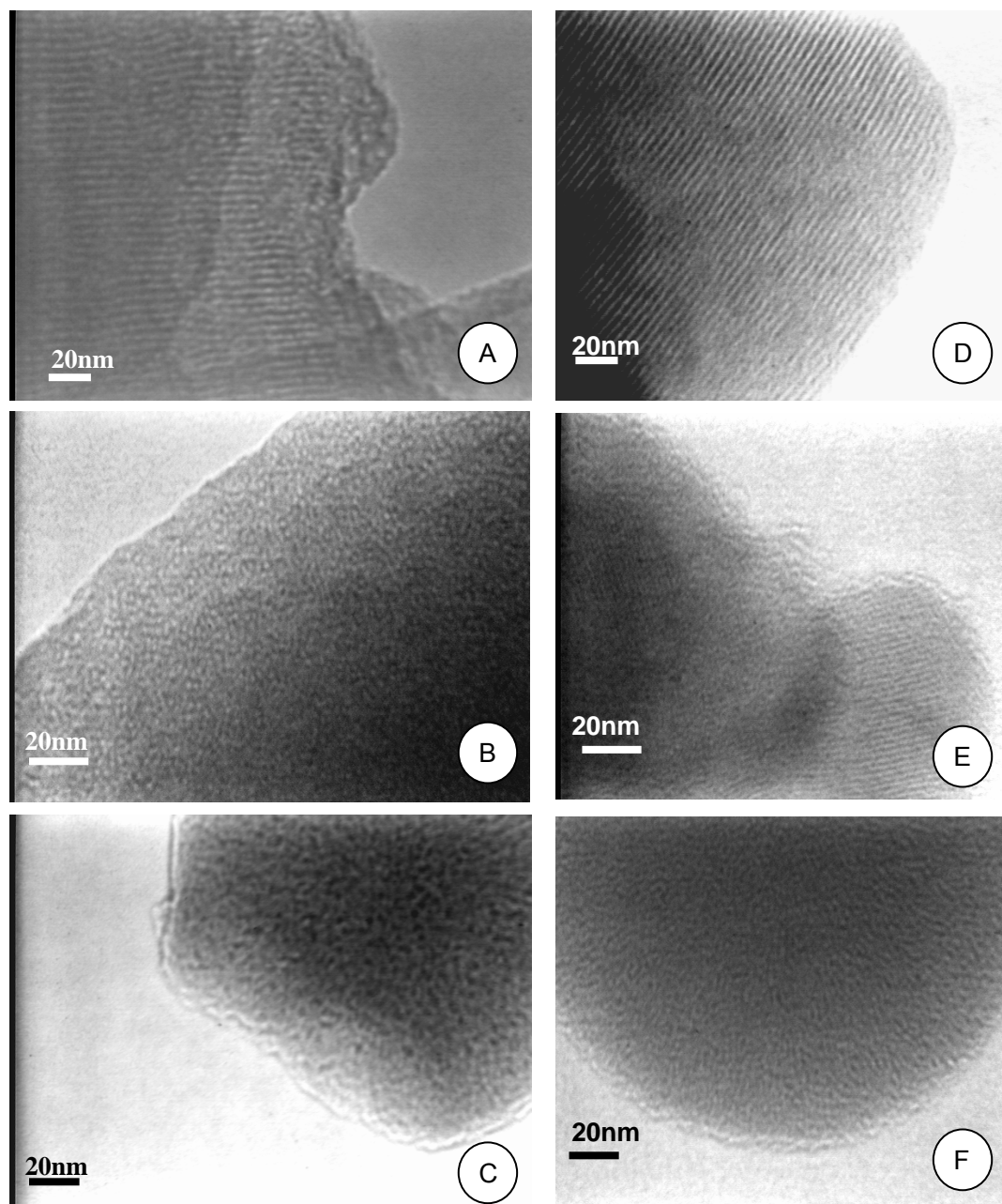


Figure 6.4: Sample TEM images of A) AP-CTAB B) AP-HFOPC C) AP-HFDePC D) AP-F₆H₂-CTAB E) AP-F₆H₂-HFOPC and F) AP-F₆H₂-HFDePC.

The effect of the self-assembly of 3-aminopropyl precursor with the surfactants is more pronounced in the presence of the fluorinated surfactants (silica materials with less long range order than CTAB template materials) which led to disordered pores. Use of TEOS to APTES ratios of 6:1 and 4:1 resulted in completely disordered silica materials

for the fluorocarbon surfactant templates, with no observable XRD reflections. Yokoi et al⁶ also observed a decrease in the order of 3-aminopropyl functionalized silica with increase in APTES to TEOS ratio using CTAB as template and synthesis in a basic medium. They observed ordered pore structure for materials synthesized with a TEOS to APTES ratio of 1:10 and disordered materials at a ratio of 1:5; no silica precipitation occurred for ratios of 7:10 and higher.

The d_{100} spacings of AP-CTAB and AP-HFOPC increase by about 0.33 nm and 0.38 nm, respectively, (Table 2) compared to that of the corresponding non-functionalized silica. An increase in (100) inter-planar spacing was also observed previously for CTAB templated 3-aminopropyl functionalized silica.⁶ This is proposed to be due to the minimal hydrophobic interaction between the uncharged hydrophilic –C₃H₆–NH₂ group and the hydrophobic core of the surfactant aggregate, which does not allow molecules of the organic group to be deeply drawn into the surfactant aggregate core.¹² However, the d_{100} spacing of the functionalized silica synthesized in an ethanol/water solution, AP-HFDePC, decreases slightly.

Incorporating a hydrophobic group in addition to the reactive aminopropyl group should minimize interactions between the silanols on the silica surface and potential adsorbate, reactive, or probe molecules. The pore order of functionalized silica improves with the incorporation of F₆H₂, in addition to the AP functional group, in silica materials templated with CTAB and HFOPC. The intensities of the (110) and (200) reflections of AP-F₆H₂-CTAB and the (100) reflection of AP-F₆H₂-HFOPC increase relative to the non-fluorinated functional material (Figure 6.3). However, a decrease in intensity of the (100) reflection (decrease in order) is observed for AP-F₆H₂-HFDePC compared to AP-

HFDePC. TEM images confirm the 2-D hexagonal pore structure (seen as channels) for AP-F₆H₂-CTAB and AP-F₆H₂-HFOPC and the disordered pore structure for AP-F₆H₂-HFDePC (Figure 6.4D – 6.4F), consistent with the XRD patterns.

As described above, the incorporation of amine groups increases the (100) inter-planar spacing for both AP-CTAB and AP-HFOPC. There is no difference in the d₁₀₀ spacing of AP-F₆H₂-CTAB compared to non-functionalized silica (CTAB), but a slightly larger d₁₀₀ spacing is observed for the fluorocarbon surfactant templated bi-functionalized materials (0.12 nm for AP-F₆H₂-HFOPC and 0.17 nm for AP-F₆H₂-HFDePC) compared to the corresponding non-functionalized silica (Table 6.2). F₆H₂ incorporation resulted in a small decrease in d₁₀₀ spacing for the CTAB template and a slight increase (HFDePC) or no change (HFOPC) in that of the fluorocarbon surfactant template silica (Table 6.2). The observed trend in the (100) inter-planar spacing of the bi-functionalized silica can be rationalized by the combination of the individual effect of the amine and fluorocarbon functional groups on the inter-planar spacing of the AP- and F₆H₂ functionalized silica.

Type IV nitrogen adsorption isotherms (typical for mesoporous materials)¹⁷⁸ are observed for all silica materials (Figure 6.5). The incorporation of the functional groups significantly reduces the sorption capacity of all templated materials. The inflection points in the isotherms move to lower relative pressures after functionalization, corresponding to smaller pore sizes. Analysis of the isotherms using the KJS method, which is based on the modified Kelvin equation,^{154,179,180} reveals a corresponding reduction in pore size (d_p), pore volume (V_p) and total surface area (S_t) (Table 2 and Figure 6.5). However, the pore wall thickness (t_{pw}; difference between hexagonal cell parameter (a₀ = 2d₁₀₀ / 3^{1/2}) and the pore size (d_p)), increases for all functionalized silica

materials (Table 2). This is consistent with the increase in d_{100} spacing observed from XRD analysis.

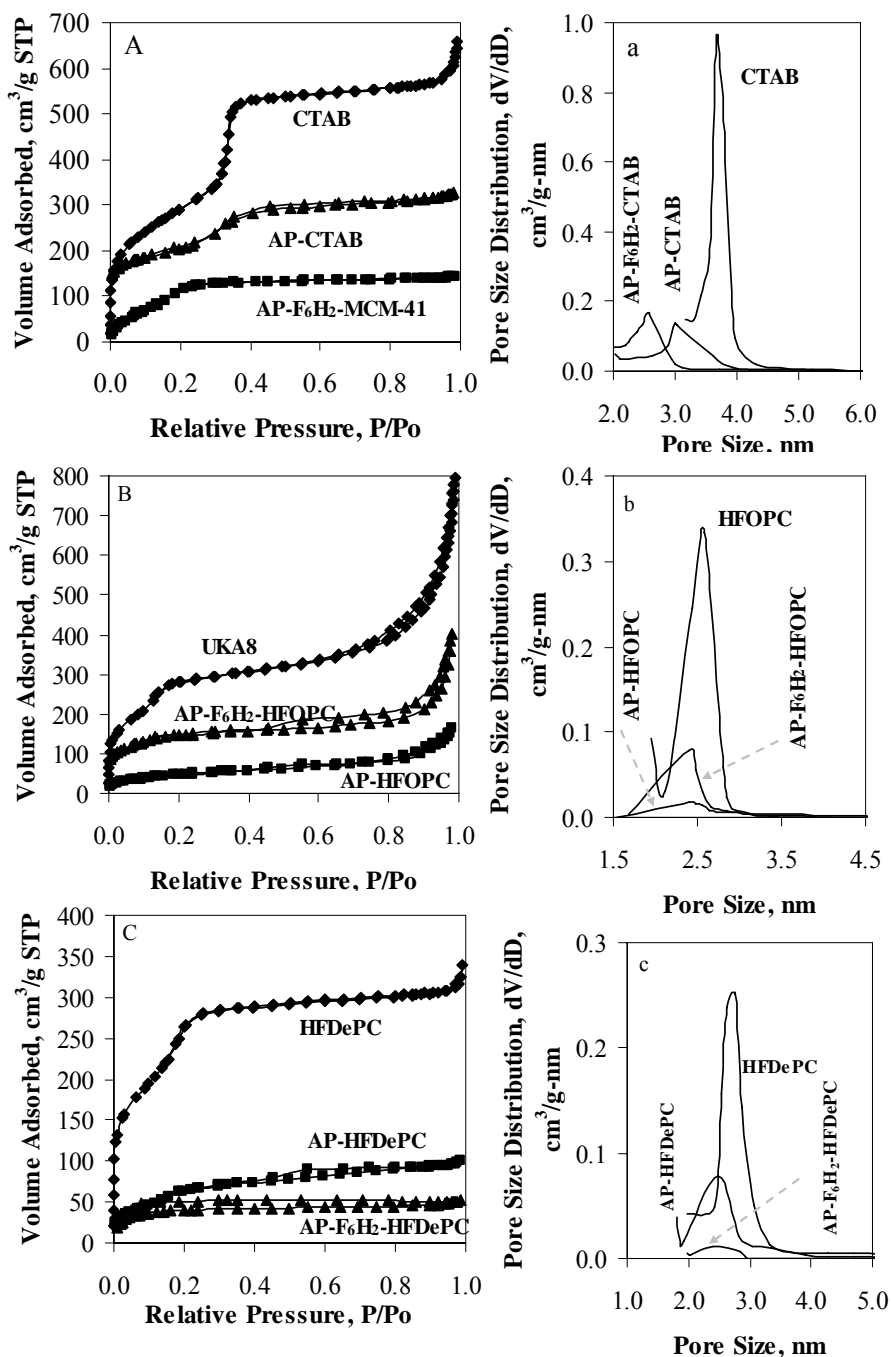


Figure 6.5 Nitrogen adsorption isotherm and pore size distribution of A) CTAB templated materials B) HFOPC templated materials and C) HFDePC template materials.

Table 6.2 Materials textural properties of non-functionalized, amine-functionalized, and bi-functionalized (amine-fluorocarbon) silica as a function of surfactant template

Material	d_{100} nm	S_{total} m^2/g	$S_{external}$ m^2/g	V_p cm^3/g	d_p nm	a_o nm	t_{pw} nm
CTAB	4.01	995	106	0.76	3.67	4.63	0.96
HFOPC	2.87	811	323	0.28	2.60	3.31	0.71
HFDDePC	3.29	739	41.0	0.40	2.77	3.80	1.03
AP-CTAB	4.34	352	52.0	0.27	3.04	5.01	1.97
AP-HFOPC	3.15	176	111	0.03	2.39	3.64	1.25
AP-HFDDePC	3.20	203	26.0	0.12	2.50	3.70	1.20
AP-F ₆ H ₂ -CTAB	4.01	520	15.0	0.25	2.56	4.63	2.07
AP- F ₆ H ₂ -HFOPC	2.99	369	117	0.10	2.39	3.45	0.88
AP- F ₆ H ₂ -HFDDePC	3.46	285	15.0	0.06	2.41	3.99	1.58
F ₆ H ₂ -CTAB	3.94	568	12.6	0.21	2.57	4.55	1.98
F ₆ H ₂ -HFOPC	2.87	675	242	0.20	2.41	3.31	0.90
F ₆ H ₂ -HFDDePC	3.37	803	21.5	0.23	2.03	3.89	1.86

The decrease in pore size is greater for AP-CTAB relative to the fluorinated templated material, and the pore walls are thicker. Amine incorporation results in an increase in pore wall thickness of 1.01 nm for AP-CTAB relative to non-functionalized silica. This suggests more condensed silica at the aggregated CTAB micelle interface during synthesis, and it is confirmed by the higher degree of amine incorporation from elemental analysis. The pore wall thickness follows the same trend (AP-CTAB > AP-HFOPC > AP-HFDDePC) as the degree of incorporation from elemental analysis.

6.4.3 Accessibility of Amine Functional Group

Fluorescein isothiocyanate incorporation in the functionalized silica, as demonstrated in fluorescence images (Fig. 6.6) obtained by confocal microscopy, confirms the accessibility of the 3-aminopropyl group. The exposure of fluorescein isothiocyanate to non-functionalized silica did not result in fluorescence (not shown). The

accessibility of amine groups can be quantified from the rate and extent of depletion of FITC from solution (Fig. 6.7) during incorporation in the amine functionalized silica. The initial rate and extent of FITC incorporation after more than 5 hours is similar for AP-CTAB and AP-HFDePC. FITC incorporation in AP-HFOPC displays the lowest initial rate (Fig. 6.7) and the lowest extent of FITC incorporation which is consistent with Figure 6.6B which show some dark (non-fluorescing) silica particles. The smaller pore size in AP-HFOPC (2.39 nm) compared to AP-CTAB (3.04 nm) could limit the accessibility of the amines by FITC (maximum global dimension; 1.55 nm). For AP-HFDePC (pore size of 2.50 nm), the possible radial orientation^{13,178} of the pores due to synthesis in homogeneous medium could contribute to the high accessibility rate (similar to AP-CTAB) even though AP-HFDePC has low amine incorporation and a relatively smaller pore size.

Accessibility of the amine group in the bi-functionalized silica materials is reduced relative to the 3-aminopropyl functionalized materials. This is not unexpected because the FITC depletion rate in Figure 6.7 is normalized by the weight of the material (10 mg) and the fluorocarbon group contributes significantly to the weight of the bi-functionalized silica. Similar initial rates are seen in the bi-functionalized silica across templates, but at steady state a slightly lower extent of FITC incorporation is observed for AP-F₆H₂-HFDePC compared to AP-F₆H₂-CTAB and AP-F₆H₂-HFOPC. The lower amine content and the higher incorporation of fluorocarbons could account for the low FITC incorporation in AP-F₆H₂-HFDePC.

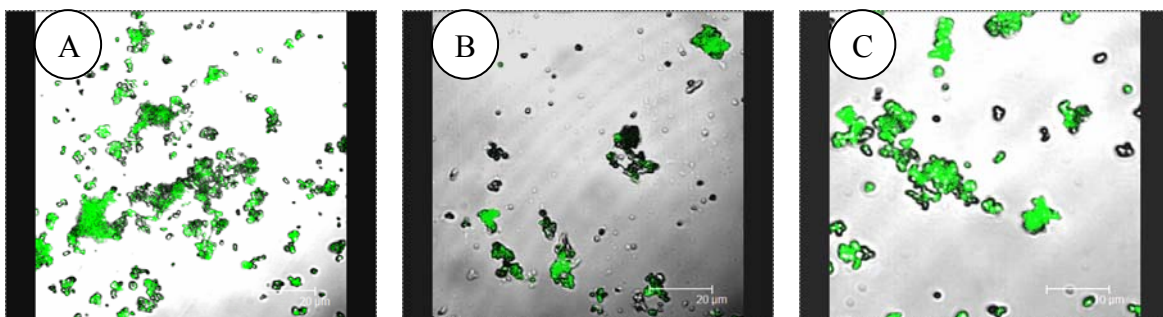


Figure 6.6 Confocal microscopy images of A) AP-CTAB B) AP-HFOPC C) AP-HFDePC

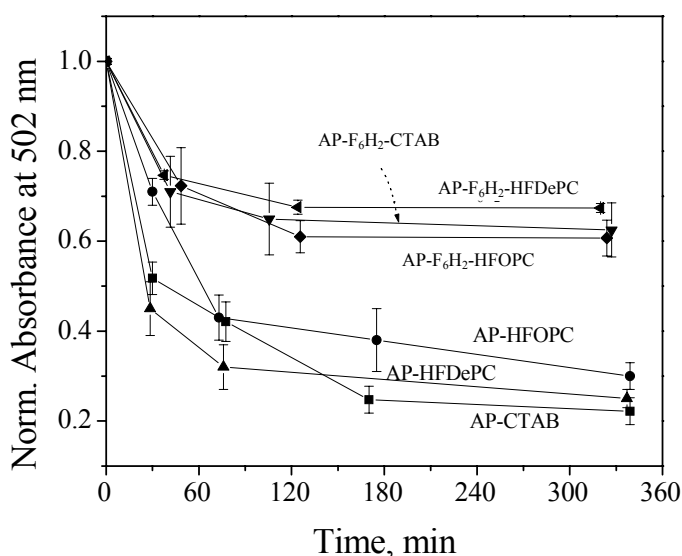


Figure 6.7: Solution phase concentration of FITC during incorporation into amine functionalized silica. Absorbance values are normalized by weight of samples (10 mg). Initial concentration of FTIC in solution is 6.89×10^{-3} mmol/L.

6.4.4 Characterization of Synthesized Silica by CO₂ Capture

CO₂ capture is a potentially sensitive means to probe the extent of amine functionalization of microporous and mesoporous silica while minimizing the steric effects associated with probe molecules such as FITC. In addition, CO₂ adsorption is sensitive to the density of amine functionalization and the surface properties (available –OH groups and adsorbed water). Previous investigations of CO₂ capture with amine-

grafted silica have reported CO₂ adsorption capacities in the range of 13.3 mg/g²⁴⁸ to 90.2 mg/g.²⁴⁰ These results suggest the promise of nanoporous silica as commercial CO₂ capture sorbents; it has been proposed that an economically ideal sorbent should have CO₂ capacity greater than 2000 μmol/g (88 mg/g).²⁴⁹

The CO₂ adsorption capacities of functionalized silica depend on the surface area, the extent amine incorporation and the accessibility of the amine group, and the type of amine group, all factors which indicate the importance of the CO₂-amine interaction.^{238,248-250} Non-functionalized silica has been explored for CO₂ capture, with reported adsorption capacities in the range from 2.2 mg/g (at 60°C)²⁵⁷ to 14 mg/g.²³⁸ 3-aminopropyl grafted on high surface area MCM-48 has shown significant pure CO₂ capture capacity of about 90.2 mg/g at STP.²³⁹ Kim et al²⁴⁸ attached monomeric (3-aminopropyl, pyrrolidinepropyl) and polymeric (polymerized aminopropyl, polyethyleneimine) amines to already synthesized MCM-48 and investigated their CO₂ adsorption capacity (0.8 mmol/g \cong 35.2 mg/g for 3-aminopropyl functionalized MCM-48). The effect of pore size on CO₂ adsorption capacity was investigated by Harlick and Sayari.²⁵⁸ Pore expanded MCM-41 (pore size 10 nm) grafted with 3-[2-(2-aminoethylamino)ethylamino]propyl trimethoxysilane (TRI) was observed to have almost two times the CO₂ adsorption capacity (from 5% CO₂-95% N₂ gas stream) of MCM-41 (pore size 3.7 nm). Humid CO₂ streams have the potential to increase the adsorption capacity for CO₂ because a carbonate or bicarbonate (requiring 1 amine group) is formed instead of a carbamate (requiring 2 amine groups and formed in dry CO₂). However, moisture in the CO₂ gas stream has been shown to have minimal effect on the amount of CO₂ adsorbed. Hiyoshi et al²⁵⁹ observed a 10 % increase in humid CO₂

adsorption capacity on triamine grafted MCM-41, whereas less than a 10% increase was seen by Harlick and Sayari.²⁵⁸

Amine-functionalized silica prepared by direct synthesis presents opportunities to tailor the degree of incorporation and uniformity in loading of the amine group for CO₂ capture. On the basis of a theoretical 3-aminopropyl content of 1.39 mmol/g_{sorbent} for the material synthesized at a TEOS:APTES ratio of 10:1, dry CO₂ sorption capacity of at least 30.6 mg/g_{sorbent} is possible with the carbamate formation reaction (involving 2 amines in close proximity and 1 CO₂ molecule). This capacity does not include the additional adsorption of CO₂ due to physisorption sites present at silica surfaces. Dry CO₂ sorption analysis performed with TGA shows a rapid increase in sample weight of the non-functionalized and all the functionalized silica (within the first 2 minutes) as a result of CO₂ uptake by the porous silica. The volume of the tubing from the gas cylinders to the TGA instrument contributes to the delay. A steady state in the uptake of dry CO₂ is reached within 15 minutes. Table 6.3 compares the steady state values (after 20 minutes) of sorbed CO₂ on non-functionalized and amine functionalized porous silica templates using the three surfactants (CTAB, HFOPC, HFDePC). The importance of surface area in the adsorbent materials and the significant capacity of non-functionalized silica for CO₂ is demonstrated by the higher CO₂ sorption capacity per gram of the non-functionalized silica than the amine functionalized silica. For instance, HFDePC templated non-functionalized silica adsorbed 22.9 mg/g of pure CO₂ at steady state as compared to 16.6 mg/g captured by AP-HFDePC. The high surface area of CTAB templated silica resulted in higher amounts of CO₂ captured per gram material (23.5 mg/g for CTAB and 22.7 mg/g for AP-CTAB). The amount of CO₂ adsorbed on the amine

functionalized silica is lower than the calculated theoretical contribution due to CO₂-amine interactions alone.

For amine functionalized silica, a high surface density of amine coupled with high surface area of silica contributes to high CO₂ uptakes, as seen in ethylenediamine modified SBA-15 mesoporous silica²⁴⁸ (86.6 mg/g pure CO₂ at 22°C) and 3-aminopropyl grafted MCM-48²³⁸ (90.2 mg/g pure CO₂ at STP). The reduced CO₂ adsorption of the synthesized silica as compared to the highest literature values (90.2 mg/g pure CO₂)²³⁸ for amine-functionalized silica may be the result of uniform distribution of functional groups in the silica materials made by direct synthesis in combination with potentially low surface amine concentration. When the amount of CO₂ sorbed is normalized by surface area of the synthesized silica, an expected increase in CO₂ sorption due to amine functionalization is observed (for HFDePC templated silica, 32.0 (± 0.1) μg/m²; for AP-HFDePC, 83.2 (± 2.3) μg/m²). HFDePC templated materials, synthesized in homogenous ethanol/water solutions, have higher CO₂ adsorption capacity per m² for both non-functionalized and amine functionalized silica than the CTAB templated and HFOPC templated materials. This is true in spite of the reduced amine incorporation in AP-HFDePC relative to the other amine-functionalized materials. Silica materials synthesized in homogeneous water/ethanol solution usually possess radial pores,^{13,181} which might have contributed to easy accessibility of adsorption sites and the amine in HFOPC templated materials. Using the smaller CO₂ molecule to probe the accessibility of the functional group results in higher CO₂ sorption capacity in AP-HFOPC comparable to AP-CTAB, reversing the trend observed in FITC incorporation.

CO₂ adsorption capacity decreases with an increase in temperature from 30 °C to 50 °C (Table 6.3) for all materials (both amine functionalized and non-functionalized). This trend is expected and the diminished role of physisorption sites at higher temperatures has been suggested to dominate this effect.²⁶⁰ A higher reduction in CO₂ sorption capacity due to increase in temperature is observed in the fluorocarbon surfactant templated silica. The greatest decrease is seen in the amine functionalized silica compared to the non-functionalized silica. The reduction of CO₂ sorption capacity of AP-HFDePC and AP-HFOPC, 20.6(± 2.3) μg/m² and 20.4(± 1.1) μg/m², respectively, is more significant than the reduction of CO₂ sorption capacity for AP-CTAB (13.2(± 1.1) μg/m²). This trend suggests that AP-HFOPC and AP-HFDePC have more physisorption sites than AP-CTAB, consistent with their lower amine incorporation.

Fluorocarbons are considered to be CO₂-philic²⁶¹⁻²⁶³, and their incorporation in ceramic (e.g. TiO₂ and γ-Al₂O₃) membranes have been previously investigated with a goal of enhancing CO₂ separation from mixed gas stream.²⁵² In this investigation, incorporation of fluorocarbon functional group in the porous silica has a marked, but unexpected, effect on surface adsorption of CO₂. Although the surface area of both F₆H₂-HFDePC and bi-functionalized AP-F₆H₂-HFDePC silica are larger than that of AP-HFDePC, the CO₂ adsorption capacities of the F₆H₂ incorporated silicas is significantly lower per gram (Table 6.3). F₆H₂-HFDePC has a higher CO₂ sorption per gram of sample than AP-F₆H₂-HFDePC, which corresponds to the increased surface area of the fluorofunctional material. When the CO₂ capacity is normalized by surface area, AP-F₆H₂-HFDePC displays the expected higher capacity [15.9 (± 2.4) μg/m²], due to the presence of amine group, than F₆H₂-HFDePC [9.20 (± 0.3) μg/m²]. However, compared to non-

functionalized silica ($32.0 (\pm 0.1) \mu\text{g}/\text{m}^2$), both fluorocarbon incorporated samples had lower CO_2 sorption capacities per surface area.

FTIR analysis of the silica samples was performed after CO_2 adsorption analysis with the TGA, to confirm the reaction of the aminopropyl functional group with CO_2 . Figure 6.8 provides an FTIR profile (taken 15 minutes after CO_2 adsorption) of AP-HFDePC before and after CO_2 capture and HFDePC after CO_2 capture. Exposure to CO_2 results in the appearance of an intense peak at wavenumber 1411 cm^{-1} for AP-HFDePC. The peak is attributed to asymmetric C–O stretch of the ammonium carbamate in dry CO_2 adsorption.^{53,263} This peak is not observed in non-functionalized silica after CO_2 adsorption (Figure 6.8).

Table 6.3 CO_2 capacity of synthesized silica as measured in dry CO_2 as a function of temperature

	Amount CO_2 sorbed			
	30°C		50°C	
	mg/g _{adsorbent}	$\mu\text{g}/\text{m}^2$	mg/g _{adsorbent}	$\mu\text{g}/\text{m}^2$
CTAB	23.6 (± 0.3)	23.7 (± 0.3)	15.5 (± 1.3)	15.6 (± 1.3)
AP-CTAB	21.5 (± 0.4)	67.1 (± 1.1)	20.0 (± 2.0)	53.9 (± 5.6)
HFOPC	20.8(± 0.4)	25.7(± 0.5)	12.9 (± 0.2)	15.9 (± 0.3)
AP-HFOPC	12.0 (± 0.2)	68.2 (± 1.1)	8.4 (± 0.1)	47.8 (± 0.5)
HFDePC	23.6 (± 0.1)	32.0 (± 0.1)	14.6 (± 2.4)	19.8 (± 3.3)
AP-HFDePC	16.9 (± 0.5)	83.2 (± 2.3)	12.7 (± 0.3)	62.6 (± 1.5)
AP-F ₆ H ₂ -HFDePC	4.50 (± 0.7)	15.9 (± 2.4)	–	–
F ₆ H ₂ -HFDePC	7.39 (± 0.2)	9.20 (± 0.3)	–	–

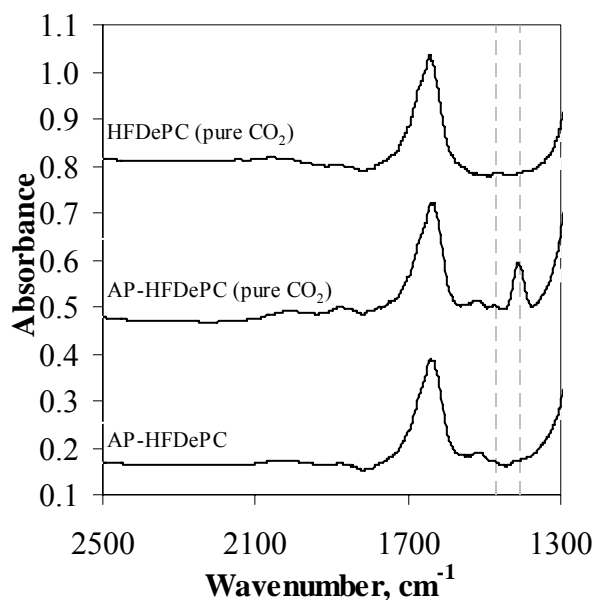


Figure 6.8 FTIR of AP-HFDePC before and 15 minutes after CO₂ adsorption. The dotted lines indicate the wavenumbers for the asymmetric C-O stretch.

6.5 CONCLUSIONS

3-Aminopropyl mesoporous silica with 2-D hexagonal (CTAB template) or disordered (fluorocarbon surfactant templates, HFOPC and HFDePC) pore structure have been synthesized by direct ('one-pot') synthesis. Functionalized silica materials with thicker pore walls are obtained due to the presence of the amine functionalized precursor during self-assembly. The degree of amine incorporation matches the thickness of the pore wall of the functionalized silica; AP-CTAB, which has the highest amine incorporation, also has a larger increase in pore wall thickness. The incorporation of a fluorocarbon functional group in addition to the amine group in bi-functionalized silica results in improved pore order, with the exception of AP-F₆H₂-HFDePC, which has reduced order due to high fluorocarbon incorporation. The 3-aminopropyl group is readily accessible in all amine functionalized silica using FITC as a probe molecule. CO₂

sorption increases (on a surface area basis) in amine functionalized silica due to the reaction of CO₂ with surface amine group. Synthesis in a homogeneous ethanol/water solution (using the HFDePC template) results in the highest CO₂ per surface area, possibly due to easy accessibility of available physisorption and amine reactive sites. Fluorocarbon functionalization reduces CO₂ sorption capacity for both fluorofunctionalized (F₆H₂) silica and bi-functionalized (AP-F₆H₂) silica, most likely due to a reduction in CO₂ physisorption sites.

An on-going investigation in our group has demonstrated the potential to expand the pores of the amine functionalized silica using pressurized CO₂. The potential to re-orient the 3-aminopropyl functional group in the pores based on CO₂-amine interaction is being investigated. Preliminary results show a substantial increase in surface area in addition to higher accessibility of the amine group in the CO₂ processed amine functionalized silica.

CHAPTER 7

CONCLUSIONS AND FUTURE WORK

7.1 CONCLUSIONS

Since the discovery of surfactant templated synthesis of mesoporous silica materials researchers have studied the effects of templates (anionic, cationic and non-ionic; hydrocarbon and fluorocarbon surfactants and block co-polymers), synthesis medium (neutral, acidic and basic), synthesis conditions (e.g. temperature) and incorporation of functional groups on the mesopore structures. Ordered mesoporous silica obtained from surfactant templating possess very high surface area and the pores can be tailored to obtain different pore structures (e.g. hexagonal, cubic or lamellar) and sizes for specific applications. The properties of fluorinated surfactants, namely their ability to self assemble at lower concentrations than their hydrocarbon counterparts and their ability to form more stable and rigid micelles with low curvature, prompted their investigation as templates for nanoporous silica. This work builds on the successful demonstration of fluorinated surfactant templating and demonstrates the synthesis and application of organic/inorganic nanoporous material silica using this class of surfactant templates. The effect of the incorporation of hydrocarbon, fluorocarbon, and amine (hydrophilic) functional precursors on degree of functional group incorporation and silica textural properties is examined as a function of the nature of the surfactant tail (hydrocarbon and fluorocarbon), its chain length, and synthesis conditions.

The initial investigation demonstrates the incorporation of vinyl (a small hydrocarbon group) in porous silica using cationic fluorocarbon surfactants templates $C_6F_{13}C_2H_4NC_5H_5Cl$ (HFOPC), $C_8F_{17}C_2H_4NC_5H_5Cl$ (HFDePC), $C_{10}F_{21}C_2H_4NC_5H_5Cl$ (HFDoDePC)) and CTAB, a hydrocarbon surfactant, for comparison. 2-D hexagonal pore structured and disordered materials are synthesized. The trend of loss of silica pore order with increase in vinyl content for the CTAB materials is also observed for the fluorocarbon surfactant template materials, except for materials made with HFDoDePC, which show an increase in order with increasing vinyl content. However, the fluorocarbon surfactant templated materials has less long range pore order when compared to the CTAB materials. The lower material order contributes to the high accessibility of the vinyl group by bromine (Br_2) molecules.

The successful use of fluorocarbon surfactants as templates to synthesize organic functionalized mesoporous silica was extended to the incorporation of long chain fluorocarbon functional group (perfluoro-decyl) and corresponding hydrocarbon group (n-decyl). The effect of the interactions between the surfactant/functional group combinations on the pore structure, degree of incorporation and material texture properties was investigated for the fluorocarbon surfactants (HFOPC and HFDePC) and CTAB. Although the pore size decreases with functional group incorporation, the long chain functional groups did not have as much of an effect on the pore size of the functionalized silica as the vinyl group. 2-D hexagonal pore structured materials were obtained with observed decrease in pore order of the silica materials upon functionalization. Fluorocarbon functionalized materials were less ordered than the decyl functionalized materials. Solubility of precursors in the synthesis medium was observed

to be a factor in the degree of functionalization. Materials synthesized in homogeneous water/ethanol solution, in which the precursors are more soluble, had high functional group incorporation leading to disordered pore structure. The incorporation of the bulky fluorocarbon group resulted in thicker silica pore walls than the hydrocarbon group. Silica functionalization conferred high surface hydrophobicity to the silica, particularly for the fluorocarbon functionalized silica.

The synthesis and application of fluorofunctionalized silica to fluorous separations was examined. The incorporation of long chain functional group was extended to perfluoro-octyl to investigate the effect of matching the surfactant hydrophobic chain length to that of the functional group. Trends in long range pore order (i.e. 2-D hexagonal pore structure with higher order in CTAB templated silica) for the perfluoro-octyl silica were similar those found with perfluorodecyl functionalized silica. However, the perfluoro-octyl functionalized materials had higher incorporation of the functional group than the perfluorodecyl silica. As in our previous investigation of combinations of fluorocarbon/hydrocarbon functionalized precursors and surfactants, matching the fluorinated functional precursor with a fluorinated surfactant with the exact same carbon chain did not result in improved incorporation. The perfluorodecyl silica materials had thicker pore walls with corresponding higher thermal stability than the perfluoro-octyl silica. These fluorocarbon functionalized materials show a great potential for use as adsorbents for separation. Performance of the fluorocarbon functionalized materials as packing for separation of hydrocarbon and fluorocarbon anthraquinone dyes was comparable to commercially available fluorinated silica gel. However, the dyes were observed to move with a narrower elution band through the synthesized fluorocarbon

functionalized silica compared to elution through the commercial fluorinated silica gel. This observation is attributed to the smaller particle and pore sizes of the synthesized silica, which led to higher retention times.

Functionalization of porous materials with reactive amine groups have numerous applications, from peptide synthesis to carbon dioxide sequestration. 3-Aminopropyl and bi-functionalized (3-aminopropyl/perfluoro-octyl) mesoporous silica materials were synthesized using the templates HFOPC, HFDePC and CTAB. CTAB templating resulted in 2-D hexagonal pore structure for both amine and bi-functionalized silica but disordered pore structures were obtained for the fluorocarbon templated silica. The exception is HFOPC templated bi-functionalized silica, which has a 2-D hexagonal pore structure. CTAB and HFOPC templated bi-functionalized materials possess better pore ordering than the amine functionalized silica synthesized with the same templates. Generally, incorporation of functional group promoted thicker silica pore walls; the presence of the amine group resulted in much thicker silica walls. The degree of amine incorporation matches the thickness of the pore wall of the functionalized silica. Functionalized silica with higher incorporation of amine has the largest pore wall thickness. The amine group is found to be accessible in both sets of materials (amine functionalized and bi-functionalized), as determined by the reactivity of the amine with the fluorescent probe molecule, fluorescein isothiocyanate (FITC). CO₂ capture acts as a probe of the amine accessibility and the surface properties of the material. CTAB templated materials had higher CO₂ capacity per gram of adsorbent than the fluorocarbon templated silica. Fluorocarbon functionalization reduces CO₂ sorption capacity for both fluorofunctionalized silica and bi-functionalized silica.

The use of perfluoroalkylpyridium chloride surfactants as templates resulted in synthesized silica materials with similar but lower long range 2-D hexagonal pore order than the CTAB template silica. On functionalization the loss of pore order, decrease in pore size, pore volume and surface area observed in CTAB templated silica materials were similarly observed in the fluorocarbon surfactant templated materials. However, the hypothesis of obtaining increased incorporation of both hydrocarbon and fluorocarbon functional groups in fluorocarbon template silica materials, due to high hydrophobicity of the fluorocarbon surfactant, was not proven when comparing syntheses in a similar medium (i.e. aqueous). In addition, simply matching the type of functional group (fluorocarbon) to the fluorocarbon surfactant hydrophobic tail did not result in improved functional group incorporation.

7.2 FUTURE WORK

The investigations on organic functionalization of fluorocarbon surfactant templated mesoporous silica have provided information on the effects of incorporating different hydrophobic chains, and hydrophilic reactive hydrocarbon functional groups on silica pore structure and order. However, information on the nature of molecular assembly during synthesis will help in designing experiments to obtain materials of required pore structure for specific applications and also give information on the location of the functional group. Molecular modeling of these systems will be a valuable tool for understanding molecular assembly inside of pores.

The size and structure of the silica particles can be tailored by following the Stöber process and vary the amount of ethanol in synthesis medium⁹¹ and several other

techniques that have been outlined in literature such as using mixtures of hydrocarbon and fluorocarbon based templates¹⁰⁰ and varying the ratio of TEOS to functionalized precursor²⁵⁵. Future research in synthesizing fluorocarbon functionalized silica with tailored particle morphology should focus on improving the use of these materials as packings in separation processes.

Comparing fluorocarbon surfactant templates with similar hydrophobic chain length and headgroup as the hydrocarbon surfactant templates will help in better understanding of the effects of the fluorocarbon chain on functional group incorporation. However, the initial idea of making functionalized materials with pores that are big enough for biomolecule attachment is still an important challenge for a number of applications. Pore expansion by compressed CO₂ on non-functionalized silica materials has been successful (ref) and can be extended to functionalized materials. Longer chain templates such as fluoropolymers and longer chain perfluoroalkyl pyridinium chlorides can also be used to obtain large pore silica particles.

The bi-functionalized silica materials possess reactive amine groups and fluorocarbons that will allow for specific biomolecule interactions when biomolecules are incorporated. CO₂ and amine groups are known to interact to form carbamates or carbonates.²⁴³ CO₂ processing of amine functionalized silica has the potential to re-orient the amine groups in the pores to make them more easily accessible. In addition fluorocarbons are CO₂-philic with the ability to solubilize CO₂. CO₂ processing of the bi-functionalized silica might provide interesting insights into the effects of CO₂ processing on amine group accessibility and surface properties of the bi-functionalized silica.

In the area of sensing applications, thin films provide the most effective geometry for sample analysis.²⁶⁵ Organic functionalization should be extended to thin films by investigating the effect of the organic groups on the silica film mesostructure. Further application of these films in pH sensing, glucose sensing and bacteria identification by incorporating active sites for attachment of these analytes will be valuable.

Finally, the advantages of the solubility of gases such as CO₂ in fluorocarbons can be utilized for CO₂ capture. Unextracted fluorocarbon surfactant templated silica particles and thin films can be investigated as adsorbents for CO₂ capture. The potential exists for these silica materials, with and without amine group, to solubilize substantial amount of CO₂.

APPENDIX A

KJS and Adsorption Potential Methods

Details of the KJS method are given below; the adsorption data for mesoporous samples in this document were analyzed by this method. The KJS method^{154,179,180} makes use of the high resolution α_s -plot. The α_s -plot method is based on the comparison between the adsorption isotherm of a porous material and that of a reference material (in our case, the well characterized Lichrospher Si-1000 (10nm pore sized silica)).¹⁷⁹ The α_s -plot is the plot of (volume of N₂ adsorbed) versus $\alpha_s = v_{\text{ref}}(P/P_o)/v_{\text{ref}}(P/P_o = 0.4)$, where $v_{\text{ref}}(P/P_o)$ is the volume adsorbed in the reference material as a function of relative pressure¹⁵⁴ (Figure A1). The linear portions in the lower α_s region (before the onset of nitrogen condensation) and higher α_s region (after nitrogen condensation in primary mesopores) are used to estimate the pore volume, the total surface area and the external surface area of the material.

The specific surface area and micropore volume are calculated from the linear equation obtained from the lower α_s region of the plot in Figure A1. The linear equation is equivalent $v = \eta + v_{\text{mi}}$, where v_{mi} is the volume of micropores present and η is used to calculate the specific (total) surface area S_t from Equation 1.

$$S_t = \frac{\eta S_{\text{BET},\text{ref}}}{v_{0.4,\text{ref}}} \quad (1)$$

$S_{\text{BET},\text{ref}}$ is the BET surface area of the reference material and $v_{0.4,\text{ref}}$ is the volume adsorbed by the reference material at P/P_o of 0.4. The linear portion in the upper α_s region of the plot in Figure A1 is equivalent to $v = \eta_2 + v_p$, where v_p is the total volume per gram

of all pores in the material. The mesopore volume is given by $v_p - v_{mi}$. The external surface area of the material is calculated from equation 2 using the coefficient η_2^{266} ;

$$S_{ex} = \frac{\eta_2 S_{BET,ref}}{v_{0.4,ref}} \quad (2)$$

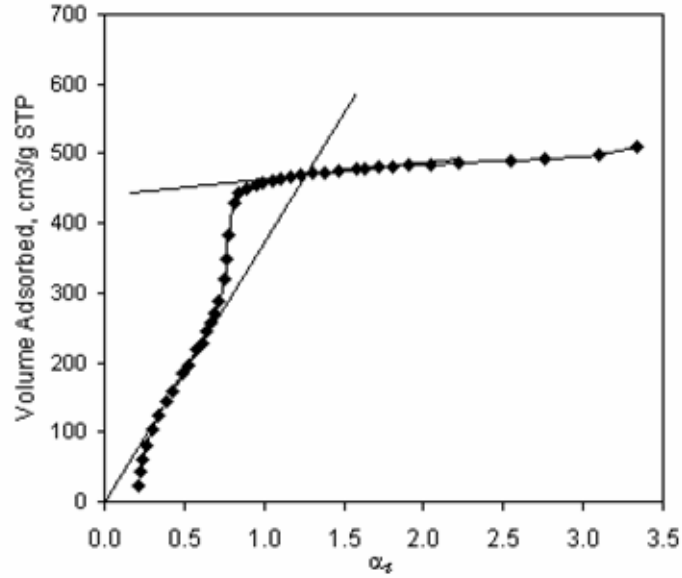


Figure A1 High resolution α_s -plot

In analyzing the data in the α_s -plot, α_s data upto about 0.3 were ignored because of anomaly in that data which is due to the limit of the transducer pressure range in the adsorption instrument.

The microporous materials, v6-HFOPC, v4-HFOPC and v4-HFDePC, were analyzed using Dubinin's and Kaganer's method¹⁷⁸, and the adsorption potential method⁶. Dubinin's and Kaganer's theories and the adsorption potential method are based on the adsorption potential theory, which assumes that the surface of a solid is made up of a series of equipotential surfaces with the same adsorption potential.⁵ The adsorption potential is given by:

$$A(\text{adsorption potential}) = RT \ln \frac{P_o}{P} \quad (3)$$

where P_o/P is the inverse of the relative pressure P/P_o .

Dubinin's method is used to find the micropore volume and Kaganer's method used to calculate the specific surface area. This is achieved by plotting $\log(\text{volume of gas adsorbed})$ against $[\log(P_o/P)]^2$, resulting in a straight line with an intercept of $\log(v_{mi})$.

Kaganer's method states that the intercept of the plot of $\log(\text{volume of gas adsorbed})$ against $[\log(P_o/P)]^2$, equals $\log(v_{st})$. The quantity (v_{st}) is then used to determine the specific surface area of the material:

$$S_t = \frac{v_{st} A_m N}{M} \quad (4)$$

where N is the Avogadro's number, M is the molecular weight of the adsorbate and A_m is the area occupied per molecule of adsorbate (for nitrogen $A_m = 1.62 \times 10^{-19} \text{ m}^2$).²⁶⁶ This analysis method implies that the point for complete pore filling is the same point for mono-layer formation.

An alternative approach in determining the pore size, specific surface area and pore volume of microporous materials, the adsorption potential method by Kruk, Jaroneic and Gadkaree²⁶⁶, states that there are two different points for monolayer formation and complete micropore filling. In this method a plot of the adsorption potential against the differential, dv/dA , gives two minimum points. An example of such a plot is shown in Figure A2. The first minimum point occurs at a lower adsorption potential (higher relative pressure) and represents the point where complete pore filling is achieved. The pore volume is calculated from this minimum point. The second minimum point,

occurring at a higher adsorption potential, corresponds to monolayer formation and is used in obtaining the specific surface area from equation 4.

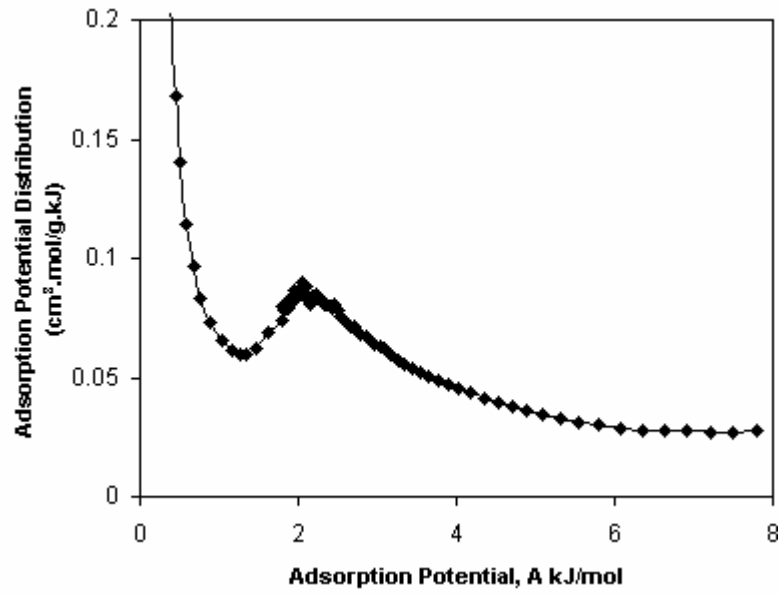


Figure A2 Adsorption potential plot for v6-HFOPC

APPENDIX B

FTIR of Representative Surfactants and Silica Precursors Used in This Investigation.

FTIR analysis of the surfactants and silica precursors provide information on the location of signature peaks of the surfactants and precursors. This information is used in identifying the peaks in the synthesized silica. HFOPC is the fluorocarbon surfactant tridecafluoro-1,1,2,2-tetrahydrooctylpyridinium chloride ($C_6F_{13}C_2H_2NC_5H_5Cl$), CPB (cetylpyridinium bromide; $C_{16}H_{33}NC_5H_5Br$) is a hydrocarbon analogue of the fluorinated surfactants and CTAB ($C_{16}H_{33}N(CH_3)_3Br$) is cetyltrimethylammonium bromide.

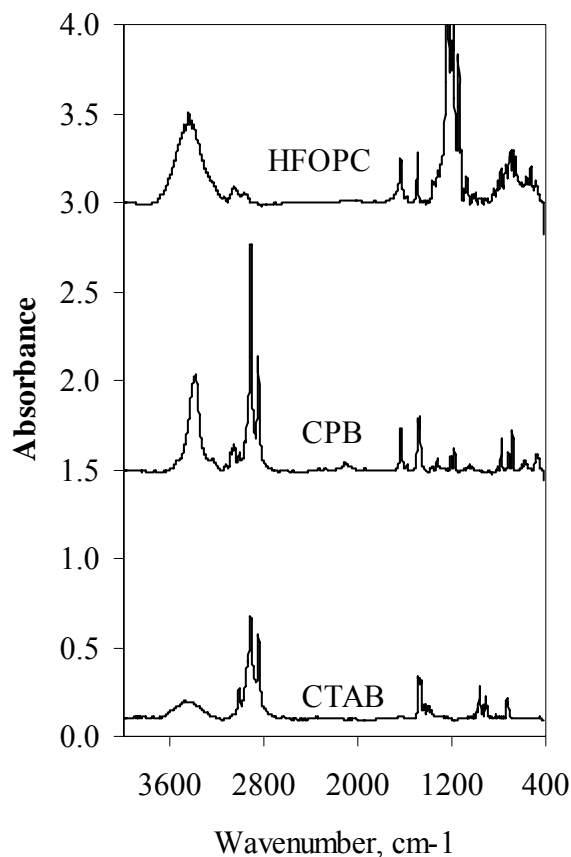


Figure B1 FTIR of representative surfactants

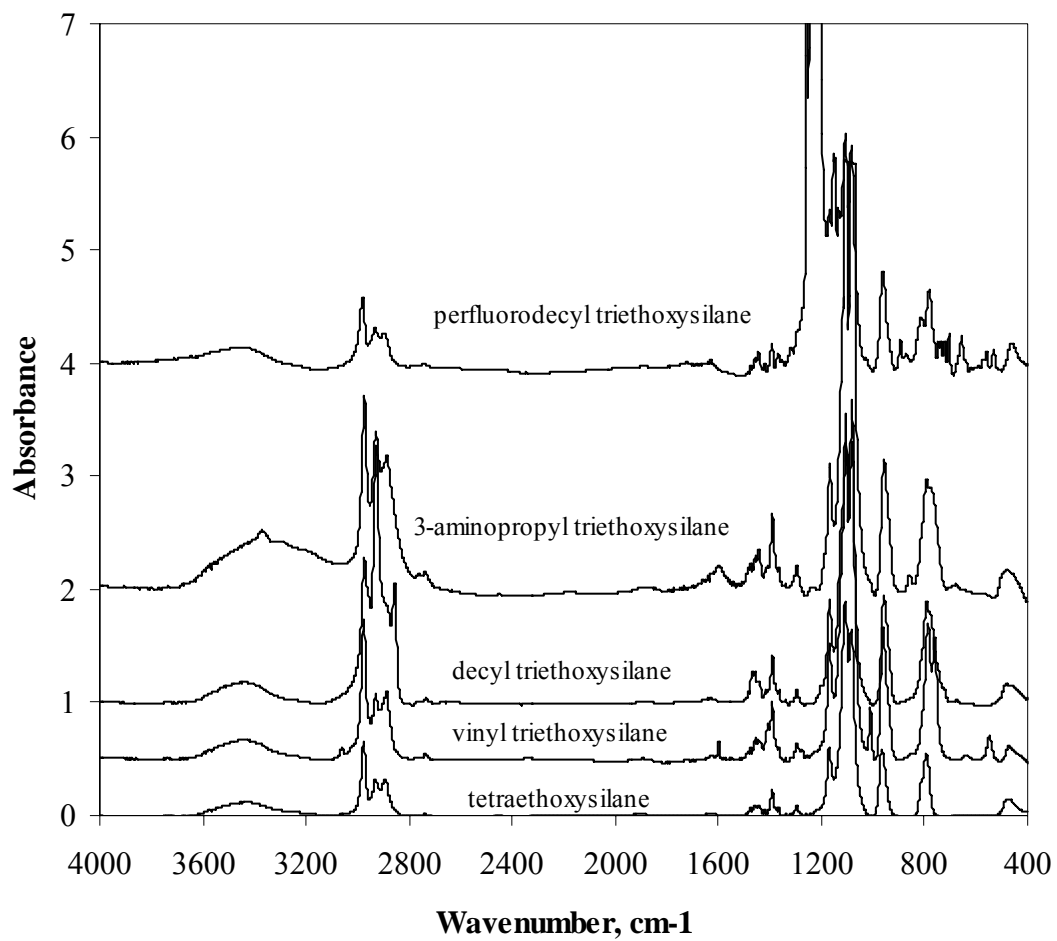


Figure B2 Transmission FTIR of precursors

APPENDIX C

FTIR of CTAB and HFOPC Templated Vinyl Functionalized Silicas

The vinyl functionalized materials were synthesized following the procedure outline in chapter 3. Bromination reaction was performed by adding 0.2 mg of the vinyl functionalized samples to 5 ml solution of bromine in dichloromethane. The solution was allowed to stir for 24 hours, the samples were filtered and washed with 20 ml of dichloromethane for 24 hours. The sample was filtered washed with ethanol and allowed to air dry for 24 hours before FTIR analysis was performed. FTIR analysis followed the procedure outlined in chapters 4, 5 and 6. The prefix Br- is used to refer to brominated samples. v4 denotes vinyl functionalized silica with 4:1 ratio of tetraethoxysilane (TEOS) to vinyltriethoxysilane (VTES). The naming follows that used in chapter 3.

FTIR analysis after bromination shows a reduction in the peak due to vinyl incorporation (at 1416 cm^{-1}). FTIR profile of the CTAB template materials, after 24 hours bromination, show greater reduction in the vinyl peak than that for HFOPC template silica.

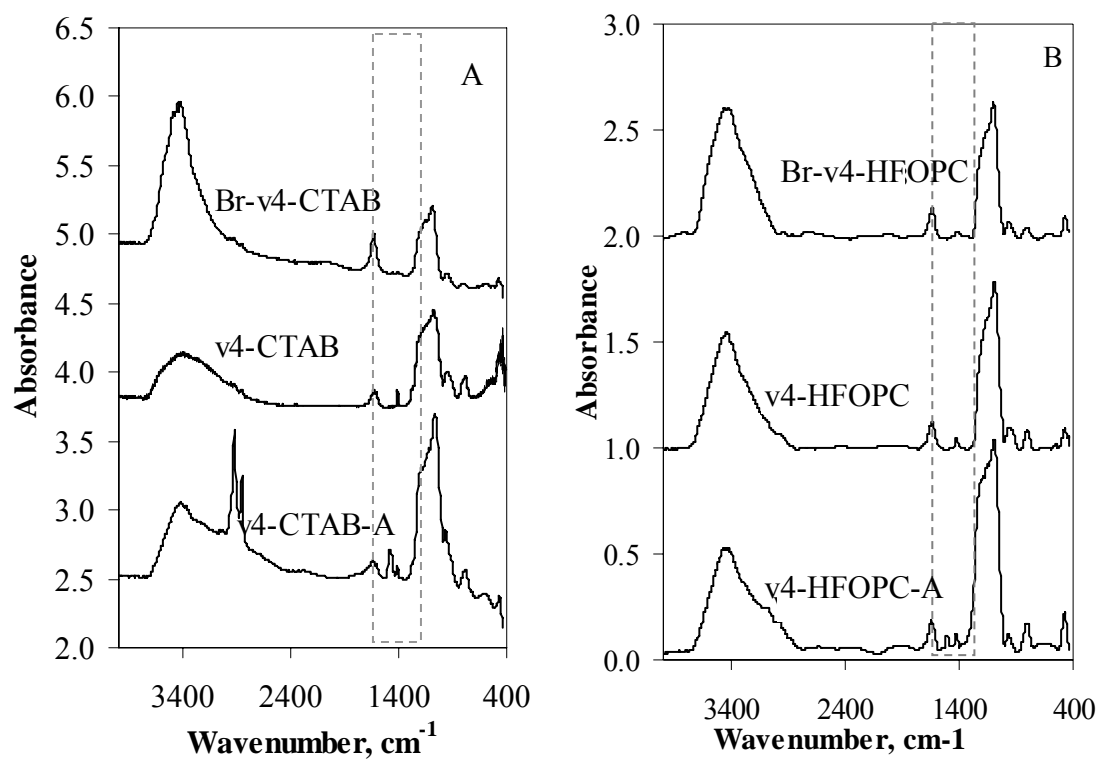


Figure C1 FTIR of A) CTAB templated and B) HFOPC templated vinyl functionalized silica.

APPENDIX D

Perfluoro-decyl (F₈H₂) Functionalized Mesoporous Silica Synthesized in Homogeneous (water/ethanol) Solution using CTAB and HFOPC Templates

These studies are performed to understand the role of homogeneous water/ethanol synthesis medium on fluorocarbon functional group incorporation. In chapters 4 and 5 functionalized silica synthesized with HFDePC template which required a homogeneous medium to obtain ordered pore structure had substantial functional group incorporation and synthesis in homogeneous medium was suggested to be a contributing factor. The letter H after the sample names is used to denote synthesis in homogeneous medium. The naming convention, synthesis and analysis procedure follows those used in chapter 4.

Table D1 Molar ratios of reagents

Sample	CTAB-H	F ₈ H ₂ -CTAB-H	HFOPC-H	F ₈ H ₂ -HFOPC-H
DIUF-Water	136	136	136	136
Surfactant	0.28	0.28	0.15	0.15
NH ₄ OH	10.6	10.6	10.6	10.6
Ethanol	64	64	64	64
TEOS	1	1	1	1
F ₈ H ₂ TES	-	0.25	-	0.25

FTIR analysis of the fluorocarbon functionalized silica synthesized in homogeneous water/ethanol medium display more intense peaks at 1217 cm⁻¹ and 1155 cm⁻¹ (characteristic of -CF₂- vibrations) compared to functionalized silica in aqueous medium. The higher intensity in the peaks suggest higher incorporation of fluorocarbon functional group in the silica synthesized in homogeneous medium. TGA analysis confirmed the high organic content in the materials synthesized in homogeneous water ethanol solution compared to materials synthesized in aqueous medium (Table D2). This

observation confirms the suggestion that synthesis in homogeneous water/ethanol medium contributed to the high incorporation of functional groups in HFDePC templated silica.

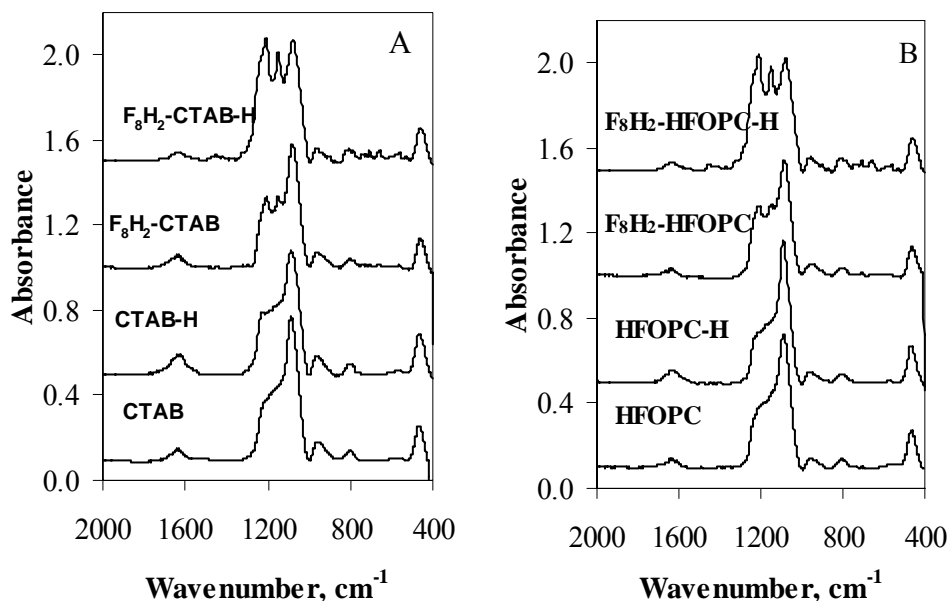


Figure D1 FTIR of A) CTAB template and B) HFOPC template materials. Where H means materials were synthesized in homogeneous water/ethanol solution.

Table D2 Organic content from TGA analysis

Material	Organic Content by TGA, mmol/g*	Theoretical Organic Content, mmol/g ⁺
F ₈ H ₂ -CTAB-H	1.42 (105 %)	
F ₈ H ₂ -HFOPC-H	1.28 (95 %)	1.35
F ₈ H ₂ -HFDePC	1.20 (89 %)	

XRD patterns for CTAB template non-functionalized and fluorocarbon functionalized silica display the (100), (110) and (200) reflections suggesting highly ordered 2-D pore structure. However, XRD patterns for both the non-functionalized and

fluorocarbon functionalized HFOPC template materials possess only one broad peak attributed to disordered pore structure.

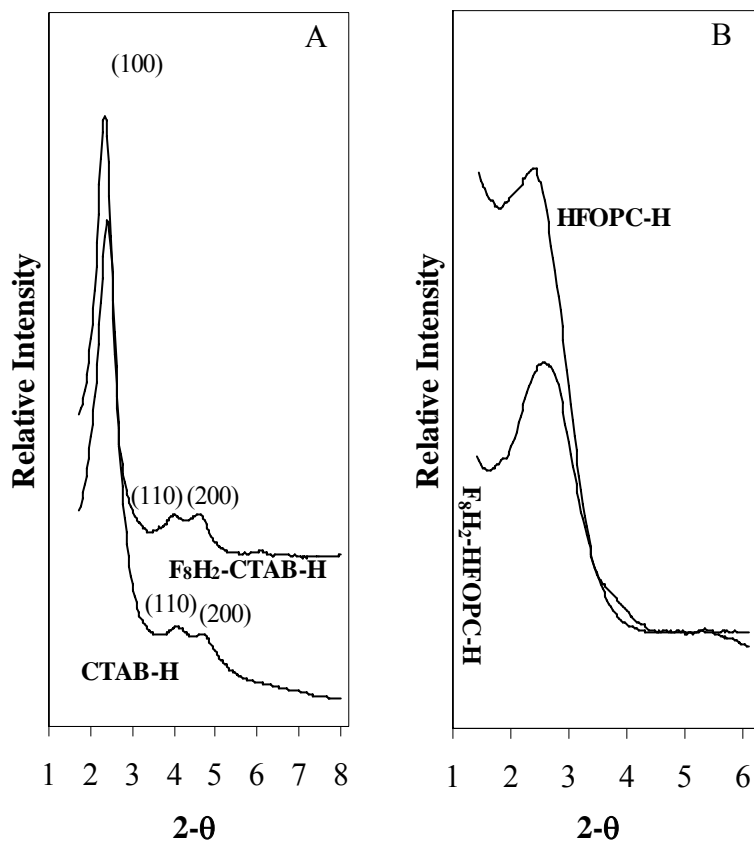


Figure D2 XRD patterns of A) CTAB template and B) HFOPC template silica materials synthesized in homogeneous water/ethanol solution.

APPENDIX E

Synthesis of organic functionalized silica using cetyltrimethyl pyridinium bromide (CPB) template

Cetylpyridinium bromide is an analogue of the perfluoroalkylpyridinium surfactants. CPB was used as template to find out if the difference in headgroup is contributing to the higher long range order in CTAB template materials compared to the fluorocarbon surfactant template materials. The synthesis and analysis conditions are similar to those in Chapters 5 and 6. The surfactant template is used to represent the synthesized silica. The prefixes to CPB stand for the incorporated functional groups.

Table E1 Molar ratios of reagents

Sample	CPB	F ₆ H ₂ -CPB	AP- CPB	AP-F ₆ H ₂ -CPB
DIUF-Water	186	186	186	186
Surfactant	0.17	0.17	0.17	0.17
NH ₄ OH	5.73	5.73	5.73	5.73
TEOS	1	1	1	1
H ₁₀ TES	-	-	-	-
F ₈ H ₂ TES	-	-	-	-
H ₈ TES	-	-	-	-
F ₆ H ₂ TES	-	0.25	-	0.25
APTES	-	-	0.1	0.10

XRD patterns (Fig. E1) show 2-D hexagonal pore structure similar to those obtained for CTAB templated silica however, comparison of the intensities of the (100), (110) and (200) reflections with those of similar CTAB template materials (e.g. Fig. E2) suggests CPB template materials possess a lower degree of pore ordering.

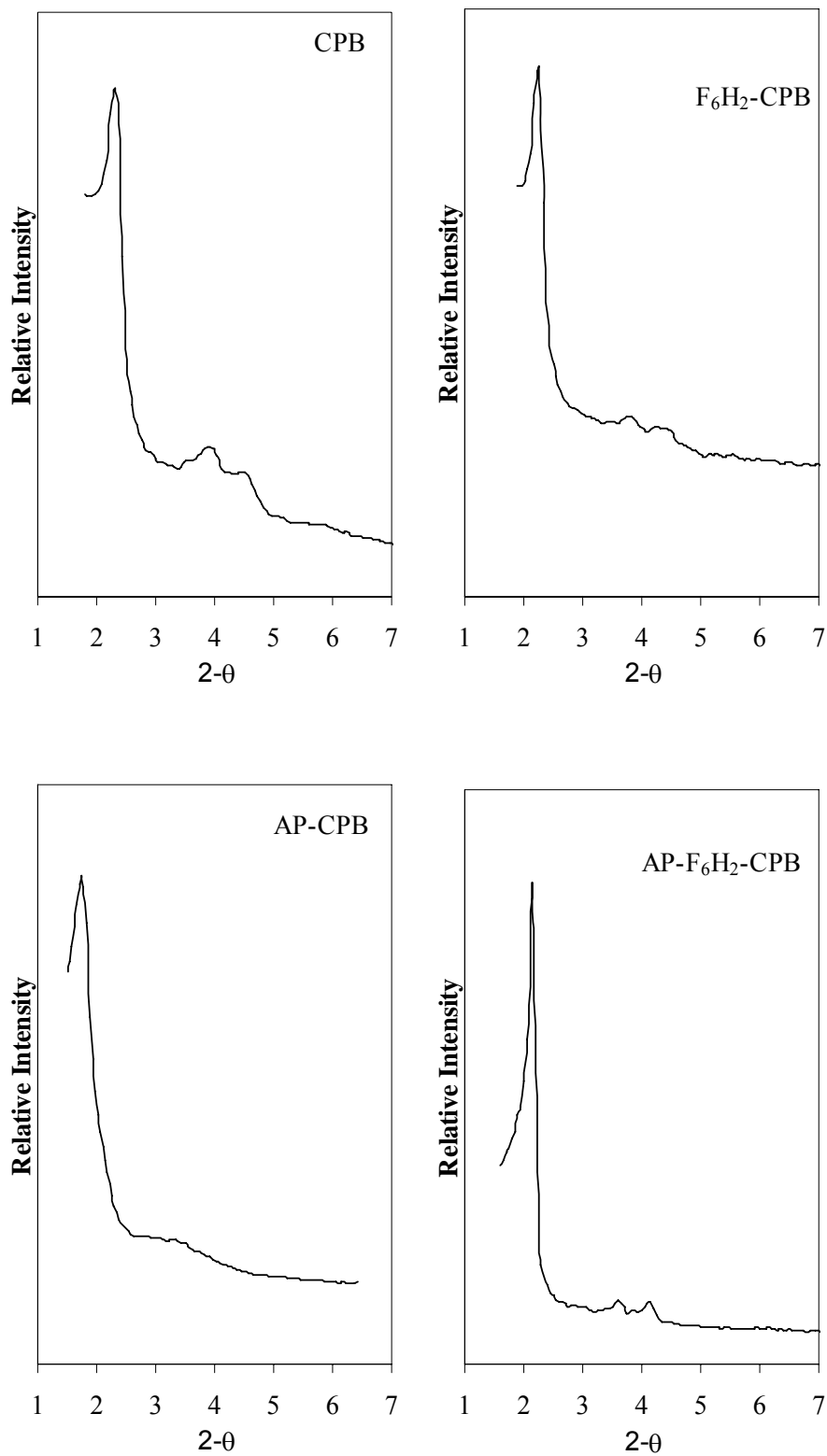


Figure E1 XRD patterns of CPB template silica materials.

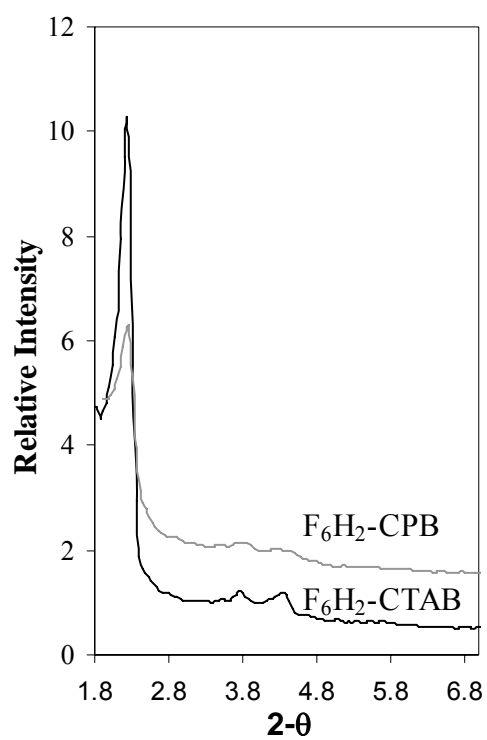


Figure E2 Comparison of XRD patterns for F₆H₂-CTAB and F₆H₂-CPB

APPENDIX F

CO₂ Capture from Humid and Low Concentration CO₂ Streams

Moisture affects the amount of CO₂ adsorbed by mesoporous silica. To investigate the effect of moisture on CO₂ adsorption, a nitrogen gas stream was passed through cold water at 4°C before it was fed into the instrument. After the pre-adsorption of moisture from the moist nitrogen stream had reached steady state (after 1 hour) the gas was switched to moist CO₂ stream. The CO₂ gas stream was also passed through water at 4°C. 26.6 µg/m² of humid CO₂ was adsorbed on AP-HFDePC (69% decrease relative to the amount of dry CO₂ adsorbed) and 6 µg/m² on HFDePC (81% decrease) (Table F1). The decrease in CO₂ adsorption is possibly due to substantial decrease in adsorption and reaction sites following the initial moisture adsorption (before switching to humid CO₂). The adsorbent AP-HFDePC shows a high capacity for moisture during the pre-CO₂ adsorption step (49 mg/g). The high amount of pre-CO₂ adsorbed moisture is observed for both functionalized and non-functionalized silica materials.

The capacity of the mesoporous silica for moisture is temperature dependent. The steady state value of moisture adsorption is reached more quickly at 50 °C (5 to 10 minutes; not shown) relative to 30 °C (45 to 60 minutes), depending on silica material. Analysis performed at 50 °C displayed a lower moisture capacity (25.6 mg/g in AP-HFDePC) for the silica materials and a concomitant increase in CO₂ adsorbed when compared to amount of CO₂ adsorbed at 30° C. AP-HFDePC adsorbed 40.6 µg/m² humid CO₂ at 50°C compared to 26.6 µg/m² at 30°C. At 50°C CO₂ sorption capacity is decreased by about 22 – 37 % for humid CO₂ intake when compared to dry CO₂ adsorption.

Table F1: Amount of CO₂ adsorbed from humid pure CO₂ stream

	Amount of humid 100% CO ₂ sorbed, mg/g	Amount of humid 100% CO ₂ sorbed, μg/m ²
Temperature	50°C	50°C
SAMPLE		
CTAB	13.0	13.1
AP-CTAB	16.3	46.3
HFOPC	10.0	12.3
AP-HFOPC	6.10	34.6
HFDePC	12.3	16.7
AP-HFDePC	8.20	40.6

CO₂ adsorption from a low concentration gas stream source (5% CO₂-95% N₂) was investigated using HFDePC and AP-HFDePC at 30°C. After a switch from dry N₂ to the dry CO₂-N₂ gas mixture, there was rapid gas adsorption after about a minute and a half followed by gradual adsorption until steady state is achieved after 40 minutes. The lower gas adsorbed per gram of aminopropyl functionalized silica in comparison to non-functionalized silica observed for pure CO₂ adsorption was also observed for the gas mixture. After normalizing by surface area, steady state gas adsorption capacity of 40 μg/m² was obtained for AP-HFDePC, as compared to 85.5 μg/m² capacity for pure CO₂ adsorption. The results show a decrease in CO₂ sorption by about 50% when a low concentration CO₂ (5% CO₂-95% N₂) gas was used instead of pure CO₂. CO₂ sorption from dry 5% CO₂-95% N₂ mix for HFDePC was 13.0 μg/m². Substantial decrease in humid CO₂ sorption from humid 5% CO₂-95% N₂ gas mix (gas mix passed through water at 4°C) was obtained after pre-adsorption of moisture. Humid low concentration CO₂ adsorption for AP-HFDePC was 9.04 μg/m² and 0.22 μg/m² for HFDePC.

REFERENCES

1. Zhao, X. S.; Bao, X. Y.; Guo W.; Lee F. Y. Immobilizing catalysts on porous materials *Materials Today* **2006**, 9 (3): 32 – 39.
2. Lin, V. S.-Y.; Motesharei, K.; Dancil, K.-P. S.; Sailor, M. J.; Ghadiri, M. R. A porous silicon-based optical interferometric biosensor, *Science* **1997**, 279: 840 – 843.
3. Zhu, Y.; Shi, J.; Shen, W.; Dong, X.; Feng, J.; Ruan, M.; Li, Y. Stimuli-responsive controlled drug release from a hollow mesoporous silica sphere/polyelectrolyte multilayer core-shell structure, *Angew. Chem. Int. Ed.* **2005**, 44, 5083 –5087
4. Zhao, (George) X. S. Novel porous materials for emerging applications, *J. Mater. Chem.* **2006**, 16: 623–625.
5. Beck, J.S.; Vartuli, J.C.; Roth, W.J.; Leonowicz, M.E.; Kresge, C.T.; Schmitt, K.D.; Chu, C.T-W.; Olson, D.H.; Sheppard, E.W.; McCullen, S.B.; Higgins, J.B.; Schlenkert, J.L. A new family of mesoporous molecular sieves prepared with liquid crystal templates, *J. Am. Chem. Soc.* **1992**, 114: 10834 - 10843.
6. Yokoi, T.; Yoshitake, H. and Tatsumi, T. Synthesis of amino-functionalized MCM-41 via direct co-condensation and post-synthesis grafting methods using mono-, di- and tri-amino-organoalkoxysilanes, *J. Mater. Chem.* **2004**, 14, 951.
7. Yokoi, T.; Yoshitake, H. and Tatsumi, T. Synthesis of anionic-surfactant-templated mesoporous silica using organoalkoxysilane-containing amino groups, *Chem. Mater.* **2003**, 15, 4536.
8. Markowitz, M. A.; Klaehn, J.; Hendel, R. A.; Qadriq, S. B.; Golledge, S. L.; Castner, D. G. and Gaber, B. P. Direct synthesis of metal-chelating mesoporous silica: effects of added organosilanes on silicate formation and adsorption properties, *J. Phys. Chem. B* **2000**, 104: 10820.
9. Zeidan, R. K.; Hwang, S-J.; Davis, M. E. Multifunctional heterogeneous catalysts: SBA-15-containing primary amines and sulfonic acids, *Angew. Chem. Int. Ed.* **2006**, 45: 6332.
- 10) Rankin, S.E.; Tan, B.; Lehmler, H-J; Hindman, K. P.; Knutson, B. L. Well-ordered mesoporous silica prepared by cationic fluorinated surfactant templating, *Microporous and Mesoporous Materials* **2004**, 73: 197.
11. Blin, J. L.; Lesieur, P.; Stebe, M. J. Nonionic Fluorinated Surfactant: Investigation of Phase Diagram and Preparation of Ordered Mesoporous Materials, *Langmuir* **2004**, 20: 491.

12. Tan, B.; Dozier, A.; Lehmler, H-J.; Knutson, B. L.; Rankin, S. E. Elongated silica nanoparticles with a mesh phase mesopore structure by fluorosurfactant templating, *Langmuir* **2004**, *20*: 6981.
13. Tan, B.; Lehmler, H-J.; Vyas, S. M.; Knutson, B. L.; Rankin, S. E. Controlling nanopore size and shape by fluorosurfactant templating of silica, *Chem. Mater.* **2005**, *17*: 916.
14. Tan, B.; Vyas, S. M.; Lehmler, H-J.; Knutson, B. L.; Rankin, S. E. Unusual dependence of particle architecture on surfactant concentration in partially fluorinated decylpyridinium templated silica, *J. Phys. Chem. B* **2005**, *109*: 23225.
15. Tan, B.; Lehmler, H-J.; Vyas, S. M.; Knutson, B. L.; Rankin, S. E. Large- and small-nanopore silica prepared with a short-chain cationic fluorinated surfactant, *Nanotechnology* **2005**, *16*: S502–S507
16. Ma, Y Qi, L.; Ma, J.; Wu, Y.; Liu, O.; Cheng, H. Large-pore mesoporous silica spheres: synthesis and application in HPLC, *Colloids and Surfaces A: Physicochem. Eng. Aspects* **2003**, *229*: 1.
17. Zheng, F.; Tran, D. N.; Busche, B. J.; Fryxell, G. E.; Addleman, R. S.; Zemanian, T. S.; Aardahl, C. L. Ethylenediamine-modified SBA-15 as regenerable CO₂ Sorbent, *Ind. Eng. Chem. Res.* **2005**, *44*: 3099.
18. Michalska, Z.M.; Rogalski, L.; Rózga-Wijas, K.; Chojnowski, J.; Fortuniak, W.; Scibiorek, M. Synthesis and catalytic activity of the transition metal complex catalysts supported on the branched functionalized polysiloxanes grafted on silica, *Journal of Molecular Catalysis A: Chemical* **2004**, *208*: 187.
19. Bois, L.; Bonhomme, A.; Ribes, A.; Pais, B.; Raffin, G.; Tessier, F. Functionalized silica for heavy metal ions adsorption, *Colloids and Surfaces A: Physicochem. Eng. Aspects* **2003**, *221*: 221 – 230
20. Zhang, H.; Sun, Y.; Ye, K.; Zhang, P.; Wang, Y. Oxygen sensing materials based on mesoporous silica MCM-41 and Pt(II)–porphyrin complexes, *J. Mater. Chem.* **2005**, *15*: 3181–3186.
21. Wight, A. P.; Davis, M. E. Design and preparation of organic-inorganic hybrid Catalysts, *Chem. Rev.*, **2002**, *102*: 3589-3614
22. Lim, M. H.; Stein, A. Comparative studies of grafting and direct syntheses of inorganic-organic hybrid mesoporous materials, *Chem. Mater.* **1999**, *11*, 3285-3295
23. Kruk, M.; Asefa, T.; Jaroniec, M.; Ozin, G. A. Metamorphosis of ordered mesopores to micropores: periodic silica with unprecedented loading of pendant reactive organic

groups transforms to periodic microporous silica with tailorable pore size, *J. Am. Chem. Soc.* **2002**, 124: 6383-6392

24. Mercier, L.; Pinnavaia, T. J. Direct synthesis of hybrid organic-inorganic nanoporous silica by a neutral amine assembly route: structure-function control by stoichiometric incorporation of organosiloxane molecules, *Chem. Mater.* **2000**, 12: 188-196.

25. Pough, F. H.; Scovil, J. *A Field Guide to Rocks and Minerals, Peterson Field Guide Series*; 7, Boston Houghton-Mifflin Trade and Reference, 1996.

26. Papirer, E. *Adsorption on Silica Surfaces*, Marcel Dekker, Inc., New York, NY, 2000.

27. Boucher, E. A. Porous materials: structure, properties and capillary phenomena, *J. Mater. Sci.* **1976**, 11: 1734-1750

28. Guan, J.; Fujimoto, K. L.; Sacks, M. S.; Wagner, W. R. Preparation and characterization of highly porous, biodegradable polyurethane scaffolds for soft tissue applications, *Biomaterials* **2005**, 26: 3961–3971.

29. Croll, L. M.; Stover, H. D. H.; Hitchcock, A. P. Composite tectocapsules containing porous polymer microspheres as release gates, *Macromolecules* **2005**, 38, 2903-2910.

30. Kumakura, M.; Kaetsu, I. Polymeric materials having a porous structure prepared by radiation polymerization, *J. of Mater. Sci.* **1984**, 19: 1616-1621.

31. Moustafa, A. B.; Faizalla, A. Synthesis and characterization of porous poly(methacrylic acid-co-triethylene glycol dimethacrylate) by seed emulsion polymerization, *J. of Applied Poly. Sci.* **2000**, 78, 6, 1209-1215.

32. Xiao C.; He, Y. Controlled synthesis and properties of degradable 3D porous lactic acid-based poly(ester–amide), *Polymer* **2006**, 47: 474–479.

33. Odian, G. *Principles of Polymerization*, 4th Ed., John Wiley and Sons, Inc., **2004**, New Jersey.

34. Wu, F.-C.; Tseng, R.-L. Preparation of highly porous carbon from fir wood by KOH etching and CO₂ gasification for adsorption of dyes and phenols from water, *J. Coll. and Inter. Sci.* **2006**, 294: 21–30.

35. Wang, Y.X.; Tan, S.H.; Jiang, D.L.; Zhang, X.Y. Preparation of porous carbon derived from mixtures of furfuryl resin and glycol with controlled pore size distribution, *Carbon* **2003**, 41: 2065–2072.

36. Job, N.; They, A.; Pirard, R.; Marien, J.; Kocon, L.; Rouzaud, J.-N.; Beguin, F.; Pirard, J.-P. Carbon aerogels, cryogels and xerogels: Influence of the drying method on the textural properties of porous carbon materials, *Carbon* **2005**, 43: 2481–2494

37. Moriguchi, I.; Nakahara, F.; Furukawa, H.; Yamada, H.; Kudo, T. Colloidal crystal-templated porous carbon as a high performance electrical double-layer capacitor material, *Electrochemical and Solid-State Letters* **2004**, 7 (8): A221-A223.
38. Smirnova, A.; Dong, X.; Hara, H.; Vasiliev, A.; Sammes, N. Novel carbon aerogel-supported catalysts for PEM fuel cell application, *International Journal of Hydrogen Energy* **2005**, 30: 149– 158.
39. Taberna, P.-L.; Chevallier, G.; Simon, P.; Plee, D.; Aubert, T. Activated carbon-carbon nanotube composite porous film for supercapacitor applications, *Materials Research Bulletin* **2006**, 41: 478–484.
40. Takagi, H.; Hatori, H.; Soneda, Y.; Yoshizawa, N.; Yamada, Y. Adsorptive hydrogen storage in carbon and porous materials, *Materials Science and Engineering B* **2004**, 108: 143–147.
41. Fang, B.; Zhou, H.; Honma, I. Ordered porous carbon with tailored pore size for electrochemical hydrogen storage application, *J. Phys. Chem. B* **2006**, 110, 4875-4880.
42. Liu, P. S.; Liang, K. M. Review functional materials of porous metals made by P/M, electroplating and some other techniques, *Journal of Materials Science* **2001**, 36: 5059 – 5072.
43. Šalák, A. *Ferrous Powder Metallurgy*, Cambridge International Science Publishing, Cambridge, England, **1995**.
44. Abbey Newsletter, Vol. 20, No. 7, Dec **1996**, Abbey Publications Inc.
45. Cundy, C. S.; Cox, P. A. The hydrothermal synthesis of zeolites: history and development from the earliest days to the present time, *Chem. Rev.* **2003** 103(3): 663 - 702
46. Rosen, M. J. *Surfactants and Interfacial Phenomena*, 3rd Edit., John Wiley & Sons, Inc., New Jersey, **2004**.
47. Kent, J. A. *Riegel's Handbook of Industrial Chemistry*, Kluwer Academic Publishers, **2003**.
48. Berthod, A.; Garcia-Alvarez-Coque, C. *Micellar Liquid Chromatography*, Chromatographic Science Series, Vol. 83, Marcel Dekker, Inc., New York, NY, **2000**, pp 19 -23.
49. Fennema, O. R.; Karel, M.; Sanderson, G. W.; Tannenbaum, S. R.; Walstra, P.; Whitaker, J. R. *Food Emulsions*, 3rd Ed., Marcel Dekker Inc., NY, **1997**.

50. Hyde, S.T.; Schröder, G.E. Novel surfactant mesostructural topologies: between lamellae and columnar (hexagonal) forms, *Current Opinion in Colloid and Interface Science* **2003**, 8: 5–14
51. Buhler, E.; Oelschlaeger, C.; Waton, G.; Rawiso, M.; Schmidt, J.; Talmon, Y.; Candau, S. J. Structural and dynamical properties of ribbonlike self-assemblies of a fluorinated cationic surfactant, *Langmuir* **2006**, 22: 2534-2542.
52. Kubo, K.; Moroi, Y.; Nomura, K.; Abe, Y.; Takahashi, T. Study on molecular aggregates of *N*-(1,1-Dihydroperfluoroalkyl)-*N,N,N*-trimethylammonium chloride, *Langmuir* **2002**, 18: 8770-8776.
53. Monduzzi, M.; Knackstedt, M. A.; Ninham, B. W. Microstructure of perfluoropolyether water/oil microemulsions, *J. Phys. Chem.* **1995**, 99: 17772 – 17777.
54. Wang, K.; Oradd, G.; Almgren, M.; Asakawa, T.; Bergenstahl, B. Phase behavior and phase structure of a cationic fluorosurfactant in water, *Langmuir* **2000**, 16, 1042-1049.
55. Kadi, M.; Hansson, P.; Almgren, M.; Furo, I. Demixing of fluorinated and hydrogenated surfactants into distinct aggregates and into distinct regions within aggregates. A combined NMR, fluorescence quenching, and cryo-TEM study, *Langmuir* **2002**, 18: 9243-9249.
56. Yoshimura, T.; Ohno, A.; Esumi, K. Equilibrium and dynamic surface tension properties of partially fluorinated quaternary ammonium salt gemini surfactants, *Langmuir* **2006**, 22: 4643-4648.
57. Can'Adas, O.; Valiente, M.; Rodenas, E. Study of the cetyltrimethylammonium bromide/ 1,6-hexanediol/water system, *J. Coll. and Inter. Sci.* **1998**, 203: 294–298.
58. Kogej, K.; Skerjanc, J. Fluorescence and conductivity studies of polyelectrolyte-induced aggregation of alkyltrimethylammonium bromides, *Langmuir* **1999**, 15: 4251-4258.
59. Bijma, K.; Rank, E.; Engberts, J. B. F. N. Effect of counterion structure on micellar growth of alkylpyridinium surfactants in aqueous solution, *J. Coll. and Inter. Sci.* **1998**, 205: 245-256.
60. Mata, J.; Varade, D.; Bahadur, P. Aggregation behavior of quaternary salt based cationic surfactants, *Thermochimica Acta* **2005**, 428: 147–155
61. Lah, J.; Pohar, C.; Vesnaver, G., Calorimetric study of the micellization of alkylpyridinium and alkyltrimethylammonium bromides in water, *J. Phys. Chem. B* **2000**, 104: 2522-2526

62. Rodríguez, A.; Muñoz, M.; del Mar Graciani, M.; Moyá, M. L. Role of the counterion in the effects of added ethylene glycol to aqueous alkyltrimethylammonium micellar solutions, *J. Coll. and Inter. Sci.* **2006**, 298: 942–951
63. Wang, K.; Karlsson, G.; Almgren, M.; Asakawa, T. Aggregation behavior of cationic fluorosurfactants in water and salt solutions. A cryoTEM survey, *J. Phys. Chem. B* **1999**, 103: 9237-9246.
64. Muto, Y.; Esumi, K.; Meguro, K.; Zana, R. Aggregation behavior of mixed fluorocarbon and hydrocarbon surfactants in aqueous solutions, *J. Coll. and Inter. Sci.* **1987**, 120: 162 – 171.
65. Almgren, M.; Garamus, V. M. Small angle neutron scattering study of demixing in micellar solutions containing CTAC and a partially fluorinated cationic surfactant, *J. Phys. Chem. B* **2005**, 109: 11348-11353.
66. Asakawa, T.; Hisamatsu, H.; Miyagishi, S. Experimental verification of demixing micelles composed of fluorocarbon and hydrocarbon surfactants via the fluorescence-quenching method, *Langmuir* **1996**, 12: 1204-1207.
67. Kadi, M.; Hansson, P.; Almgren, M.; Bergstrom, M.; Garamus, V. M. Mixed micelles of fluorocarbon and hydrocarbon surfactants. A small angle neutron scattering study, *Langmuir* **2004**, 20: 3933-3939.
68. Tornblom, M.; Henriksson, U. Effect of solubilization of aliphatic hydrocarbons on size and shape of rodlike C₁₆TABr micelles studied by ²H NMR relaxation, *J. Phys. Chem. B* **1997**, 101: 6028-6035
69. Hoffmann, H.; Ulbricht, W. Transition of rodlike to globular micelles by the solubilization of additives, *J. of Coll. and Inter. Sci.* **1989**, 129, 2: 388 – 405.
70. Karukstis, K. K.; D'Angelo, N. D.; Loftus, C. T. Using the optical probe methyl orange to determine the role of surfactant and alcohol chain length in the association of 1-alkanols with alkyltrimethylammonium bromide micelles, *J. Phys. Chem. B* **1997**, 101: 1968-1973.
71. Eda, Y.; Takisawa, N.; Shirahama, K. Solubilization of 1-alkanols in ionic micelles measured by piezoelectric gas sensors, *Langmuir* **1996**, 12: 325-329.
72. Li, W.; Han, Y.-C.; Zhang, J.-L.; Wang, B.-G. Effect of Ethanol on the Aggregation Properties of Cetyltrimethylammonium Bromide Surfactant, *Colloid Journal, Vol. 67, No. 2*, **2005**, pp. 159–163
73. Huo, Q.; Margolese, D. I.; Ciesla, U.; Feng, P.; Gier, T. E.; Sieger, P.; Leon, R.; Petroff, P. M.; Schuth, F.; Stucky, G. D. Generalized synthesis of periodic surfactant/inorganic composite materials, *Nature* **1994**, 368: 317 – 321.

74. Gao, C.; Qiu, H.; Zeng, W.; Sakamoto, Y.; Terasaki, O.; Sakamoto, K.; Chen, Q.; Che, S. Formation mechanism of anionic surfactant-templated mesoporous silica, *Chem. Mater.* **2006**, *18*: 3904-3914
75. Pang, J.; Na, H.; Lu, Y. Effect of ionic polymer on cetyltrimethyl ammonium bromide templated synthesis of mesoporous silica, *Microporous and Mesoporous Materials* **2005**, *86*: 89–95.
76. Pinnavaia, T. J.; Thorpo, M. F. *Access in Nanoporous Materials*, Fundamental Materials Research Series, Kluwer Academic Publishers, USA, **2002**.
77. Palmqvist, A. E. C. Synthesis of ordered mesoporous materials using surfactant liquid crystals or micellar solutions, *Current Opinion in Colloid and Interface Science* **2003**, *8* 145–155
78. Zhao, D, Y.; Huo, Q. S.; Feng, J. L.; Chmelka, B. F.; Stucky, G. D. Nonionic triblock and star diblock copolymer and oligomeric surfactant syntheses of highly ordered, hydrothermally stable, mesoporous silica structures, *J. Am. Chem. Soc.* **1998**, *120*: 6024.
79. Reed, J. S. *Principles of Ceramics Processing*, 2nd Ed., John Wiley & Sons, Inc., 1995 pp 571-572.
80. Ryoo, R.; Park, I-S; Jun, S.; Lee, C. W.; Kruk, M.; Jaroniec, M. Synthesis of Ordered and Disordered Silicas with Uniform Pores on the Border between Micropore and Mesopore Regions Using Short Double-Chain Surfactants, *J. Am. Chem. Soc.* **2001**, *123*: 1650-1657.
71. Pinnavaia, T. J.; Thorpo, M. F. *Access in Nanoporous Materials*, Fundamental Materials Research Series, Kluwer Academic Publishers, USA, **2002**.
82. Kumar, D.; Schumacher, K.; Fresne von Hohenesche, C.; Grun, M.; Unger, K. K. MCM-41, MCM-48 and related mesoporous adsorbents: their synthesis and characterization, *Colloids Surf. A* **2001**, *187–188*: 109.
83. Tanev, P. T.; Pinnavaia, T. J. A Neutral templating route to mesoporous molecular sieves, *Science* **1995**, *267*: 865 – 867.
84. Ryoo, R.; Kim, J. M.; Ko, C. H.; Shin, C. H. Disordered molecular sieve with branched mesoporous channel network, *J. Phys. Chem.* **1996**, *100*, 17718-17721.
85. Zhao, D.; Huo, Q.; Feng, J.; Chmelka, B. F.; Stucky, G. D. Nonionic triblock and star diblock copolymer and oligomeric surfactant syntheses of highly ordered, hydrothermally stable, mesoporous silica structures, *J. Am. Chem. Soc.* **1998**, *120*, 6024-6036.

86. Kim, T.-W.; Kleitz, F.; Paul, B.; Ryoo, R. MCM-48-like large mesoporous silicas with tailored pore structure: facile synthesis domain in a ternary triblock copolymer-butanol-water system, *J. Am. Chem. Soc.* **2005**, 127, 7601-7610
87. Nakao K.; Shimizu R.; Kubota H.; Yasuhara M.; Hashimura Y.; Suzuki T.; Fujita T.; Ohmizu H.; Tanev P.T.; Pinnavaia T.J. Biomimetic assembly of porous lamellar silica molecular sieves with a vesicular particle architecture, *Supramolecular Science* **1998**, 5: 399 – 404.
88. Tanev, P. T.; Liang, Y.; Pinnavaia, T. J. Assembly of mesoporous lamellar silicas with hierarchical particle architectures, *J. Am. Chem. Soc.* **1997**, 119, 8616-8624.
89. Inagaki, S.; Fukushimaa, Y.; Kurodab, K. Synthesis of highly ordered mesoporous materials from a layered polysilicate, *J. Chem. Soc., Chem. Commun.* **1993**, 8, 680 – 682.
90. Endo, A.; Miyata, T.; Akiya, T.; Nakaiwa, M.; Inagi, Y.; Nagamine, S. Synthesis of ordered microporous silica by the solvent evaporation method, *J. Mater. Sci.* **2004**, 39: 1117 – 1119.
91. Ryoo, R.; Park, I-S; Jun, S.; Lee, C. W.; Kruk, M.; Jaroniec, M. Synthesis of Ordered and Disordered Silicas with Uniform Pores on the Border between Micropore and Mesopore Regions Using Short Double-Chain Surfactants, *J. Am. Chem. Soc.* **2001**, 123: 1650-1657.
92. Stober, W.; Fink, A.; Bohn, E. Controlled growth of monodisperse silica spheres in the micron size range, *J. Colloid Interface Sci.* **1968**, 26, 62.
93. Grun, M.; Lauer, I.; Unger, K. K. The synthesis of micrometer- and submicrometer-size spheres of ordered mesoporous oxide MCM-41, *Adv. Mater.* **1997**, 9, 254.
94. Liu, S. Q.; Cool, P.; Collart, O.; Van der Voort, P.; Vansant, E. F.; Lebedev, O. I.; Van Tendeloo, G.; Jiang, M. H. The influence of the alcohol concentration on the structural ordering of mesoporous silica: cosurfactant versus cosolvent, *J. Phys. Chem. B* **2003**, 107, 10405.
95. van Tendeloo, G.; Lebedev, O. I.; Collart, O.; Cool, P.; Vansant, E. F. Structure of nanoscale mesoporous silica spheres?, *J. Phys. Cond. Matter* **2003**, 15, S3037.
96. Grun, M.; Unger, K. K.; Matsumoto, A.; Tsutsumi, K. Novel pathways for the preparation of mesoporous MCM-41 materials: control of porosity and morphology, *Micropor. Mesopor. Mater.* **1999**, 27, 207.
97. Meng, X.; Di, Y.; Zhao, L.; Jiang, D.; Li, S.; Xiao, F.-S. Semi-fluorinated surfactant syntheses of ordered porous materials with tailorable pore sizes, *Chem. Mater.* **2004**, 16, 5518-5526.

98. Han, Y.; Li, D.; Zhao, L.; Song, J.; Yang, X.; Li, N.; Di, Y.; Li, C.; Wu, S.; Xu, X.; Meng, X.; Lin, K.; Xiao, F-S. High-temperature generalized synthesis of stable ordered mesoporous silica-based materials by using fluorocarbon-hydrocarbon surfactant mixtures, *Angew. Chem. Int. Ed.* **2003**, *42*, 3633–3637.
99. Li, D.; Han, Y.; Song, J.; Zhao, L.; Xu, X.; Di, Y.; Xiao, F-S. High-temperature synthesis of stable ordered mesoporous silica materials by using fluorocarbon-hydrocarbon surfactant mixtures, *Chem. Eur. J.* **2004**, *10*, 5911–5922.
100. Han, Y.; Ying, J.-Y. Generalized fluorocarbon-surfactant-mediated synthesis of nanoparticles with various mesoporous structures, *Angew. Chem. Int. Ed.* **2005**, *44*, 288–292.
101. Zhu, H.; Liang, C.; Yan, W.; Overbury, S. H.; Dai, S. Preparation of highly active silica-supported Au catalysts for CO oxidation by a solution-based technique, *J. Phys. Chem. B* **2006**, *110*, 10842-10848.
102. Shao, Y.; Wang, L.; Zhang, J.; Anpo, M. Synthesis of hydrothermally stable and long-range ordered Ce-MCM-48 and Fe-MCM-48 materials, *J. Phys. Chem. B* **2005**, *109*, 20835-20841.
103. Nowak, I.; Ziolk, M.; Jaroniec, M. Synthesis and characterization of polymer-templated mesoporous silicas containing Niobium, *J. Phys. Chem. B* **2004**, *108*, 3722-3727.
104. He, X.; Antonelli, D. Recent advances in synthesis and applications of transition metal containing mesoporous molecular sieves, *Angew. Chem. Int. Ed.* **2002**, *41*, 214–229.
105. Yan, Z.; Li, G.; Muab, L.; Tao, S. Pyridine-functionalized mesoporous silica as an efficient adsorbent for the removal of acid dyestuffs, *J. Mater. Chem.* **2006**, *16*, 1717–1725.
106. Liang, Y.; Hanzlik, M.; Anwender, R. Periodic mesoporous organosilicas: mesophase control via binary surfactant mixtures, *J. Mater. Chem.* **2006**, *16*, 1238–1253.
107. Zhang, C.; Zhou, W.; Liu, S. Synthesis and characterization of organofunctionalized MCM-41 by the original stepped templated sol-gel technology, *J. Phys. Chem. B* **2005**, *109*, 24319-24325.
108. Hatton, B.; Landskron, K.; Whitnall, W.; Perovic, D.; Ozin, G. A. Past, present, and future of periodic mesoporous organosilicas-the PMOs, *Acc. Chem. Res.* **2005**, *38*, 305-312.

109. Huh, S.; Wiench, J. W.; Yoo, J.-C.; Pruski, M.; Lin, V. S.-Y. Organic functionalization and morphology control of mesoporous silicas via a co-condensation synthesis method, *Chem. Mater.* **2003**, *15*, 4247-4256
110. Yiu, H. H. P.; Wright, P. A. Enzymes supported on ordered mesoporous solids: a special case of an inorganic–organic hybrid, *J. Mater. Chem.* **2005**, *15*, 3690–3700.
111. Qhobosheane, M.; Santra, S.; Zhang, P.; Tan, W. Biochemically functionalized silica nanoparticles, *Analyst* **2001**, *126*, 1274–1278
112. Walcarius, A.; Sayen, S.; Gérardin, C.; Hamdounb, F.; Rodehüser, L. Dipeptide-functionalized mesoporous silica spheres, *Colloids and Surfaces A: Physicochem. Eng. Aspects* **2004**, *234*: 145–151
113. Fan, J.; Shui, W.; Yang, P.; Wang, X.; Xu, Y.; Wang, H.; Chen, X.; Zhao, D. Mesoporous silica nanoreactors for highly efficient proteolysis, *Chem. Eur. J.* **2005**, *11*, 5391 – 5396.
114. Bois, L.; Bonhomme, A.; Ribes, A.; Pais, B.; Raffin, G.; Tessier, F. Functionalized silica for heavy metal ions adsorption, *Colloids and Surfaces A: Physicochem. Eng. Aspects* **2003**, *221*: 221 – 230
115. Bibby, A.; Mercier, L. Mercury (II) ion adsorption behavior in thiol-functionalized mesoporous silica microspheres, *Chem. Mater.* **2002**, *14*, 1591-1597.
116. Liu, A. M.; Hidajat, K.; Kawi, S.; Zhao D. Y., A new class of hybrid mesoporous materials with functionalized organic monolayers for selective adsorption of heavy metal ions, *Chem. Commun*, **2000**, 1145–1146
117. Sayari, A.; Hamoudi, S.; Yang, Y. Applications of pore-expanded mesoporous silica. 1. Removal of heavy metal cations and organic pollutants from wastewater, *Chem. Mater.* **2005**, *17*, 212-216.
118. Lai, C.-Y.; Trewyn, B. G.; Jęftinija, D. M.; Jęftinija, K.; Xu, S.; Jęftinija, S.; Lin, V. S.-Y. A mesoporous silica nanosphere-based carrier system with chemically removable CdS nanoparticle caps for stimuli-responsive controlled release of neurotransmitters and drug molecules, *J. Am. Chem. Soc.*, **2003**, *125*, 4451-4459.
119. Fagundes, L.B.; Sousa, T.G.F.; Sousa, A.; Silva, V.V.; Sousa, E.M.B. SBA-15-collagen hybrid material for drug delivery applications, *Journal of Non-Crystalline Solids* **2006**, *352*: 3496–3501
120. Qu, F.; Zhu, G.; Lin, H.; Zhang, W.; Sun, J.; Li, S.; Qiu, S. A controlled release of ibuprofen by systematically tailoring the morphology of mesoporous silica materials, *Journal of Solid State Chemistry* **2006**, *179*: 2027–2035

121. Tozuka, Y.; Oguchi, T.; Yamamoto, K. Adsorption and entrapment of salicylamide molecules into the mesoporous structure of folded sheets mesoporous material (FSM-16), *Pharmaceutical Research* **2003**, *20*, 6: 926 - 930.
122. Hampsey, J. E.; Arsenault, S.; Hu, Q.; Lu, Y. One-step synthesis of mesoporous metal-SiO₂ particles by an aerosol-assisted self-assembly process, *Chem. Mater.* **2005**, *17*, 2475-2480.
123. Im, H.-J.; Yang, Y.; Allain, L. R.; Barnes, C. E.; Dai, S.; Xue, Z. Functionalized sol-gels for selective copper(II) separation, *Environ. Sci. Technol.* **2000**, *34*, 2209-2214
124. Zheng, F.; Tran, D. N.; Busche, B. J.; Fryxell, G. E.; Addleman, R. S.; Zemanian, T. S.; Aardahl, C. L. Ethylenediamine-modified SBA-15 as regenerable CO₂ sorbent, *Ind. Eng. Chem. Res.* **2005**, *44*, 3099.
125. Kim, S.; Ida, J.; Gulians, V. V.; Lin, Y. S. Tailoring pore properties of MCM-48 silica for selective adsorption of CO₂, *J. Phys. Chem. B* **2005**, *109*, 6287-6293.
126. Wang, X.; Lin, K. S. K.; Chan, J. C. C.; Cheng, S. Direct synthesis and catalytic applications of ordered large pore aminopropyl-functionalized SBA-15 mesoporous materials, *J. Phys. Chem. B* **2005**, *109*, 1763-1769.
127. Ma, Y.; Qi, L.; Ma, J.; Wu, Y.; Liu, O.; Cheng, H. Large-pore mesoporous silica spheres: synthesis and application in HPLC, *Colloids and Surfaces A: Physicochem. Eng. Aspects* **2003**, *229*: 1–8.
128. Moelans, D.; Cool, P.; Baeyens, J.; Vansant, E. F. Immobilisation behaviour of biomolecules in mesoporous silica materials, *Catal. Comm.* **2005**, *6*: 591–595.
129. Ravindra, R.; Zhao, S.; Gies, H.; Winter, R. Protein encapsulation in mesoporous silicate: the effects of confinement on protein stability, hydration, and volumetric properties, *J. Am. Chem. Soc.* **2004**, *126*, 12224-12225.
130. Ryoo, R.; Jun, S.; Kim, J. M.; Kim, M. J. Generalised route to the preparation of mesoporous metallosilicates via post-synthetic metal implantation, *Chem. Commun.* **1997**; 2225 – 2226.
131. Lesaint, C.; Lebeau, B.; Marichal, C.; Patarin, J. Synthesis of mesoporous silica materials functionalized with n-propyl groups, *Micro. Meso. Mater.* **2005**, *83*; 76–84.
132. Wang, L.; Qi, T.; Zhang, Y. Novel organic–inorganic hybrid mesoporous materials for boron adsorption, *Colloids and Surfaces A: Physicochem. Eng. Aspects* **2006** *275*; 73–78

133. Yan, Z.; Tao, S.; Yin, J.; Li, G. Mesoporous silicas functionalized with a high density of carboxylate groups as efficient absorbents for the removal of basic dyestuffs, *J. Mater. Chem.* **2006**, 16; 2347–2353.
134. Kao, H.-M.; Wu, J.-D.; Cheng, C.-C.; Chiang, A. S. T. Direct synthesis of vinyl-functionalized cubic mesoporous silica SBA-1, *Microporous and Mesoporous Materials* **2006**, 88; 319–328.
135. Huq, R.; Mercier, L.; Kooyman, P. J. Incorporation of cyclodextrin into mesostructured silica, *Chem. Mater.* **2001**, 13, 4512-4519.
136. Shylesh, S.; Jha, R.K.; Singh, A.P. Assembly of hydrothermally stable ethane-bridged periodic mesoporous organosilicas with spherical and wormlike structures, *Microporous and Mesoporous Materials* **2006**, 94; 364–370.
137. Robinson, J. W. Undergraduate Instrumental Analysis, 5th Ed., Marcel Dekker, Inc., New York, NY, **1995**.
138. Stuart, B. H. Infrared Spectroscopy: Fundamentals and Applications, John Wiley & Sons Ltd, West Sussex, England, **2004**.
139. ThermoNicolet,
T N - 0 0 1 2 8, www.thermo.com/eThermo/CMA/PDFs/Product/productPDF_21615.pdf
140. Speyer, R. F. Thermal Analysis of Materials, Marcel Dekker, Inc, New York, NY, **1994**.
141. Hatakeyama, T.; Liu, Z. Handbook of Thermal Analysis, John Wiley & Sons Ltd, West Sussex, England, 1998.
142. Fifield, F.W.; Kealey, D. Principles and Practice of Analytical Chemistry, 5th ed., Blackwell Science Ltd, **2000**.
143. Will, G. Powder Diffraction The Rietveld Method and the Two Stage Method to Determine and Refine Crystal Structures from Powder Diffraction Data, Springer-Verlag Berlin Heidelberg, Germany, **2006**.
144. Chung, F. H.; Smith, D. K. Industrial Applications of X-Ray Diffraction, Marcel Dekker, Inc., USA, **2000**.
145. Irene, E. A. Electronic Materials Science, John Wiley & Sons, Inc., Hoboken, New Jersey, **2005**.
146. Heiney, P. A. <http://www.physics.upenn.edu/~heiney/talks/hires/whatis.html>.

147. Williams, D. B.; Carter, C. B. Transmission Electron Microscopy, Vol. 1, Plenum Press, New York, **1996**.
148. Bozzola, J. J.; Russell, L. D. Electron Microscopy Principles and Techniques for Biologists, 2nd Edition, Jones and Bartlett Publishers Canada, **1999**.
149. Keller, J. U.; Staudt, R. Gas Adsorption Equilibria Experimental Methods and Adsorptive Isotherms, Springer Science Business Media, Inc., Boston, USA, **2005**.
150. Sing, K. S. W. Reporting physisorption data for gas/solid systems with special reference to the determination of surface area and porosity, *Pure & Appl.Chem.* **1982**, Vol.54, No.11; 2201—2218.
151. Brunauer, S.; Emmet, P. H.; Teller, E. Adsorption of Gases in Multimolecular Layers, *J. Am. Chem. Soc.* **1938**; 60(2): 309-319
152. Barrett, E. P.; Joyner, L. G.; Halenda, P. P. The determination of pore volume and area distributions in porous substances. I. Computations from nitrogen isotherms, *J. Am. Chem. Soc.* **1951**, 73; 373.
153. Groen, J. C.; Peffer, L. A. A.; Perez-Ramirez, J. Pore size determination in modified micro- and mesoporous materials. Pitfalls and limitations in gas adsorption data analysis, *Microporous and Mesoporous Materials* **2003**, 60; 1–17.
154. Kruk, M.; Jaroniec, M.; Sayari, A. Application of large pore MCM-41 molecular sieves to improve pore size analysis using nitrogen adsorption measurements, *Langmuir*, **1997**, 13, 6267 – 6273
155. Horvath, G.; Kawazoe, K. Method for the calculation of effective pore distribution in molecular sieve carbon, *J. Chem. Eng. Jpn*, **1983**, 16; 470 – 475.
156. Herdes, C.; Santos, M. A.; Medina, F.; Vega, L. F. Pore size distribution analysis of selected hexagonal mesoporous silicas by grand canonical Monte Carlo simulations, *Langmuir* **2005**, 21, 8733-8742.
157. Kruk, M.; Jaroniec, M.; Gadkaree, K. P. Determination of the specific surface area and the pore size of microporous carbons from adsorption potential distributions, *Langmuir* **1999**, 15, 1442 – 1448.
158. Selvam, P.; Bhatia, S. K.; Sonwane, C. G. Recent advances in processing and characterization of periodic mesoporous MCM-41 silicate molecular sieves, *Ind. Eng. Chem. Res.* **2001**, 40; 3237.
159. Han, S., Xu, J., Hou, W., Yu, X.; Wang, Y. Synthesis of high-quality MCM-48 mesoporous silica using gemini surfactant dimethylene-1,2-bis(dodecyldimethylammonium bromide), *J. Phys. Chem. B.* **2004**, 108; 15043.

160. El Haskouri, J.; Cabrera, S.; Gomez-Garcia, C. J.; Guillem, C.; Latorre, J.; Beltran, A.; Beltran, D.; Marcos, M. D.; Amoros, P. High cobalt content mesoporous silicas, *Chem. Mater.* **2004**, 16; 2805.
161. Sorensen, A. C.; Fuller, B. L.; Eklund, A. G.; Landry, C. C. Mo-doped mesoporous silica for thiophene hydrodesulfurization: comparison of materials and methods, *Chem. Mater.* **2004**, 16; 2157.
162. Guo, X.; Lai, M.; Kong, Y.; Ding, W.; Yan, Q.; Au, C. T. P. Novel coassembly route to Cu-SiO₂ MCM-41-like mesoporous materials, *Langmuir* **2004**, 20; 2879.
163. Aguado, J.; Arsuaga, J. M.; Arencibia, A. Adsorption of aqueous mercury(II) on propylthiol-functionalized mesoporous silica obtained by cocondensation, *Ind. Eng. Chem. Res.* **2005**, 44; 3665.
164. Hunks, W. J.; Ozin, G. A. Periodic mesoporous organosilicas with phenylene bridging groups, 1,4-(CH₂)_nC₆H₄ (n = 0-2), *Chem. Mater.* **2004**, 16; 5465.
165. Wang, Y. Q.; Yang, C. M.; Zibrowius, B.; Spliethoff, B.; Linden, M.; Schuth, F. Directing the formation of vinyl-functionalized silica to the hexagonal SBA-15 or large-pore Ia3d Structure, *Chem. Mater.* **2003**, 15; 5029.
166. Walcarius, A.; Delacote, C. Rate of access to the binding sites in organically modified silicates. 3. Effect of structure and density of functional groups in mesoporous solids obtained by the co-condensation route, *Chem. Mater.* **2003**, 15; 4181.
167. Andersson, J.; Rosenholm, J.; Areva, S.; Linden, M. Influences of material characteristics on ibuprofen drug loading and release profiles from ordered micro- and mesoporous silica matrices, *Chem. Mater.* **2004**, 16; 4160.
168. Gong, Y. J.; Li, Z. H.; Wu, D.; Sun, Y. H.; Deng, F.; Luo, Q.; Yue, Y. Synthesis and characterization of ureidopropyl-MSU-X silica, *Micropor. Mesopor. Mater.* **2001**, 49; 95.
169. Doyle, A.; Hodnett, B. K. Synthesis of 2-cyanoethyl-modified MCM-48 stable to surfactant removal by solvent extraction: Influence of organic modifier, base and surfactant, *Micropor. Mesopor. Mater.* **2003**, 58; 255.
170. Sierra, L.; Guth, J.-L. Synthesis of mesoporous silica with tunable pore size from sodium silicate solutions and a polyethylene oxide surfactant, *Micropor. Mesopor. Mater.* **1999**, 27; 243.
171. Kekicheff, P.; Tiddy, G.J.T. Structure of the intermediate phase and its transformation to lamellar phase in the lithium perfluorooctanoate/water system, *J. Phys. Chem.* **1989**, 93; 2520.

172. Giuleri, F.; Krafft, M.P. Self-organization of single-chain fluorinated amphiphiles with fluorinated alcohols, *Thin Solid Films* **1996**, 284-285; 195.
173. Asakawa, T.; Hisamatsu, H.; Miyagishi, S. Micellar pseudophase separation regions of 1H,1H,2H,2H-perfluoroalkylpyridinium chloride and hydrocarbon surfactants by group contribution method, *Langmuir* **1995**, 11; 478.
174. Bore, M. T.; Rathod, S. B.; Ward, T. L.; Datye, A. K. Hexagonal mesostructure in powders produced by evaporation-induced self-assembly of aerosols from aqueous tetraethoxysilane solutions, *Langmuir* **2003**, 19; 256.
175. Areal, C. O.; Delgado, M. R.; Montouillout, V.; Lavalley, J.C.; Fernandez, C.; Pascual, J. J. C.; Parra, J.B. NMR and FTIR spectroscopic studies on the acidity of gallia-silica prepared by a sol-gel route, *Micropor. Mesopor. Mater.* **2004**, 67; 259.
176. Dollish, F.R.; Fateley, W.G.; Bentley, F.F. Characteristic Raman Frequencies of Organic Compounds, John Wiley and Sons Inc., **1974**.
177. Weidkamp, K. P.; Hacker, C. A.; Schwartz, M. P.; Cao, X.; Tromp, R. M.; Hamers, R. J. Interfacial chemistry of pentacene on clean and chemically modified silicon (001) surfaces, *J. Phys. Chem. B* **2003**, 107; 11142.
178. Gregg, S.J.; Sing, K.S.W. Adsorption, Surface Area and Porosity, Academic Press: London, **1967**.
179. Jaroniec, M.; Kruk, M.; Olivier, J. P. Standard nitrogen adsorption data for Characterization of Nanoporous Silicas, *Langmuir* **1999**, 15; 5410.
180. Kruk, M.; Jaroniec, M. Gas Adsorption characterization of ordered organic-inorganic nanocomposite materials, *Chem. Mater.* **2001**, 13; 3169.
181. Osei-Prempeh, G.; Lehmler, J.H.; Knutson, B.L.; Rankin, S.E. Fluorinated surfactant templating of vinyl-functionalized nanoporous silica, *Micropor. Mesopor. Mater.* **2005**, 85, 16.
182. Guari, Y.; Thieuleux, C.; Mehdi, A.; Reye, C.; Corriu, R.J.P.; Gomez-Gallardo, S.; Philippot, K.; Chaudret, B. In situ formation of gold nanoparticles within thiol functionalized HMS-C₁₆ and SBA-15 type materials via an organometallic two-step approach, *Chem. Mater.* **2003**, 15, 2017.
183. Ganesan, V.; Walcarius, A. Surfactant templated sulfonic acid functionalized silica microspheres as new efficient ion exchangers and electrode modifiers, *Langmuir* **2004**, 20, 3632.

184. Kosuge, K.; Murakami, T.; Kikukawa, N. and Takemori, M. Direct synthesis of porous pure and thiol-functional silica spheres through the S^+X-I^+ assembly pathway, *Chem. Mater.* **2003**, *15*, 3184.
185. Walcarius, A.; Etienne, M.; Lebeau, B. Rate of access to the binding sites in organically modified silicates. 2. ordered mesoporous silicas grafted with amine or thiol groups, *Chem. Mater.* **2003**, *15*, 2161.
186. Shea, K. J.; Loy, D. A. Bridged polysilsesquioxanes. Molecular-engineered hybrid organic-inorganic materials, *Chem. Mater.* **2001**, *13*, 3306.
187. Kapoor, M. P.; Yang, O.; Inagaki, S. Self-assembly of biphenylene-bridged hybrid mesoporous solid with molecular-scale periodicity in the pore walls, *J. Am. Chem. Soc.* **2002**, *124*, 15176.
188. Huh, S.; Chen, H.-T.; Wiench, J. W.; Pruski, M.; Lin, V. S.-Y. Cooperative catalysis by general acid and base bifunctionalized mesoporous silica nanospheres, *Angew. Chem., Int. Ed.* **2005**, *44*, 1826.
189. Han, L.; Ruan, J.; Li, Y.; Terasaki, O.; Che, S. Synthesis and characterization of the amphoteric amino acid bifunctional mesoporous silica, *Chem. Mater.* **2007**, *19*, 11; 2860 - 2867
190. Lei, C.; Shin, Y.; Liu, J.; Ackerman, E. J. Entrapping enzyme in a functionalized nanoporous support, *J. Am. Chem. Soc.* **2002**, *124*, 11242.
191. Wang, Y.; Caruso, F. Mesoporous silica spheres as supports for enzyme immobilization and encapsulation, *Chem. Mater.* **2005**, *17*, 953.
192. Kim, M. J.; Ryoo, R. Synthesis and pore size control of cubic mesoporous silica SBA-1, *Chem. Mater.* **1999**, *11*, 487.
193. Flodstrom, K.; Alfredsson, V.; Kallrot, N. Formation of a new $Ia\bar{3}d$ cubic mesostructured silica via triblock copolymer-assisted synthesis, *J. Am. Chem. Soc.* **2003**, *125*, 4402.
194. Berggren, A.; Palmqvist, A. E. C.; Holmberg, K. Surfactant-templated mesostructured materials from inorganic silica, *Soft Matter*, 2005, *1*, 219–226.
195. Rankin, S. E.; Tan, B.; Lehmler, H.-J.; Knutson, B. Fluorinated surfactant templating of ordered nanoporous silica, *Mat. Res. Soc. Symp. Proc.* **2003**, *775*, 47.
196. Meng, X.; Di, Y.; Zhao, L.; Jiang, D.; Li, S.; Xiao, F.-S. Semi-fluorinated surfactant syntheses of ordered porous materials with tailorable pore sizes, *Chem. Mater.* **2004**, *16*, 5518.

197. Burkett, S. L.; Sims, S. D.; Mann, S. Synthesis of hybrid inorganic–organic mesoporous silica by co-condensation of siloxane and organosiloxane precursors, *Chem. Commun.* **1996**, 11, 1367.
198. Fowler, C. E.; Burkett, S. L.; Mann, S. Synthesis and characterization of ordered organo–silica–surfactant mesophases with functionalized MCM-41-type architecture, *Chem. Commun.* **1997**, 18, 1769.
199. Bae, J. Y.; Jung, J.-I.; Bae, B.-S. Photochromism in spiropyran impregnated fluorinated mesoporous organosilicate films, *J. Mater. Res.*, **2004**, 19, 8, 2503.
200. Patist, A.; Chhabra, V.; Pagidipati, R.; Shah, R.; Shah, D. O. Effect of chain length compatibility on micellar stability in sodium dodecyl sulfate/alkyltrimethylammonium bromide solutions, *Langmuir* **1997**, 13, 432.
201. Kamiusuki, T.; Monde, T.; Nakayama, N.; Yano, K.; Yoko, T.; Konakahara, T. Interaction between a solute molecule and a fluorocarbon bonded layer in reversed-phase high-performance liquid chromatography, *J. Colloid Interface Sci.* **1999**, 220, 123
202. Lebeau, B.; Marichal, C.; Mirjol, A.; Soler-Illia, G. J. de A.A.; Buestrich, R.; Popall, M.; Mazerolles, L.; Sanchez, C. Synthesis of highly ordered mesoporous hybrid silica from aromatic fluorinated organosilane precursors, *New J. Chem.* **2003**, 27, 166.
203. Jung, J.-I.; Bae, J. Y.; Bae, B.-S. Characterization and mesostructure control of mesoporous fluorinated organosilicate films, *J. Mater. Chem.* **2004**, 14, 1988.
204. Pagliaro, M.; Ciriminna, R. New fluorinated functional materials, *J. Mater. Chem.*, **2005**, 15, 4981–4991.
205. Porcherie, O.; Guari, Y.; Reye, C. Direct syntheses using a fluorinated surfactant of silicas containing organofluorinated groups, *New J. Chem.*, **2005**, 29, 538 – 543.
206. Gladysz, J. A.; Curran, D. P.; Horvath, I. T. *Handbook of Fluorous Chemistry*; Wiley-VCH: Germany, **2004**.
207. Curran, D.; Lee, Z. Fluorous techniques for the synthesis and separation of organic molecules, *Green Chemistry* **2001**, 3, G3
208. Gu, Z.-Z.; Uetsuka, H.; Takahashi, K.; Nakajima, R.; Onishi, H.; Fujishima, A.; Sato, O. Structural color and the lotus effect, *Angew. Chem. Int. Ed.* **2003**, 42 (8), 894.
209. Tung, C.-H.; Ji, H.-F. Aggregation behavior of mixed fluorocarbon and hydrocarbon molecules in aqueous organic solvents. Nonideality and ideality of mixing, *J. Phys. Chem.* **1995**, 99, 8311.
210. Kamiusuki, T.; Monde, T.; Yano, K.; Yoko, T.; Konakahara, T. Preparation of branched-polyfluoroalkylsilane-coated silica gel columns and their HPLC separation characteristics, *Chromatographia* **1999**, 49, 11/12, 649 -656.

211. Kadi, M.; Hansson, P.; Almgren, M. Demixing of fluorinated and hydrogenated surfactants into distinct aggregates and into distinct regions within aggregates. A combined NMR, fluorescence quenching, and cryo-TEM Study, *Langmuir* **2002**, *18*, 9243-9249.
212. Lo Nostro, P.; Scalise, L.; Baglioni, P. Phase separation in binary mixtures containing linear perfluoroalkanes, *J. Chem. Eng. Data* **2005**, *50*, 1148 -1152.
213. Lin-Vien, D.; Colthup, N.B.; Fateley, W.G.; Grasselli, J.G., *The Handbook of Infrared and Raman Characteristic Frequencies of Organic Molecules*, Academic Press, Inc., San Diego, CA, **1991**.
214. Holmes, S.M.; Zholobenko, V.L.; Thursfield, A.; Plaisted, R.J.; Curdy, C.S.; Dweyer, J. In situ FTIR study of the formation of MCM-41, *J. Chem. Soc. Faraday Trans.* **1998**, 2025.
215. Jaroniec, C. P.; Gilpin, R. K.; Jaroniec, M. Adsorption and thermogravimetric studies of silica-based amide bonded phases, *J. Phys. Chem. B* **1997**, *101*, 6861-6866.
216. Hatakeyama, T.; Quinn, F.X.; *Thermal Analysis Fundamentals and Applications to Polymer Science*; 2nd Ed, John Wiley & Sons: England; **1999**
217. Asakawa, T.; Hisamatsu, H.; Miyagishi, S. Micellar pseudophase separation regions of 1H,1H,2H,2H-perfluoroalkylpyridinium chloride and hydrocarbon surfactants by group contribution method, *Langmuir* **1995**, *11*, 478-482.
218. Seong Huh, Jerzy W. Wiench, Ji-Chul Yoo, Marek Pruski, and Victor S.-Y. Lin, Organic functionalization and morphology control of mesoporous silicas via a co-condensation synthesis method, *Chem. Mater.* **2003**, *15*, 4247-4256
219. Sayari, A.; Hamoudi, S. Periodic mesoporous silica-based organic-inorganic nanocomposite materials, *Chem. Mater.* **2001**, *13*, 3151
220. Tan, B.; Rankin, S. E. Interfacial alignment mechanism of forming spherical silica with radially oriented nanopores, *J. Phys. Chem. B* **2004**, *108*, 20122-20129
221. Liu, S.; Cool, P.; Collart, O.; Van der Voort, P.; Vansant, E. F.; Lebedev, O. I.; Tendeloo, G. V.; Jiang, M. The influence of the alcohol concentration on the structural ordering of mesoporous silica: cosurfactant versus cosolvent, *J. Phys. Chem. B* **2003**, *107*, 10405-10411
222. Borman, S. Combinatorial Chemistry, *Chemical & Engineering News*, February 24, **1997**

223. Yan, B. *Analytical Methods in Combinatorial Chemistry*; Technomic Publishing Company, Inc: USA, **2000**.
224. Zhang, W.; Curran, D. P.; Chen, C. H.-T. Use of fluoruous silica gel to separate fluoruous thiol quenching derivatives in solution-phase parallel synthesis, *Tetrahedron* **2002**, *58*, 3871.
225. Zhang, W.; Luo, Z.; Chen, C. H.-T. Curran, D. P. Solution-phase preparation of a 560-compound library of individual pure mappicine analogues by fluoruous mixture synthesis, *J. Am. Chem. Soc.* **2002**, *124*, 10443.
226. Zhang, Q; Luo, Z.; Curran, D. P. Separation of "Light Fluoruous" reagents and catalysts by fluoruous solid-phase extraction: Synthesis and study of a family of triarylphosphines bearing linear and branched fluoruous tags, *J. Org. Chem.* **2000**, *65*, 8866.
227. Brittain, S. M.; Ficarro, S. B.; Brock, A.; Peters, E. C. Enrichment and analysis of peptide subsets using fluoruous affinity tags and mass spectrometry. *Nat. Biotech.* **2005**, *23*, 4, 463.
228. Krafft, M. P.; Riess, J. G. Highly fluorinated amphiphiles and colloidal systems, and their applications in the biomedical field. A contribution. *Biochimie* **1998**, *80*, 489.
229. Zhang, W.; Lu, Y.; Nagashima, T. Plate-to-plate fluoruous solid-phase extraction for solution-phase parallel synthesis. *J. Comb. Chem.* **2005**, *7*, 893.
230. Palmqvist, A. E. C. Synthesis of ordered mesoporous materials using surfactant liquid crystals or micellar solutions. *Current Opinion in Coll. and Inter. Sci.* **2003**, *8*, 145.
231. Cardia, M. C.; Begala, M.; DeLogu A. Maccioni, E. Synthesis and biological evaluation of some differently substituted 9,10-anthracenediones. *Il Farmaco* **2001**, *56*, 549.
232. Simpson, N. J. K. *Solid-Phase Extraction: Principles, Techniques and Applications*; Marcel Dekker Inc: New York, **2000**.
233. Innocenzi, P.; Falcaro, P.; Grosso, D.; Babonneau, F. Order-disorder transitions and evolution of silica structure in self-sssembled mesostructured silica films studied through FTIR spectroscopy. *J. Phys. Chem. B* **2003**, *107*, 4711.
234. Zhang, W. Fluoruous synthesis of heterocyclic systems. *Chem. Rev.* **2004**, *104*, 2531.
235. Unsal, E.; Caml, S. T.; Irmak, T.; Tuncel, M.; Tuncel, A. Monodisperse Poly(Styrene-co-Divinylbenzene) particles (3.2 μm) with relatively small pore size as HPLC packing material. *Chromatographia* **2004**, *60*, 553.

236. Bowe, C. A.; Poore', D. D.; Benson, R. F.; Martin, D. F. Extraction of heavy metals by amines adsorbed onto silica gel, *J. Environ. Sci. and Health part A*, **2003**, 38, 11, 2653.
237. Im, H.-J.; Yang, Y.; Allain, L. R.; Barnes, C. E.; Dai, S.; Xue, Z. Functionalized sol-gels for selective copper(II) separation, *Environ. Sci. Technol.* **2000**, 34, 2209.
238. Huang, H. Y.; Yang, R. T.; Chinn, D.; Munson, C. L. Amine-grafted MCM-48 and silica xerogel as superior sorbents for acidic gas removal from natural gas, *Ind. Eng. Chem. Res.* **2003**, 42, 2427
239. Zhu, G.; Yang, Q.; Jiang, D.; Yang, J.; Zhang, L.; Li, Y.; Li, C. Synthesis of bifunctionalized mesoporous organosilica spheres for high-performance liquid chromatography, *J. Chromatography A* **2006**, 1103, 257.
240. Wang, X.; Tseng, Y.-H.; Chan, J. C. C.; Cheng, S. Catalytic applications of aminopropylated mesoporous silica prepared by a template-free route in flavanones synthesis, *J. Catalysis.* **2005**, 233; 266.
241. a. Osei-Prempeh, G; Lehmler, J. H.; Rankin, S.E.; Knutson, B.L. Application of fluoro-functionalized mesoporous silica to fluoruous separations, Submitted, *Ind. Eng. Chem. Res.*, April, **2007** b.Osei-Prempeh, G; Lehmler, J. H.; Rankin, S.E.; Knutson, B.L. Comparison of fluorocarbon and hydrocarbon functional group incorporation into nanoporous silica employing fluorinated and hydrocarbon surfactants as templates, *Unpublished.*
242. Khatri, R. J.; Chuang, S. C. C.; Song, Y.; Gray, M. Thermal and chemical stability of regenerable solid amine sorbent for CO₂ capture. *Energy and Fuels* **2006**, 20, 1514.
243. Meisen, A.; Shuai, X. Research and development issues in CO₂ capture, *Energy Convers. Mgmt* 1997, 38, S37.
244. Leci, C. L. Development requirements for absorption processes for effective CO₂ capture from power plants. *Energy Convers. Mgmt.* **1997**, 38, S45-S50.
245. Zheng, F.; Tran, D. N.; Busche, B. J.; Fryxell, G. E.; Addleman, R. S.; Zemanian, T. S.; Aardahl, C. L. Ethylenediamine-Modified SBA-15 as Regenerable CO₂ Sorbent, *Ind. Eng. Chem. Res.* **2005**, 44, 3099-3105.
246. Kim, S.; Ida, J.; Guliants, V. V.; Lin, J. Y. S. Tailoring pore properties of MCM-48 silica for selective adsorption of CO₂, *J. Phys. Chem. B* **2005**, 109, 6287-6293.
247. Hiyoshi, N.; Yogo, K.; Yashima, T. Adsorption characteristics of carbon dioxide on organically functionalized SBA-15, *Microporous and Mesoporous Materials* **2005**, 84: 357-365.

248. Leal, O.; Bolivar, C.; Ovalles, C.; Garcia, J. J.; Espidel, Y. Reversible adsorption of carbon dioxide on amine surface-bonded silica gel. *Inorg. Chim. Acta* **1995**, *240*, 183.
249. Chang, A. C. C.; Chuang, S. S. C.; Gray, M.; Soong, Y. In-situ infrared study of CO₂ adsorption on SBA-15 grafted with γ -(aminopropyl)triethoxysilane, *Energy & Fuels* **2003**, *17*, 468-473.
250. Macario, A.; Katovic, A.; Giordano, G.; Iucolano, F.; Caputo, D. Synthesis of mesoporous materials for carbon dioxide sequestration, *Microporous and Mesoporous Materials* **2005**, *81*, 139 – 147.
251. Abidi, N.; Sivadea, A.; Bourret, D.; Larbot, A.; Boutevin, B.; Guida-Pietrasanta, F.; Ratsimihety, A. Surface modification of mesoporous membranes by fluoro-silane coupling reagent for CO₂ separation, *Journal of Membrane Science* **2006**, *270*: 101–107
252. Innocenzi, P.; Falcaro, P.; Grosso, D.; Babonneau, F. Order-disorder transitions and evolution of silica structure in self-assembled mesostructured silica films studied through FTIR spectroscopy. *J. Phys. Chem. B* **2003**, *107*, 4711.
253. Wei, Q.; Nie, Z.-R.; Hao, Y.-L.; Liu, L.; Chen, Z.-X.; Zou, J.-X. Effect of synthesis conditions on the mesoscopical order of mesoporous silica SBA-15 functionalized by amino groups, *J Sol-Gel Sci Techn* **2006**, *39*:103–109.
254. Huh, S.; Wiench, J.W.; Yoo, J.-C.; Pruski, M.; Lin, V. S.-Y. Organic functionalization and morphology control of mesoporous silicas via a co-condensation synthesis method, *Chem. Mater.* **2003**, *15*, 4247-4256
255. Sadasivan, S.; Khushalanib, D.; Mann, S. Synthesis and shape modification of organo-functionalised silica nanoparticles with ordered mesostructured interiors, *J. Mater. Chem.* **2003**, *13*, 1023–1029.
256. Hiyoshi, N.; Yogo, K.; Yashima, T. Adsorption characteristics of carbon dioxide on organically functionalized SBA-15, *Microporous and Mesoporous Materials* **2005**, *84*: 357–365.
257. Harlick, P. J. E.; Sayari, A. Applications of pore-expanded mesoporous silicas. 3. triamine silane grafting for enhanced CO₂ adsorption, *Ind. Eng. Chem. Res.* **2006**, *45*, 3248-3255.
258. Hiyoshi, N.; Yogo, D K.; Yashima, T. Adsorption of carbon dioxide on amine modified SBA-15 in the presence of water vapor. *Chem. Lett.* **2004**, *33*, 510.
259. Knowles, G. P.; Delaney, S. W.; and Chaffee, A. L. Diethylenetriamine[propyl(silyl)]-functionalized (DT) mesoporous silicas as CO₂ adsorbents. *Ind. Eng. Chem. Res.* **2006**, *45*, 2626.

260. Tham, M. K.; Walker, R. D. Jr.; Model, J. H. Physical properties and Gas Solubilities in Selected Fluorinated Ethers, *Journal of Chemical and Engineering Data* **1973**, 18, 4: 385.
261. Cece, A.; Jureller, S. H.; Kerschner, J. L.; Moschner, K. F. Molecular modeling approach for contrasting the interaction of ethane and hexafluoroethane with carbon dioxide, *J. Phys. Chem.* **1996**, 100, 7435-7439.
262. Dias, A. M. A.; Carrier, H.; Daridon, J. L.; Pa`mies, J. C.; Vega, L. F.; Coutinho, J. A. P.; Marrucho, I. M. Vapor-liquid equilibrium of carbon dioxide-perfluoroalkane mixtures: experimental data and SAFT modeling, *Ind. Eng. Chem. Res.* **2006**, 45, 2341-2350.
263. Meng, L.; Burris, S.; Bui, H.; Pan, W.-P. Development of an analytical method for distinguishing ammonium bicarbonate from the products of an aqueous ammonia CO₂ scrubber, *Anal. Chem.* **2005**, 77, 5947.
264. Hooker, S.A. Nanotechnology Advantages Applied to Gas Sensor Development, *The Nanoparticles 2002 Conference Proceedings*, Business Communications Co., Inc., Norwalk, CT USA
265. Jaroniec, M.; Kruk, M.; Shin, H. Y.; Ryoo, R.; Sakamoto, Y.; Terasaki, O. Comprehensive characterization of highly ordered MCM-41 silicas using nitrogen adsorption, thermogravimetry, X-ray diffraction and transmission electron microscopy, *Microporous and Mesoporous Materials*, **2001**, 48, 127 – 134.
266. Kruk, M.; Jaroniec, M.; Gadkaree, K. P. Determination of the specific surface area and the pore size of microporous carbons from adsorption potential distributions, *Langmuir* **1999**, 15, 1442 – 1448.

VITA

Date of Birth: February 26, 1975

Place of Birth: Accra, Ghana

EDUCATION

M.S. Chemical Engineering, North Carolina A&T State University (July, 2002)

B.S. Chemical Engineering, University of Science and Technology, Ghana (July, 1999)

HONORS

3rd Place Award, poster presentation, 79th ACS Colloid and Surface Science Symposium, Clarkson University, Potsdam, NY (June 2005).

PUBLICATIONS

Osei-Prempeh, G., Knutson, B.L., Rankin, S.E., Lehmler, H.-J., 'Application of Fluorocarbon Functionalized Mesoporous Silica to Fluorous Separations.' Submitted, Industrial & Engineering Chemistry Research (April, 2007).

Osei-Prempeh, G., Knutson, B.L., Rankin, S.E., Lehmler, H.-J., 'Synthesis of Vinyl Functionalized Mesoporous Silica using Fluorinated Surfactant Templates,' Microporous and Mesoporous Materials 85 (2005) 16–24.

PRESENTATIONS

Osei-Prempeh, G., Knutson, B.L., Rankin, S.E., Lehmler, H.-J., 'Synthesis and Applications Of Fluorocarbon Functionalized Porous Silica,' AIChE annual meeting, San Francisco, CA (November 2006)

Osei-Prempeh, G., Knutson, B.L., Rankin, S.E., Lehmler, H.-J., 'Bi-Functionalized Mesoporous Silica Synthesized using Fluorinated Surfactants As Template' Cincinnati, Oh (November 2005)

Osei-Prempeh, G., Knutson, B.L., Rankin, S.E., Lehmler, H.-J., 'Fluorocarbon Functionalized Mesoporous Silica using Fluorinated Surfactants as Templates,' Poster presentation, ACS Colloid and Surface Science Symposium, Clarkson University, Potsdam, NY (June 2005)

Osei-Prempeh, G., Knutson, B.L., Rankin, S.E., Lehmler, H.-J., 'Fluorocarbon Functionalized Mesoporous Silica using Fluorinated Surfactants as Templates,' AIChE annual meeting, Austin, TX (November 2004)

Osei-Prempeh, G., Knutson, B.L., Rankin, S.E., Lehmler, H.-J., 'Synthesis of Vinyl Functionalized Mesoporous Silica using Fluorinated Surfactant Templates,' AIChE annual meeting, San Francisco, CA (November 2003)

Gifty Osei Prempeh